DESIGN, MODELLING AND CONTROL OF HYBRID ENERGY STORAGE SYSTEM FOR ELECTRIC VEHICLES

TAHA MOHAMMED AHMED SADEQ

DOCTOR OF PHILOSOPHY (ENGINEERING)

LEE KONG CHIAN FACULTY OF ENGINEERING AND SCIENCE
UNIVERSITI TUNKU ABDUL RAHMAN
OCTOBER 2021

DESIGN, MODELLING AND CONTROL OF HYBRID ENERGY STORAGE SYSTEM FOR ELECTRIC VEHICLES

By

TAHA MOHAMMED AHMED SADEQ

A thesis submitted to the Department of Electrical and Electronic Engineering,
Lee Kong Chian Faculty of Engineering and Science,
Universiti Tunku Abdul Rahman,
in partial fulfilment of the requirements for the degree of
Doctor of Philosophy (Engineering)
October 2021

ABSTRACT

DESIGN, MODELLING AND CONTROL OF HYBRID ENERGY STORAGE SYSTEM FOR ELECTRIC VEHICLES

Taha Mohammed Ahmed Sadeq

The energy storage system (ESS) is a critical factor in electric vehicle (EV) applications. Batteries represent a wide solution for clean energy, and they are among the most popular energy storage devices. Low power density and limited life-time are the main defects in Pure Battery Electric Vehicles (PBEVs). The Hybrid energy storage system (HESS) is the solution to the disadvantages of the single energy storage system in EV applications. In HESS, the battery is used to supply the low traction power and steady-state load current; whereas the supercapacitor is used to supply the peak demand current and absorb the regenerative energy during braking. This research aims to design a battery-supercapacitor HESS for EV. A semi-active topology had been used to interface the battery and supercapacitor with the DC bus. The energy consumption of the selected drive cycles was estimated considering the topographical information. The contour positioning system (CPS) was used to extract the road slope of the selected drive cycle along the journey. The proposed energy management strategy of HESS includes three control layers. The standard rule-based controller, the optimal adaptive rule-based controller, and the fuzzy adaptive rule-based controller were proposed to manage the energy flow of the HESS. The linear quadratic regulator (LQR) was designed to control the current flow of the DC-DC converter. To validate the proposed control strategies, the system was modelled and tested in Matlab/Simulink environment. The proposed control algorithms were tested in three real drive cycles (uphill, downhill, and city-tour) at three different speeds (50, 60, and 70 Km/h) and in three different standard drive cycles (UDDS, NYCC, and Japan1015). The results of the proposed energy management system proved that the controller succeeded in reducing the battery stress compared to that of the single energy storage battery system. The results of the proposed HESS using the optimal adaptive controller succeed to extend the number of possible drive cycles compared to those of the rule-based controller and the fuzzy adaptive controller.

Specially dedicated to
my beloved wife, my parents and, my family for their
patience, support, prayers, encouragement and blessings

ACKNOWLEDGEMENT

First and foremost, I would like to express my thanks to Allah Subhanho wa ta'ala who is lead me to finish this study. Second, I would like to express my sincere appreciation to my supervisor, Ts. Dr. CHEW KUEW WAI for his continuous guidance, professional advices, support, motivation, and encouragement to complete this study. Also, I would like to extend my thanks to my co-supervisor, Dr. EZRA MORRIS ABRAHAM GNANAMUTHU for his effort and guidance.

Moreover, I would like to express my gratitude to all my professors, lecturers, and staff in Universiti Tunku Abdul Rahman for their continuous guidance and help during my study.

Last but not least, I would like to extend my grateful thanks to Universiti Tunku Abdul Rahma Research Fund (UTARRF), KL Automation Engineering Sdn Bhd, and Ministry of Higher Education and Scientific Research-YEMEN for supporting my study.

APPROVAL SHEET

This dissertation/thesis entitled "**DESIGN, MODELLING AND CONTROL OF HYBRID ENERGY STORAGE SYSTEM FOR ELECTRIC VEHICLES**" was prepared by TAHA MOHAMMED AHMED SADEQ and submitted as partial fulfillment of the requirements for the degree of Doctor of Philosophy (Engineering) at at Universiti Tunku Abdul Rahman.

Approved by:

____

(Ts. Dr. CHEW KUEW WAI)
Date: 27-Oct-2021
Supervisor
Department of Electrical and Electronic Engineering
Lee Kong Chian Faculty of Engineering and Science
Universiti Tunku Abdul Rahman

____

(Dr. EZRA MORRIS ABRAHAM GNANAMUTHU)
Date: 27-10-2021
Co-supervisor
Department of Electrical and Electronic Engineering
Lee Kong Chian Faculty of Engineering and Science
Universiti Tunku Abdul Rahman

LEE KONG CHIAN FACULTY OF ENGINEERING AND SCIENCE

UNIVERSITI TUNKU ABDUL RAHMAN

Date: 18/10/2021

SUBMISSION OF THESIS

It is hereby certified that **TAHA MOHAMMED AHMED SADEQ** (ID No: **16UED01149**) has completed this final thesis entitled "*DESIGN, MODELLING AND CONTROL OF HYBRID ENERGY STORAGE SYSTEM FOR ELECTRIC VEHICLES*" under the supervision of Ts. Dr. CHEW KUEW WAI (Supervisor) from the Department of Electrical and Electronic Engineering, Lee Kong Chian Faculty of Engineering and Science, and Dr. EZRA MORRIS ABRAHAM GNANAMUTHU (Co-Supervisor) from the Department of Electrical and Electronic Engineering, Lee Kong Chian Faculty of Engineering and Science.

I understand that University will upload softcopy of my thesis in pdf format into UTAR Institutional Repository, which may be made accessible to UTAR community and public.

Yours truly,

(*TAHA MOHAMMED AHMED SADEQ*)

*

DECLARATION

I hereby declare that the dissertation is based on my original work except for quotations and citations which have been duly acknowledged. I also declare that it has not been previously or concurrently submitted for any other degree at UTAR or other institutions.

Name: TAHA MOHAMMED AHMED SADEQ

Date: 18/10/2021

TABLE OF CONTENTS

	Page
ABSTRACT	**iv**
ACKNOWLEDGEMENTS	**vii**
APPROVAL SHEET	
viii	
SUBMISSION SHEET	**ix**
DECLARATION	**x**
LIST OF TABLES	**xv**
LIST OF FIGURES	**xvii**
LIST OF ABBREVIATIONS	**xxiii**

CHAPTER

1.0	**INTRODUCTION**	**1**
1.1	Background of Study	1
1.2	Problem Statement	6
1.3	Research Objectives	8
1.4	Scopes of Work	9
1.5	Thesis Organizations	10
1.6	List of Publications	11
2.0	**A REVIEW OF HYBRID ENERGY STORAGE SYSTEM OF ELECTRIC VEHICLES**	**12**
2.1	Introduction	12
2.2	Electric vehicles	13
2.3	Energy Sources in Electric Vehicles	14

2.3.1 Batteries 15
2.3.2 Supercapacitors 17
2.3.3 Fuel Cells 19
2.3.4 Flywheels 19
2.4 The Topologies of the Hybrid Energy Storage System 21
2.5 The Energy Management Strategy of the HESS 23
2.5.1 Optimization Energy Management Strategy 24
2.5.2 Rule-based Energy Management Strategy 31
2.5.3 Pattern recognition Energy Management Strategy 36
2.6 The Impact of the Topography on the Energy Consumption for Electric Vehicle 37
2.7 Chapter Summary 39

3.0 MODELLING THE HYBRID ENERGY STORAGE SYSTEM AND ELECTRIC VEHICLE 41
3.1 Introduction 41
3.2 System Modelling and Configuration 42
3.2.1 Battery Model 43
3.2.2 Supercapacitor Model 47
3.2.3 DC-DC converter Model 50
3.3 Electric Vehicle Model 53
3.4 Contour Positioning System 57
3.5 Standard drive cycles 61
3.6 Sizing the Hybrid energy storage system 64
3.7 Chapter Summary 67

4.0 ENERGY MANAGEMENT SYSTEM OF HYBRID ENERGY STORAGE SYSTEM 68
4.1 Introduction 68
4.2 The Rule-Based Controller of HESS 69

4.3 The Adaptive Rule-Based Controller of HESS 71
4.3.1 The Optimal Adaptive Rule-Base Controller of HESS 71
4.3.2 The Fuzzy Adaptive Rule-Base Controller of HESS 74
4.4 The Linear Quadratic Regulator (LQR) 76
4.5 The Proposed Hybrid Energy Storage System Model in Matlab 80
4.6 Chapter Summary 84

5.0 RESULTS AND DISCUSSION 85
5.1 Introduction 85
5.2 Single Energy Storage Battery System 86
5.2.1 Uphill Drive Cycle 86
5.2.2 Downhill Drive Cycle 88
` 5.2.3 City-tour Drive Cycle 91
5.2.4 Standard Drive Cycles 94
5.3 The Results of Rule-Based Controller for HESS 96
5.3.1 Uphill Drive Cycle 97
5.3.2 Downhill Drive Cycle 100
` 5.3.3 City-tour Drive Cycle 104
5.3.4 Standard Drive Cycles 107
5.4 The Results of the Optimal Adaptive Rule-Based Controller for HESS 112
5.4.1 Uphill Drive Cycle 112
5.4.2 Downhill Drive Cycle 116
` 5.4.3 City-tour Drive Cycle 119
5.4.4 Standard Drive Cycles 123
5.5 The Results of Fuzzy Adaptive Rule-Based Controller for HESS 128
5.5.1 Uphill Drive Cycle 128
5.5.2 Downhill Drive Cycle 132
` 5.5.3 City-tour Drive Cycle 135

5.5.4 Standard Drive Cycles 138
5.6 Chapter Summary 143

6.0 CONCLUSION AND FUTURE WORK 145
6.1 Conclusion 145
6.2 Limitations and Future Work 148

LIST OF REFERENCES 149

LIST OF TABLES

Table		Page
1.1	List of the Publication of this research	11
3.1	The parameters of battery model	47
3.2	The Parameters of Supercapacitor Model	50
3.3	The Parameters of Electric Vehicle Model	57
4.1	The transient time characteristics for different values of q and R	78
5.1	The effect of considering road slope in the uphill drive cycle	88
5.2	The effect of considering road slope in the downhill drive cycle	91
5.3	The effect of considering road slope in the city-tour drive cycle	93
5.4	The total energy consumption in a standard drive cycle	96
5.5	The HESS details in uphill drive cycle using a rule-based controller	100
5.6	The HESS details in downhill drive cycle using a rule-based controller	103
5.7	The HESS details in city-tour drive cycle using a rule-based controller	107
5.8	The HESS details in UDDS, NYCC, and Japan 1015 drive cycles using a rule-based controller	110
5.9	The battery energy reduction ratio using the rule-based controller	111
5.10	The HESS details in uphill drive cycle using an optimal adaptive rule-based controller	115
5.11	The HESS details in downhill drive cycle using an optimal adaptive rule-based controller	119
5.12	The HESS details in city-tour drive cycle using an	123

optimal adaptive rule-based controller

5.13 The HESS details in UDDS, NYCC, and Japan 1015 drive cycles using an optimal adaptive rule-based controller 127

5.14 The battery energy reduction ratio using the optimal adaptive rule-based controller 127

5.15 The HESS details in uphill drive cycle using fuzzy adaptive rule-based controller 131

5.16 The HESS details in downhill drive cycle using a fuzzy adaptive rule-based controller 135

5.17 The HESS details in city-tour drive cycle using a fuzzy adaptive rule-based controller 137

5.18 The HESS details in UDDS, NYCC, and Japan 1015 drive cycles using an optimal adaptive rule-based controller 142

5.19 The battery energy reduction ratio using the fuzzy adaptive rule-based controller 143

5.20 The number of the possible drive cycles using the proposed controllers 144

LIST OF FIGURES

Figures		Page
1.1	The main components for the Battery Electric Vehicles	2
1.2	Ragone chart and location of several storage devices	4
2.1	The architecture of the main types of HEV in the market (Richardson, 2013)	14
2.2	Schematic of Li-ion cell (Zhang et al., 2018)	16
2.3	The schematic of charged Electrostatic double-layer capacitor (Conway, 2013)	18
2.4	The schematic diagram of a FC (Fathabadi, 2018)	19
2.5	The main component of flywheel (Dixon, 2010)	20
2.6	The main topologies for the HESS in literature	22
2.7	The Classification of Energy Management System for HESS	24
2.8	The topology of the HESS in (Zheng et al., 2018)	25
2.9	The Architecture of the HESS in (Pan et al., 2019)	26
2.10	The topology of the proposed HESS in (Lu et al., 2019)	27
2.11	The Schematic of the driving cycle prediction algorithm in (Zhao et al., 2019)	28
2.12	The structure of the optimization level of the EMS in (Gonsrang and Kasper, 2018)	29
2.13	The HESS load power based on the proposed EMS in (Mesbahi et al., 2017)	30
2.14	The scheme of the three control modes of HESS in (Veneri et al., 2018)	32
2.15	The diagram of the control strategy of HESS in (Liu et al., 2020)	33

2.16	The flowchart of the fuzzy logic controller in (Sellali et al., 2019)	34
2.17	The structure of the fuzzy logic controller in (Wang et al., 2016)	35
2.18	The configuration of the EV in (Eckert et al., 2020)	35
2.19	The configuration of the HESS in (Javorski Eckert et al., 2018)	3.6
3.1	Architecture of HESS for Electric Vehicle in this research	42
3.2	Different equivalent circuit model of the battery (a) Thevenin model, (b) impedance model, and (c) runtime-based electrical battery model(Chen and Rincon-Mora, 2006)	44
3.3	Equivalent model of the battery in SimPowerSystems library	46
3.4	Equivalent circuit models for the supercapacitor in literature	48
3.5	The main components of the DC-DC converter	51
3.6	The equivalent model of the DC-DC converter	53
3.7	The Forces affect the vehicle during movement	54
3.8	The dynamic model of vehicle in Matlab\Simulink	57
3.9	The uphill drive cycle (a) road elevation, (b) road slope	59
3.10	The downhill drive cycle (a) road elevation, (b) road slope	60
3.11	The city-tour drive cycle (a) road elevation, (b) road slope	61
3.12	The UDDS speed profile	62
3.14	The NYCC speed profile	63
3.14	The Japan1015 speed profile	63
3.15	The sizing step for electric vehicle application (Sadoun et al., 2011)	64

3.16	The steps to select the supercapacitor size for HESS	65
3.17	The steps to select the maximum value of the battery current (I_{b_max})	66
4.1	The flowchart of the proposed rule-based controller	70
4.2	Flowchart of optimal adaptive rule-based controller	73
4.3	The fuzzy logic controller surface	74
4.4	Flowchart of Fuzzy adaptive rule-based controller	75
4.5	The feedback gains of the LQR controller	77
4.6	The transient responses of battery current with several values of q and R	78
4.7	MATLAB/Simulink model of the EV using the single energy storage battery based on the real drive cycles	80
4.8	MATLAB/Simulink model of the EV using the single energy storage battery based on the standard drive cycles	81
4.9	MATLAB/Simulink model of the HESS using the rule-based controller based on the real drive cycles	82
4.10	MATLAB/Simulink model of the HESS using the rule-based controller based on the standard drive cycles	82
4.11	MATLAB/Simulink model of the HESS using the adaptive rule-based controller based on the real drive cycles	83
4.12	MATLAB/Simulink model of the HESS using the adaptive rule-based controller based on the standard drive cycles	84
5.1	Total EV load currents based on an uphill drive cycle for a single energy storage battery system (a) 50km/h, (b) 60km/h, and (c) 70km/h	87
5.2	The battery states of charge in an uphill drive cycle for a single energy storage battery system	88
5.3	Total EV load currents based on a downhill drive cycle for a single energy storage battery system (a) 50km/h, (b) 60km/h, and (c) 70km/h	90

5.4	The battery states of charge in a downhill drive cycle for a single energy storage battery system	90
5.5	Total EV load currents based on a city-tour drive cycle for a single energy storage battery system (a) 50km/h, (b) 60km/h, and (c) 70km/h	92
5.6	The battery states of charge in city-tour drive cycle for a single energy storage battery system	93
5.7	Total EV load currents for a single energy storage battery system based on (a) UDDS, (b) NYCC, and (c) Japan1015 drive cycles	95
5.8	The battery states of charge in UDDS, NYCC and Japan1015 drive cycles for a single energy storage battery system	96
5.9	Total HESS currents based on uphill drive cycle using the rule-based controller (a) 50km/h, (b) 60km/h and (c) 70km/h	98
5.10	The battery states of charge in an uphill drive cycle using the rule-based controller	99
5.11	The supercapacitor states of charge in an uphill drive cycle using the rule-based controller	99
5.12	Total HESS currents based on downhill drive cycle using the rule-based controller (a) 50km/h, (b) 60km/h and (c) 70km/h	101
5.13	The battery states of charge in a downhill drive cycle using the rule-based controller	102
5.14	The supercapacitor states of charge in a downhill drive cycle using the rule-based controller	103
5.15	Total HESS currents based on city-tour drive cycle using the rule-based controller (a) 50km/h, (b) 60km/h and (c) 70km/h	105
5.16	The battery states of charge in city-tour drive cycle using the rule-based controller	105
5.17	The supercapacitor states of charge in city-tour drive cycle using the rule-based controller	106
5.18	Total HESS currents based on standard drive cycle using the rule-based controller (a) UDDS, (b)	108

NYCC and (c) Japan1015

5.19 The battery states of charge in UDDS, NYCC, and Japan1015 drive cycles using the rule-based controller 109

5.20 The supercapacitor states of charge in UDDS, NYCC, and Japan1015 drive cycles using the rule-based controller 109

5.21 Total HESS currents based on uphill drive cycle using optimal adaptive rule-based controller (a) 50km/h, (b) 60km/h and (c) 70km/h 113

5.22 The battery states of charge in an uphill drive cycle using the optimal adaptive rule-based controller 114

5.23 The supercapacitor states of charge in an uphill drive cycle using the optimal adaptive rule-based controller 115

5.24 Total HESS currents based on downhill drive cycle using optimal adaptive rule-based controller (a) 50km/h, (b) 60km/h and (c) 70km/h 117

5.25 The battery states of charge in a downhill drive cycle using the optimal adaptive rule-based controller 118

5.26 The supercapacitor states of charge in a downhill drive cycle using the optimal adaptive rule-based controller 118

5.27 Total HESS currents based on city-tour drive cycle using optimal adaptive rule-based controller (a) 50km/h, (b) 60km/h and (c) 70km/h 121

5.28 The battery states of charge in city-tour drive cycle using the optimal adaptive rule-based controller 121

5.29 The supercapacitor states of charge in city-tour drive cycle using the optimal adaptive rule-based controller 122

5.30 Total HESS currents based on standard drive cycle using the optimal adaptive rule-based controller (a) UDDS, (b) NYCC and (c) Japan1015 124

5.31 The battery states of charge in UDDS, NYCC, and Japan1015 drive cycles using the optimal adaptive 125 rule-based controller

5.32 The supercapacitor states of charge in UDDS, NYCC, and Japan1015 drive cycles using the optimal adaptive rule-based controller 126

5.33 Total HESS currents based on uphill drive cycle using the fuzzy adaptive rule-based controller (a) 50km/h, (b) 60km/h and (c) 70km/h 129

5.34 The battery states of charge in an uphill drive cycle using the fuzzy adaptive rule-based controller 130

5.35 The supercapacitor states of charge in an uphill drive cycle using the fuzzy adaptive rule-based controller 131

5.36 Total HESS currents based on a downhill drive cycle using the fuzzy adaptive rule-based controller (a) 50km/h, (b) 60km/h and (c) 70km/h 133

5.37 The battery states of charge in a downhill drive cycle using the fuzzy adaptive rule-based controller 133

5.38 The supercapacitor states of charge in a downhill drive cycle using the fuzzy adaptive rule-based controller 134

5.39 Total HESS currents based on city-tour drive cycle using the fuzzy adaptive rule-based controller (a) 50km/h, (b) 60km/h and (c) 70km/h 136

5.40 The battery states of charge in city-tour drive cycle using the fuzzy adaptive rule-based controller 137

5.41 The supercapacitor states of charge in city-tour drive cycle using the fuzzy adaptive rule-based controller 137

5.42 Total HESS currents based on standard drive cycle using the fuzzy adaptive rule-based controller (a) UDDS, (b) NYCC and (c) Japan1015 140

5.43 The battery states of charge in UDDS, NYCC, and Japan1015 drive cycles using the fuzzy adaptive rule-based controller 140

5.44 The supercapacitor states of charge in UDDS, NYCC, and Japan1015 drive cycles using the fuzzy adaptive rule-based controller 141

LIST OF ABBREVIATIONS

ESS	Energy Storage System
EV	Electric Vehicles
HEV	Hybrid Electric Vehicles
ICE	Internal Combustion Engine
BEV	Battery Electric Vehicle
HESS	Hybrid Energy Storage System
DC	Direct Current
CPS	Contour Positioning System
LQR	Linear Quadratic Regulator
FCV	Fuel Cell Vehicles
NiCad	Nickel Cadmium
NiMH	Nickel Metal Hydride
PbO_2	Lead Oxide
Pb	Pure-Lead
H_2SO_4	Sulphuric Acid
H_2O	Water
ε_r	Electrolyte Dielectric Constant
ε_0	Permittivity Of A Vacuum
d	Effective Thickness of the EDL
v	Cell Voltage
C	Cell Capacity
FC	Fuel Cell
CO_2	Carbon Dioxide

SOC	State Of Charge
DP	Dynamic Programming
MDP	Markov Decision Process
CBDC	China Bus Driving Cycle
UDDS	Urban Dynamometer Driving Schedule
MOO	Multi-Objective Optimization
NYCC	New York City Cycle
NMPC	Non-Linear Model Predictive Control
LMPC	Linear Model Predictive Control
Q	Electric Charge
I_b	Battery Current
r_b	Battery Internal Resistance
E_b	Battery Potential
t	Time
V_b	Battery Terminal Voltage
SOC(0)	Initial State of Charge
C_{sc}	Total Capacity of Supercapacitor module
V_{sc}	Terminal Voltage of Supercapacitor module
PWM	Pulse Width Modulation
IGBT	Insulated-Gate Bi-polar Transistor
d	Switching period (duty cycle)
r_c	Capacitor Resistance
r_L	Inductor Resistance
F_{total}	Total Vehicle Forces
F_{aero}	Aerodynamic Force

F_{roll}	Rolling Force
F_{gr}	Grading Force
F_{accel}	Acceleration force
ρ	Air Density
A_f	Vehicle Front Area
C_d	Drag Coefficient
μ_{rr}	Rolling Resistance Coefficient
g	Earth Gravity
Mv	Vehicle Mass
J_{eq}	Total Value Of Moment Of Inertia Indicates To Motor Shaft
Jm	Total Moment Of Inertia Of The Electrical Motor
V	Vehicle Speed
θ	Road Angle
D(k)	Distance
E(k)	Elevation
N_{bat_s}	Number Of The Batteries In Series
N_{bat_P}	Number Of The Batteries In Parallel
P_{bat}	Battery Power
P_{sc}	Supercapacitor Power
It	Total Electric Vehicle Load Current
Ico	DC-DC Converter Output Current
I_{b_max}	Maximum Value Of Battery Current
SOC_{sc}	Supercapacitor State of Charge
SOC_{sc_mn}	Minimum Supercapacitor State Of Charge

SOC_{sc_max}	Maximum Supercapacitor State Of Charge
R	Percentage Of Power Split Between The Battery And Supercapacitor
I_{reg}	Total Regenerative Current
I_{tp}	Total Positive EV Load Current
q	Weighting element of states
R_r	Weighting Matrix of Inputs
Q_r	Weighting Matrix of States
SOC_b	Battery State of Charge
EnVar	Energy Variance

CHAPTER 1

INTRODUCTION

1.1 Background of Study

The considerable interest around the Energy Storage System (ESS) is motivated by a necessity to employ renewable resources to produce energy instead of fossil fuel. This need is related to two concerns: the depletion of petroleum reservoir in the future and global warming. Nowadays, based on the drive trains, the landed vehicles are classified into three main categories; conventional motor vehicles, hybrid electric vehicles (HEV), and electric vehicles (EV). The most common types are the conventional vehicles that use the internal combustion engine (ICE). The chemical energy resources such as (gasoline, ethanol, diesel, etc.) are converted to kinetic energy in a complicated process in poor efficiency by using ICE.

On the other hand, EV is an alternative-design automobile that uses an electric motor to power the vehicle with ESS's electricity. Furthermore, ICE and electrical motor with ESS are the two types of energy sources that power the HEVs. It combines the benefits of high fuel economy and low emissions. A strong support is given to HEVs and EVs' development to reduce air pollution and harmful vehicle emissions.

There are six main styles of the EV's in the market classified as follows: The pure battery electric vehicle BEV which comes first to ordinary people's minds when the electric vehicles are mentioned. The second type is the hybrid electric vehicle which depends on an ICE and ESS; this type became the most common type in the market in the last few years. Thirdly, vehicles that rely on power lines to move. Fourthly, vehicles that are supplied by replaceable energy sources such as metal-air batteries or fuel cells. Fifthly, vehicles that use alternative means to store the power like supercapacitor or flywheels. Sixthly, vehicles that are directly supplied by solar systems (Larminie and Lowry, 2003).

The numbers of electric vehicles increase significantly in today's market due to the advancement in the power electronic converter, being environmentally friendly, and the possibility of energy regeneration through braking. The efficiency of the EV's is better than that of the conventional vehicles. In addition, the maintenance of the EVs is less due to the limited moving parts. Furthermore, they have a high impact to reduce air pollution. Figure 1.1 represents the main components of the battery electric vehicles.

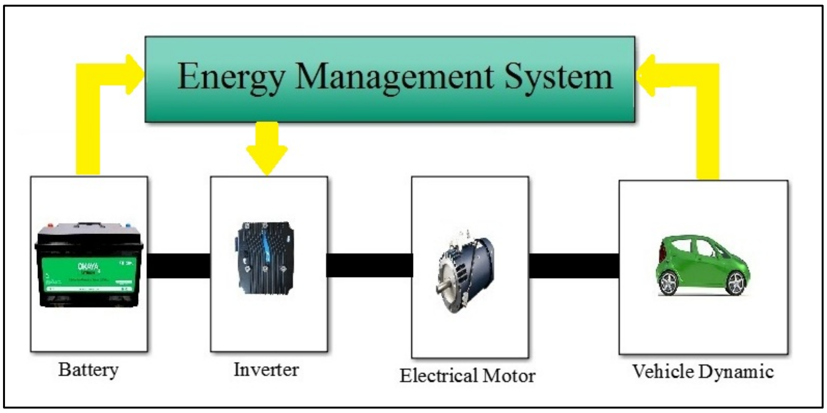

Figure 1.1 The main components of the Battery Electric Vehicles

An electric vehicle is a vehicle energized by electricity in the ESS. Batteries are one of the most common energy storage devices, and they represent a significant promise of the clean energy (Paladini et al., 2007). Many researchers (Udhaya Sankar et al., 2019, Ren et al., 2019, Fotouhi et al., 2016, Devillers et al., 2014) have demonstrated that in order to achieve a performance similar to that of the internal combustion engines, a single electric system (like a fuel cell) is not enough. Many efforts are devoted to studying the battery cell for electric vehicles in which the battery provides the main power.

Batteries, which are stacked cells, convert chemical energy to electrical energy and vice versa. The batteries use energy and power capacities as rating terms. Batteries play a major role in improving the ESS asset utilization, reliability, energy availability, and performance. They also provide economical ESS for the big sectors of energy management and power system applications. The main drawbacks of batteries are the need for a long time to charge, a low power density, and a short lifetime. Furthermore, the battery's lifetime is reduced by instantly responding to high load changes in charging and discharging.

Lead-acid batteries are the most popular battery type and dominate approximately 40–45% of the total universal battery sales. Lead-acid batteries can be found in several designs and sizes in the market. The availability, reliability, and low cost are the strengths of this kind of batteries (Balog and Davoudi, 2013). Lithium-Ion batteries are used widely in the EV application due to their high rate of specific power. BEVs require to have the minimum specific capacity 0.470 KW/kg and particular energy of 0.235 KWh/kg. Also, the user of the electrical vehicle has to drive in a range of 20,000 km per year. The standard vehicle consumes about 2.7 kWh for every 50 km of a driving distance. To have a driving range of 500 KM, 100 Kg of Lithium-Ion is used which is equivalent to the energy of one tank of petrol (Pearre et al., 2011, Neubauer et al., 2014). Figure 1.2 represents the specific energy against specific power of several energy storage devices in the market (Shim et al., 2013).

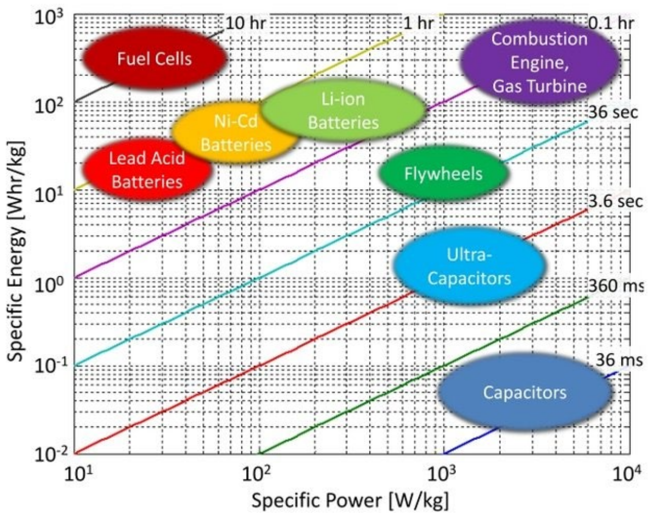

Figure 1.2 Ragone chart and location of several storage devices

The ESS of EV also needs a charging system. The charging system needs to be capable to reduce the losses of the battery pack during charging and to charge the batteries in a short time. Various energy sources can be implemented to charge the batteries. Moreover, the regenerative braking system in the EVs is used to harvest energy instead of dissipating it in a form of heat during braking. Nevertheless, the number of EVs sold are not comparable to that of the conventional vehicles due to the cost and driving range of EVs.

The electric vehicles are still facing many issues that need to be developed (Schaltz, 2011, Jordán et al., 2018, Ren et al., 2019). The limited lifetime and the low power density are the main issues in Battery Electric Vehicle. Hybrid Energy Storage System (HESS) is the practical solution that can be implemented for EV applications (Li et al., 2019b, Veneri et al., 2018, Capasso et al., 2018). HESS is a combination of two different types or more energy storage devices like batteries, fuel cells, flywheel, or supercapacitor. In HESS, a primary storage device with high energy density like batteries or fuel cells is used to provide constant power to the load while an auxiliary storage device with high power density like supercapacitor or flywheel is used to provide a fast dynamic response for load power changes (Mellor et al., 2000, Zhang et al., 2008).

The supercapacitor is a regular capacitor that allows to store a high amount of energy in a limited space. Unlike the electrochemical process of the battery, supercapacitor store energy as a static electronic charge and that makes them have a higher power density. It is then advantageous to combine these two energy storage devices to gain a better power and energy performances. The supercapacitor are implemented to supply the fast power load changes while the battery is used as primary ESS to meet the energy demand (Zhang et al., 2008).

In this research, the implementation of a battery-supercapacitor HESS in an EV is studied. Batteries remain the primary energy storage devices due to their high energy density. On the other hand, a supercapacitor has a lower energy density but a higher power density. The supercapacitor possesses the unique properties that can complement the other energy storage technologies.

Generally, a HESS is designed using a bidirectional DC-DC converter to mitigate the limitations of a supercapacitor-battery combination. One of the primary challenges in HESS design is the configuration of the supercapacitor and battery with the DC bus.

1.2 Problem Statement

Nowadays, the number of electric vehicles in the roads is still limited due to the limited driving range, the long charging time, and the short lifetime of the battery. All these challenges are related to the ESS of the EV. The ESS should contain enough energy to have a specific driving range, and it should also have a sufficient power capability for the accelerations and decelerations. Many researchers are trying to improve the efficiency of and ESS for the EV by using a combination of two or more energy storage devices. The fused device is called Hybrid Energy Storage System (HESS). In HESS, the batteries can supply the main power to the load due to its high energy density; however, they cannot supply peaks of power in short periods due to its limited power density. Likewise, supercapacitor have a low energy density but a high power density. Therefore, combining these two devices can achieve an efficient, light, and high-performance ESS for the EV (Gonzlez, 2009).

The energy storage hybridization in HESS will improve the energy storage system efficiency and extend the battery lifetime of the electric vehicles. Furthermore, the regenerative braking energy can be absorbed by the HESS instead of converting the kinetic energy into heat via friction brakes. HESS possesses two critical issues: the topology of HESS and the Energy Management System (EMS). There are several topologies of HESS used in literature, and each topology has its advantages and disadvantages. On the other hand, EMS is a critical affair to control the power flow between the HESS and the load. There are several control strategies used to manage HESS power such as the optimisation control strategies and the rule-based strategies. EMS aims to improve the performance and efficiency of HESS. The control strategy of the EV is implemented in a standalone mode to manage the power flow in real-time. Therefore, most of the optimised control strategies presented in literature require high computational time.

Many studies in the literature proved the advantage of HESS for electric vehicles in extending the battery lifetime, the energy availability, and the reduction of the battery temperature. Also, road conditions have a significant impact on the total energy demand in a drive cycle. Neglecting this factor leads to an inaccurate estimation of the EV energy consumption. Most of these researches ignored the road slope in the drive cycles and considered standard drive cycles to validate the performance of HESS for electric vehicle applications. Furthermore, the control strategies in the literature did not consider the conditions which guarantee the ability of HESS to operate continuously for various types of drive cycles.

1.3 Research Objectives

This research aims to propose an energy management system of HESS for EV to prolong the battery lifetime and enhance the vehicle performance. The aim of the proposed management system is to utilise the terrain information of the drive cycle to improve the performance of the HESS and achieve a maximum number of drive cycles. This objective includes the following:

i. To model the battery, the supercapacitor, the DC-DC converter, and the electric vehicle. The accurate model of HESS and electric vehicle leads to achieve the optimal design for the close-loop control system and the valid estimation of the EV energy consumption.

ii. To determine the drive cycles road slope angle and estimate the energy consumption and the regenerative energy along with the drive cycles by using Contour Positioning System (CPS).

iii. Design the optimal adaptive rule-based controller which guarantees the ability of HESS to operate continuously along with various drive cycles and obtain the maximum number of cycles.

iv. To design a Linear Quadratic Regulator (LQR) controller to control the energy flow between the supercapacitor and the DC-Bus by driving the bidirectional DC-DC converter.

v. To validate the proposed control algorithms of HESS for EV in three different types of real-drive cycles (Uphill, Downhill and City tour) in three different speeds and three different types of standard drive cycles (UDDS, NYCC and Japan1015).

1.4 Scope of the Work

The scope of the current research is as follows:

i. Design the HESS of pure electric vehicles without considering other vehicles like Hybrid Electric Vehicles containing Internal Combustion Engine.

ii. This research employs the lithium-ion battery and the supercapacitor module as the energy storage devices for the HESS of EV. A semi-active topology is used to interface the supercapacitor in parallel with the battery through a bidirectional DC-DC converter.

iii. Other energy devices like fuel cells or flywheel are not considered in the scope of this research.

iv. Matlab/Simulink software is used to model and simulate the system components such as the battery, the supercapacitor, the DC-DC Converter, and EV. The response of the proposed energy management system is tested in Matlab/Simulink environment as well.

v. The proposed energy management system is tested with real drive cycles. The driver is required to set the driving speed before the commencement of the journey.

vi. During the deceleration, the regenerative braking energy is to be solely absorbed by the supercapacitor to avoid the fast charging of the battery.

1.5 Thesis Organisation

This thesis is organised into six chapters. The outline of the chapters is described below. After the current introductory chapter, the literature review of the energy management system and HESS architectures for an electric vehicle is summarised in Chapter 2. The main challenge is to control the load current of the electric vehicle.

Chapter 3 presents the topology and the configuration of the proposed HESS. The details of the HESS components mathematical models for the battery, the supercapacitor, and the bidirectional DC-DC are explained. The model of the electric vehicle is described clearly. Furthermore, the contour positioning system, the selected real drive cycles, and the standard drive cycles are explained. Finally, the sizing method for the battery and supercapacitor is investigated.

Chapter 4 includes the design of the proposed energy management system of the HESS for the EV. The designs of the rule-based controller and the proposed algorithms of the adaptive rule-based controller are explained in details.

The results and the discussions of the proposed controllers are presented in Chapter 5. While chapter 6 highlights the conclusions, limitations, and the future work of this research.

1.6 List of the Publications

The presented findings in this thesis have been published in the international conferences and peer review journals as listed in Table 1.1.

Table 1.1 List of the Publication of this research.

No	Authors/ Title/ Status/ Link	Journal/ Conference	Index/ Impact factor
1	Sadeq, Taha, and Chew Kuew Wai. "Model the DC-DC Converter with Supercapacitor Module based on System Identification." (published) DOI:10.1109/i2cacis.2019.8825095	2019 IEEE International Conference on Automatic Control and Intelligent Systems (I2CACIS)	SCOPUS
2	Sadeq, Taha, and Chew Kuew Wai. "Linear Quadratic Regulator Control Scheme on Hybrid Energy Storage System" (published) DOI: 10.1109/i2cacis49202.2020.9140093	2020 IEEE International Conference on Automatic Control and Intelligent Systems (I2CACIS)	SCOPUS
3	Sadeq, Taha, Chew Kuew Wai, Ezra Morris, Qazwan A. Tarbosh, and Ömer Aydoğdu. "Optimal Control Strategy to Maximise the Performance of Hybrid Energy Storage System for Electric Vehicle Considering Topography Information." (published) DOI: 10.1109/access.2020.3040869	IEEE Access	ISI/Q1 3.75
4	Sadeq, Taha, Chew Kuew Wai, Ezra Morris," Current Control of Battery-Supercapacitor System for Electric Vehicle based on Rule-Base Linear Quadratic Regulator". (published) DOI: 10.25046/aj060107	Advances in Science, Technology and Engineering Systems Journal (ASTESJ)	SCOPUS

CHAPTER 2

A REVIEW OF HYBRID ENERGY STORAGE SYSTEM OF ELECTRIC VEHICLES

2.1 Introduction

Nowadays, attention is highly demanded to green and clean technologies. In today's cities, transport has experienced a high rate of growth. The typical internal combustion engine vehicle emits gases such as carbon dioxides, carbon monoxide, oxides of nitrogen, hydrocarbons, and water resulting in a higher earth's surface temperature. Electric cars are one of the best solutions to degrade fossil fuels and global warming. Many scientists focus primarily on Energy Storage System (ESS) in terms of cost reduction, rise in age, and growth in energy density. In the industrial section, the ESS is motivated by the necessity to employ renewable resources to produce energy instead of fossil fuels.

This chapter discusses the hybrid energy storage system for electric vehicles. The current state-of-the-art is summarized to solve the limitations of the energy storage systems in EVs. The advantages and disadvantages of several types of energy storage devices are presented. The combination of a high energy density energy storage technology and high power density technology offers a solution to solve energy storage device challenges.

2.2 Electric vehicles

The development of electrical vehicles (EVs) started in the second half of the 19th century, and they were used in Europe in the early 1880s (Haley, 2012). In current days, many researchers consider electric vehicles in their researches due to their features like high efficiency, elimination of local pollution, absence of noise, and provision of opportunities for a transportation sector powered by renewable energy. However, electric vehicles are still facing critical challenges that need to be solved (Schaltz, 2011).

This research will focus on electric vehicles that use energy storage devices to produce power. There are three main types of these vehicles: Battery Electric Vehicle (BEV), Hybrid Electric vehicles (HEV), and Fuel Cell Vehicles (FCV). BEV is fully powered by grid electricity stored in a large on-board battery. Several types of the battery had been used with EV as presented in the studies of (Yang and Knickle, 2002, Thomas, 2009, Khaligh and Li, 2010). HEV is a combination of a conventional vehicle and an electric vehicle, and it is driven by four different parts: electric motor, ESS, ICE, and transmission system.

Furthermore, the architecture of HEV is classified into two basic types: series and parallel. But presently, HEVs are classified into four kinds: series hybrid, parallel hybrid, series-parallel hybrid, and complex (Ehsani et al., 2009). FCV is another category of an electric vehicle. In this type, the fuel cell is used to generate the electrical power through an electrochemical reaction in the fuel cell chamber. FCV has an on-board fuel source, like hydrogen or natural gas. It also can either be fully dependent on the fuel cell or designed with a battery in a hybrid arrangement (Richardson, 2013). Figure 2.1 illustrates the architecture of the most common types of HEV in the market.

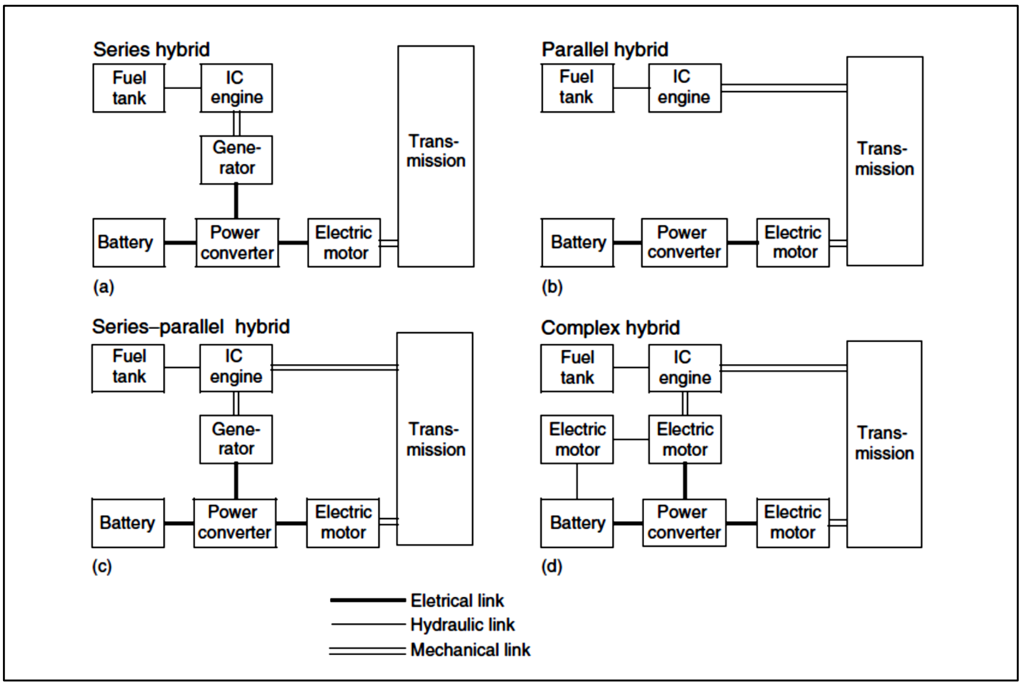

Figure 2.1 The architecture of the main types of HEV in the market (Richardson, 2013)

2.3 Energy Sources in Electric Vehicles

The energy storage devices are used to supply the electric vehicle with the needed traction power. The main characteristics that should be offered in ESS are energy density, power density, lifetime, cost, and maintenance-free. Various types of energy storage devices are used in EVs such as batteries, supercapacitor, flywheels, and fuel cell.

2.3.1 Batteries

A battery is a storage device that consists of one or more electrochemical cells that convert the stored chemical energy into electrical energy. Batteries have many features such as high energy density, compact size, and reliability. Due to these characteristics, the batteries became widely used in electric vehicles. On the other hand, there are some energy losses from the battery cells during the charging and/or discharging due to the internal resistance of the battery.

Currently, there are several kinds of chemical batteries available in the market and the most commonly used in the EV are Lead-Acid, Nickel Cadmium (NiCad), Nickel Metal Hydride (NiMH), and Lithium-Ion (Tie and Tan, 2013). In general terms, the lead-acid cell consists of a lead oxide (PbO_2) cathode and a pure-lead (Pb) anode immersed in aqueous sulphuric acid ($H_2SO_4 + H_2O$) (Reddy, 2002). Equation 2.1 and Equation 2.2 describe the overall chemical reaction during charge and/or discharge for lead-acid and lithium-ion batteries, respectively.

$$PbO_2 + Pb + 2H_2SO_4 \leftrightarrow 2PbSO_4 + 2H_2O \qquad (2.1)$$

$$C_6Li_x + M_yO_z \leftrightarrow 6C + Li_xM_yO_z \qquad (2.2)$$

Batteries are designated by the nominal capacity in ampere-hours (Ah) and the nominal voltage which has been standardized at 2.1V/cell for the lead-acid battery. This value applies to the nominal electrolyte temperature and density. Higher voltages are achieved by the series connection of individual cells. Battery capacity is increased by using cells of greater capacity rather than a parallel connection. The parallel connection of cells increases reliability but this increases the total battery weight.

The common battery type in mobile electronics is Lithium-ion; however, these days it can be implemented in high power demand applications such as grid systems and electric vehicles. Lithium-ion batteries have a long life-time comparing with other kinds of batteries like lead-acid. Since the emergence of Lithium-ion batteries in 1991, Lithium batteries occupied the second place of the most consumed mobile energy in the market. Lithium-ion batteries have high specific energy density because Lithium is the lightest of all metals and has the greatest electrochemical potential. Low weight, temperature, volume, and, sensitivity are the main features of Lithium-ion batteries. Figure 2.2 shows the schematic of a single Lithium-ion battery.

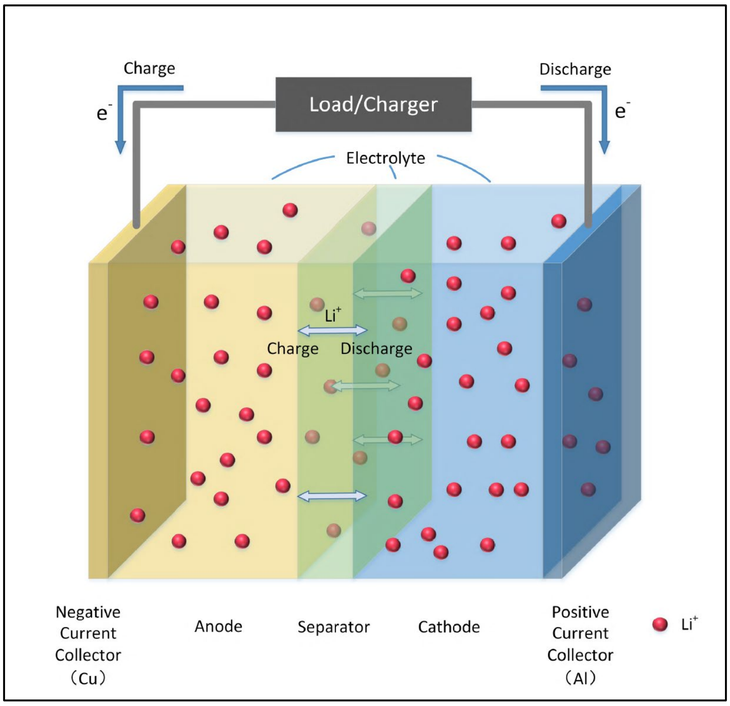

Figure 2.2 Schematic of Li-ion cell (Zhang et al., 2018).

2.3.2 Supercapacitor

There are two different ways to store the electrical energy: indirectly in batteries as potentially available in chemical energy which requires Faradaic oxidation and reduction of the electrochemically active reagents to release charges that can perform electrical work and directly in an electrostatic way as negative and positive electric charges on the plates of a capacitor, a process known as non-Faradaic electrical energy storage (Conway, 2013). Generally, capacitors consist of two metallic plates separated and insulated from each other by a non-conductive material such as glass or porcelain, Supercapacitor is a regular capacitor with very high capacitance in a small package (Burke, 2000). Supercapacitor are based on the double-layer capacitance concept, first described by the German physicist Hermann von Helmholtz in 1853. The first patent based on the double-layer structure was taken out by General Electric Company in 1957 (Becker, 1957).

Supercapacitor have two types: the electric double-layer capacitor (EDLC) and the pseudo-capacitor, and every type differs in the way of charge storing (Sharma and Bhatti, 2010). The supercapacitor has relatively high specific power and relatively low specific energy compared to those of the chemical batteries. Due to their low specific energy density and the dependence of voltage on the SOC, it is difficult to use supercapacitor alone as an energy storage device for high load applications. Nevertheless, some advantages can be achieved by using the supercapacitor as an auxiliary power source (Ehsani et al., 2009). Figure 2.3 represents the Schematic of EDLC.

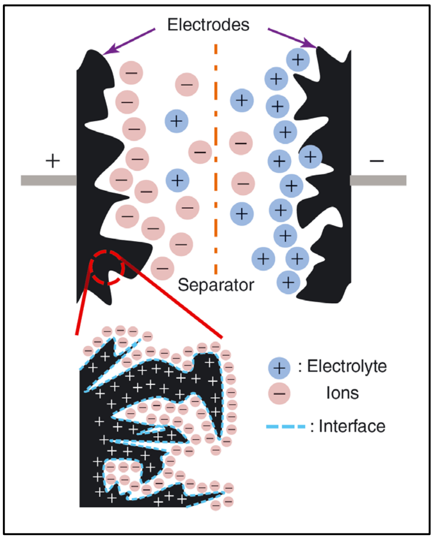

The main limitation of the supercapacitor is its low operation voltage. The maximum voltage that can be offered by a supercapacitor is nearly 2.5 V but most powerful applications require considerably higher voltages. To reach the required application voltage, the supercapacitor are connected in series. The capacity and the stored energy of the supercapacitor can be calculated using Equations 2.3 and 2.4, respectively.

$$C = \frac{\varepsilon_r \varepsilon_0}{d} A \tag{2.3}$$

$$E = \frac{1}{2} C V^2 \tag{2.4}$$

Where:

ε_0 ≡ the permittivity of a vacuum.

ε_r ≡ the electrolyte dielectric constant.

A ≡ the specific surface area of the electrode accessible to electrolyte ions.

d ≡ the effective thickness of the EDL (the Debye length).

C ≡ the capacitance of the cell (in farads).

V ≡ the cell voltage (in volts).

2.3.3 Fuel Cells

Fuel cells (FC) are electrochemical instrument used to convert energy from a chemical form to an electrical form directly. The FC generates the electrical energy as long as the reactant flows are maintained. The main advantages of FC are high conversion efficiency, low emission of Carbon dioxide CO2, quiet operation, fuel flexibility, durability waste heat recoverability, and reliability (Khaligh and Li, 2010). Figure 2.4 presents the schematic diagram of the FC.

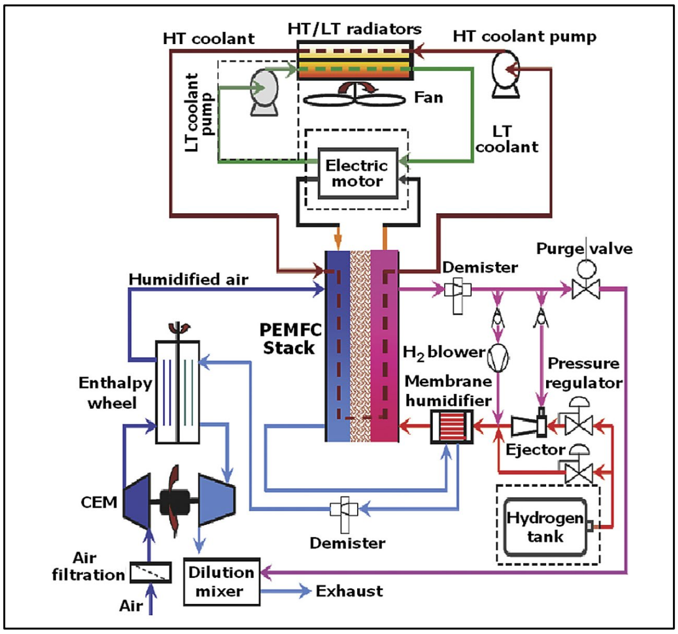

Figure 2.4 The schematic diagram of the FC (Fathabadi, 2018)

2.3.4 Flywheels

A flywheel energy storage system is a mechanical device that stores kinetic energy. FC consists of a cylinder with a shaft connected to an electrical generator. Electric energy is converted by the generator to kinetic energy which is stored by increasing the flywheel rotational speed. The stored energy is converted to electric energy via the generator (Rekioua, 2014). Flywheel is classified as an electro-mechanical battery made of wheel of carbon fibre, bearing, converter and generator (Dixon, 2010). Figure 2.5 shows the main components of the flywheel. The flywheel characteristics as following:

- Low Specific energy.
- High Specific power.
- No pollution.
- Long life-cycle.
- High efficiency.
- Less maintenance

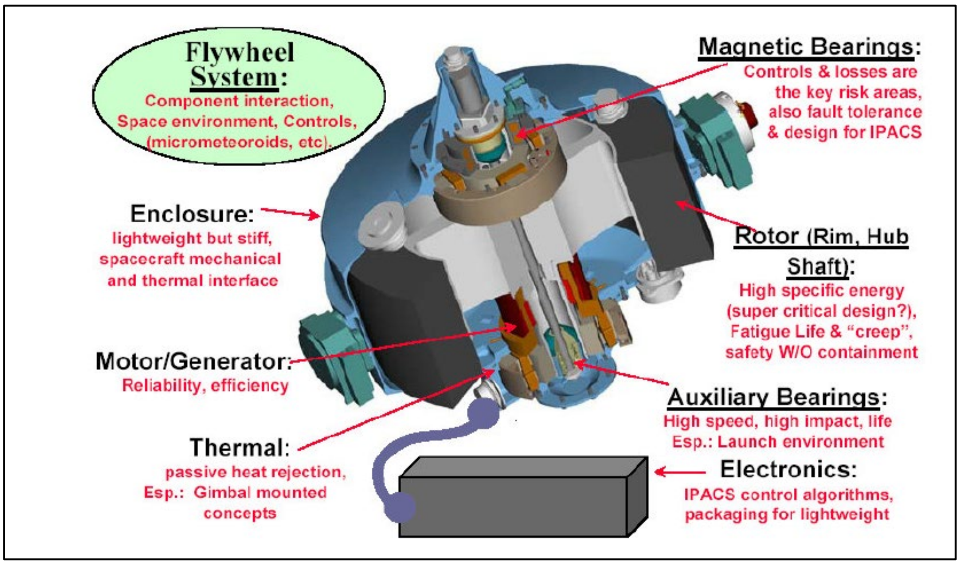

Figure 2.5 The main component of flywheel (Dixon, 2010)

2.4 The Topologies of the Hybrid Energy Storage System

The storage technology, operational characteristics, and particular strengths are varied in the energy storage devices. Different structures of hybrid energy storage systems were compared such as battery-Supercapacitor and battery-flywheel in (Kędra and Malkowski, 2018). The conclusion of this comparison is that the flywheel required special work conditions such as maintain the speed of the wheel while the main limitation of the supercapacitor is that has a fast drop in the terminal voltage. For EV applications the auxiliary energy storage device like supercapacitor and flywheel is used to store the regenerative energy during the braking. Due to the operation limitation of the flywheel and the big size of the flywheel compare with the supercapacitor module the battery-supercapacitor hybrid energy storage system was selected to supply the energy of the electric vehicle in this research.

Generally, HESS is designed by interfacing the supercapacitor and battery via a bidirectional DC-DC converter to take advantage of the two and mitigate their limitations. Many topologies for battery-supercapacitor interfaces have been attempted. Numerous studies in the literature have attempted to design battery-supercapacitor hybrid energy storage systems for EVs with various topologies to interface between the battery and the supercapacitor (Tie and Tan, 2013, Ju et al., 2014, Cao and Emadi, 2012, Xiang et al., 2014). Figure 2.6 illustrates different topologies of HESS. Furthermore, different types of bidirectional DC-DC converters have been used in a HESS for EV applications (Ostadi et al., 2013).

Figure 2.6(a) presents the simplest topology of a battery-supercapacitor system. Due to the direct connection, the battery and the supercapacitor voltage terminal is the same, and the DC-DC converter is used to maintain the power flow. In this topology, the supercapacitor characteristics are limited. Furthermore, a full-sized DC-DC converter is needed to manage the delivered energy (Aharon and Kuperman, 2011).

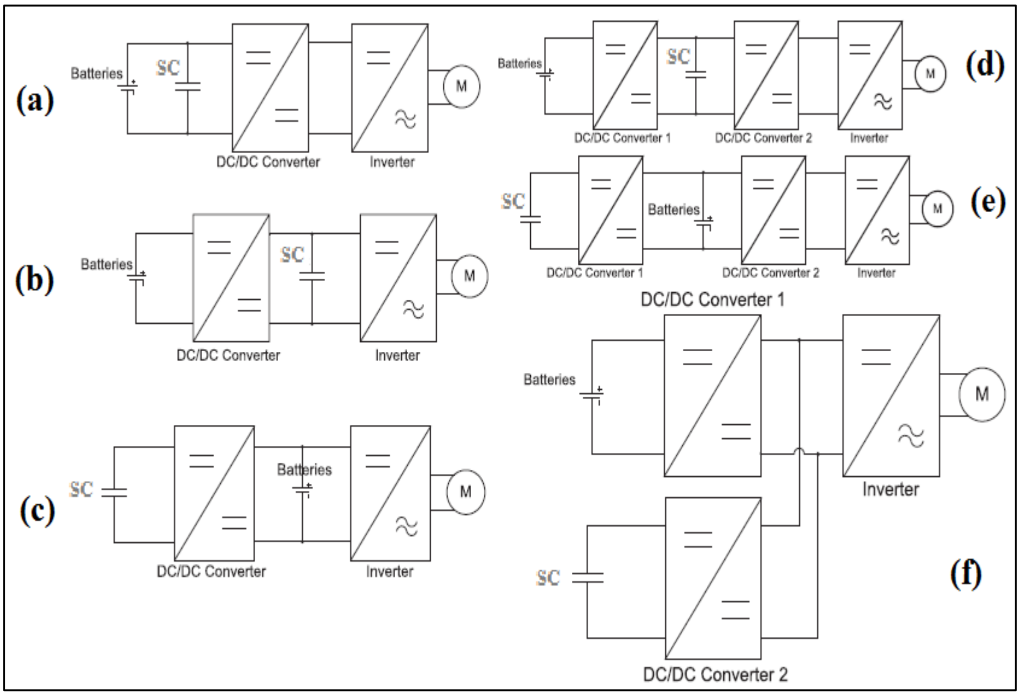

Figure 2.6 The main topologies for the HESS in literature

Another configuration of a HESS is shown in Figure 2.6(b). In this topology, the power flow of the battery is maintained within a safe range via the DC-DC converter. The supercapacitor operational range is limited, and it responds as an energy buffer (Ju et al., 2014).

The configuration in Figure 2.6(c) is widely used in literature (Iannuzzi and Tricoli, 2012, Armenta et al., 2015). The DC-DC converter was inserted between the supercapacitor and the DC bus as an interface to control the power flow from the supercapacitor. This topology offers a wide range of voltage for the supercapacitor and enhances the performance of the battery by decreasing the battery current. The reliability is another feature of this topology; the power flow is not affected by the failure of the DC-DC converter. This configuration is known as the semi-active HESS.

The topologies represented in Figure 2.6(d, e) use two DC-DC converters to manage the power flow from the battery and supercapacitor separately. These topologies require a full and medium-size DC-DC converter for every source. Besides, the loss, cost, and weight are increased in these topologies compared with the other topologies regarding the need for full-sized DC-DC converters (Kuperman and Aharon, 2011, Laldin et al., 2013).

The scheme in Figure 2.6(f) uses a parallel connection of batteries and supercapacitor via two DC-DC converters separately and suffers from the same constraints in Figure 2.2(d, e). This configuration is called the active HESS.

2.5 The Energy Management Strategy of the HESS

The Energy Management System (EMS) is the most critical issue in the active and semi-active topologies of HESS. The EMS aims to split the power between the battery and the supercapacitor and increase the performance of the HESS. Currently, the EMS of EV can be mainly categorized into optimization energy management strategies, rule-based energy management strategies, and pattern recognition energy management strategies. Various researches highlighted the different characteristics of energy management strategies. This section summarises the information and the various aspects of the energy management strategies. Figure 2.7 summarized the main categories of energy management system.

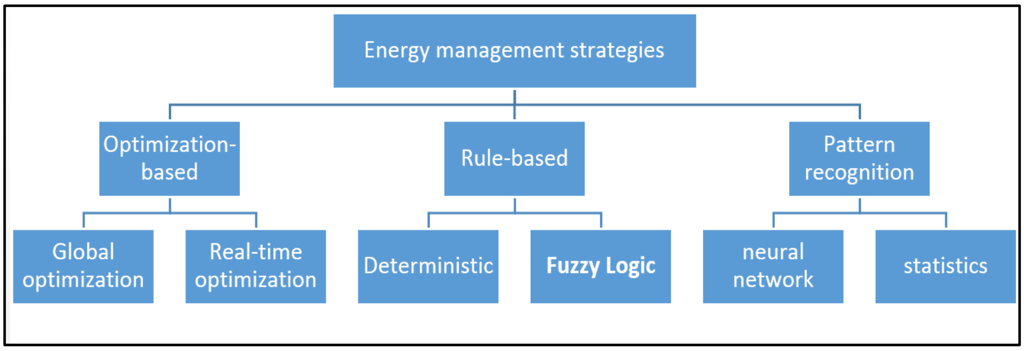

Figure 2.7 The Classification of Energy Management System for HESS

2.5.1 Optimization Energy Management Strategy

The energy management system uses an optimization method to improve the performance of the EV. The diversity of the control problems leads to the description of several cost functions. There are two different optimization energy management systems introduced in the literature; the real-time optimization energy management strategy and the global optimization energy management strategy.

The work in (Zheng et al., 2018) proposed an energy management system for HESS based on Pontryagin's minimum principle to extend the battery life-time and achieve extra driving hours compared with the rule-based management system and single storage system. The semi-active topology was used to interface the battery and supercapacitor of HESS. Figure 2.8 presents the topology of HESS in this work. The proposed controller estimates the optimal supercapacitor state of charge (SOC) for the selected drive cycle and finds the required battery and supercapacitor energy to supply the EV to follow the estimated SOC of the supercapacitor. The proposed controller in this research was validated by being tested on three drive cycles: FTP72, NEDC, and Japan1015 drive cycles.

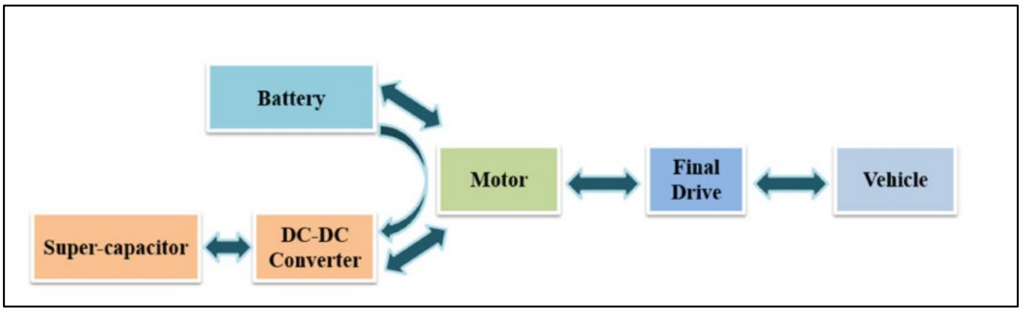

Figure 2.8 The topology of the HESS in (Zheng et al., 2018).

Other works consider the dynamic programming (DP) optimization method to manage energy flow in the battery-supercapacitor system presented in (Pan et al., 2019). The semi-active HESS is used to validate the proposed controller. The architecture of the HESS in this work is presented in Figure 2.9. The proposed controller reduced the energy consumption of an EV by 17.6% compared to the energy consumption when a battery was used.

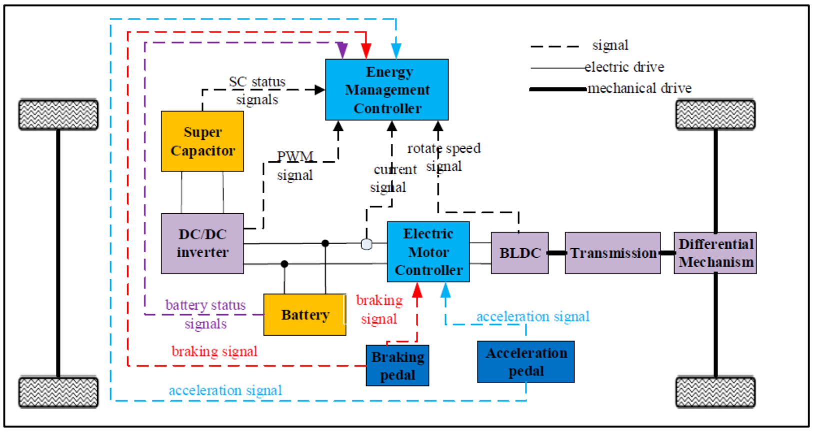

Figure 2.9 The architecture of the HESS in (Pan et al., 2019).

Other works presented in (Li et al., 2019a) proposed an energy management system using the Markov Decision Process (MDP) to manage the power flow for HESS of an EV. The active topology of HESS using two DC-DC converters was implemented in this research. The controllers aimed to reduce the battery fluctuation current to extend the battery life. China Bus Driving Cycle (CBDC) drive cycle and Urban Dynamometer Driving Schedule (UDDS) were used to test the controller response. A down-scale prototype of HESS was used to verify the proposed controller experimentally.

A real-time control strategy for HESS was studied in (Lu et al., 2019). The Multi-Objective Optimization (MOO) problem was formulated using three loss functions which are the battery life-cycle, power loss, and the stability of DC link voltage. The no-preference method and weighted method are two different methods used to change the optimized problem to a unity problem. The HESS model and controller algorithm were tested using ADVISOR. The proposed controllers were validated with four standard drive cycles UDDS, NYCC, NEDC, and INDIA_URBAN_SAMPLE. The proposed EMS in this work managed the energy flow from the battery in semi-active HESS as illustrated in Figure 2.10. The results proved the proposed control strategy enhances the performance of the HESS in terms of minimizing the power loss, extends the battery life-cycle, and maintains the voltage of the dc-link in a stable range.

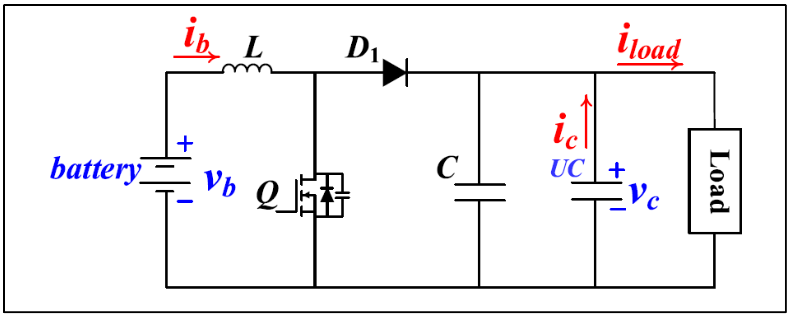

Figure 2.10 The topology of the proposed HESS in (Lu et al., 2019).

A comparative study was done to compare the control response of a Non-Linear Model Predictive Control (NMPC), rule-base control and Linear Model Predictive Control (LMPC) for the battery supercapacitor HESS in EVs (Golchoubian and Azad, 2017). A Toyota Rav4EV model was tested and showed the improved response of NMPC compared to that of LMPC.

A more complex control scheme was designed to split the load power between the battery and supercapacitor to increase the efficiency of the HESS and overall battery life in (Shen and Khaligh, 2016b). The predictive controller was used to manipulate the duty cycle of the DC-DC converter to control the current of the supercapacitor during operations. Furthermore, the predictive controller reduced the frequent variation of battery load in the EV's HESS. A non-uniform sampling time approach was investigated in (Gomozov et al., 2016).

The Markov Chain method was cooperated with the Monte Carlo method to propose a stochastic model from the history of the driving cycle in (Zhao et al., 2019). The predictive drive cycle was used to update the equivalent consumption minimization strategy in real-time. The proposed energy management strategy was validated for HEV model. Figure 2.11 represents the schematic of the driving cycle prediction algorithm.

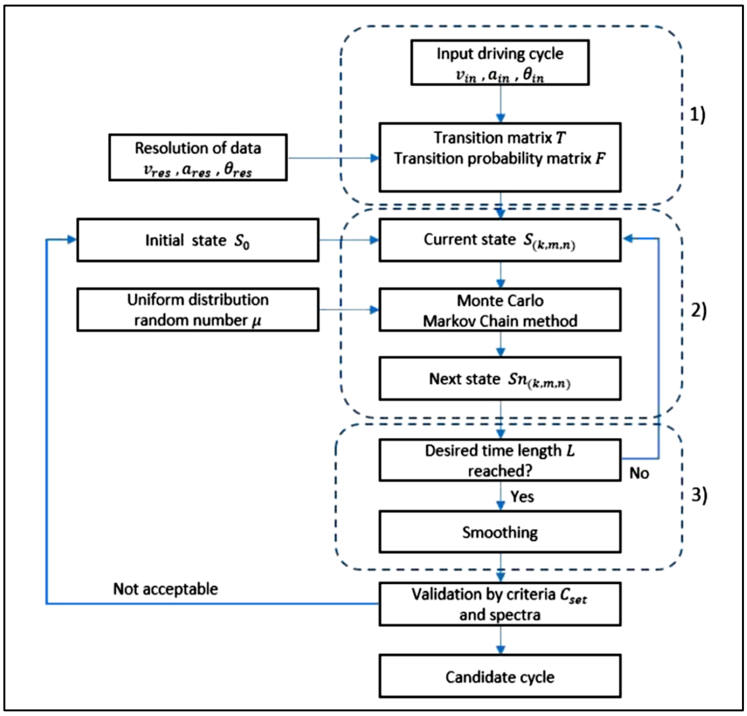

Figure 2.11 The schematic of the driving cycle prediction algorithm in (Zhao et al., 2019)

A new control strategy was proposed in (Hu et al., 2020) based on the driving pattern recognition. The driving cycle was classified into different patterns based on the historical driving data. An adaptive wavelet transform was used to assign the high power demand to the supercapacitor while the low frequency power demand was supplied by a battery. This strategy was implemented in a standard drive cycle and decreased the maximum charge/discharge current of the battery, improved the battery lifetime, and extended the vehicle range.

In (Gonsrang and Kasper, 2018), the power management system was proposed for HESS to extend the driving range of the electric vehicle. The proposed EMS aimed to split the vehicle load power between the battery and supercapacitor based on solving the formulated problem. The implementation of the proposed EMS in real-time could be achieved due to the small computation time. Multiple objectives problem was formulated based on the driving speed, the terminal voltage of the supercapacitor, and the battery peak power demand. The optimization problem was solved by a nonlinear model predictive control program and constrained quadratic program. Figure 2.12 shows the structure of the optimization level.

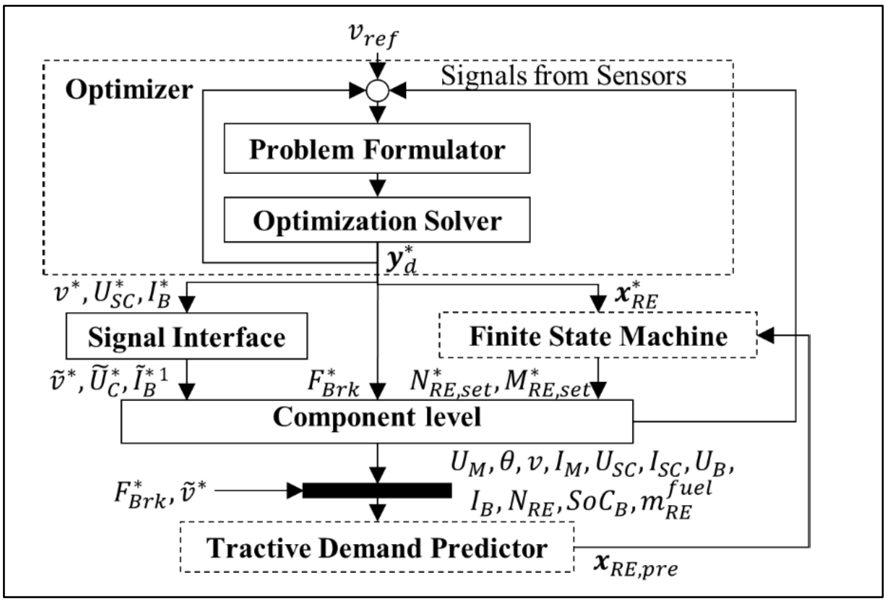

Figure 2.12 The structure of the optimization level of the EMS in (Gonsrang and Kasper, 2018).

The optimal energy management strategy was designed in (Mesbahi et al., 2017) to manage the battery/supercapacitor HESS. The proposed EMS aimed to manage the supercapacitor SOC around the initial value. The integration of the Particle Swarm Optimization and the Nelder–Mead was used to define the control parameter of the proposed EMS. The ARTEMIS drive cycle was used to test the performance of the proposed EMS. The results proved that the proposed EMS decreases the battery stress, reduces the system cost, and increases the battery life-time. Figure 2.13 represents the power split concept of the proposed controller in this research.

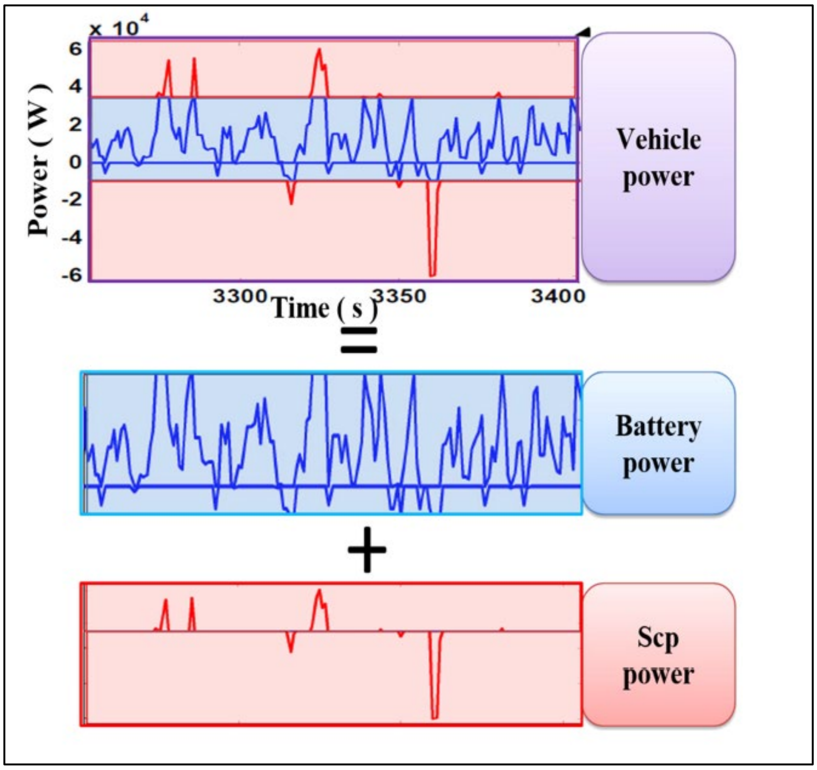

Figure 2.13 The HESS load power based on the proposed EMS in (Mesbahi et al., 2017).

The power management strategy based on dynamic programming (DP) was proposed to prolong the battery lifetime and extend the driving range of the

EV in (Chen et al., 2014). The performance of the DP was investigated with two cost functions: battery loss oriented and fuel loss oriented power management strategies. The minor drawback of the DP is the complicated interpolation and quantization; therefore, it needs a super microprocessor for implementation.

Rule-based control system is a group of rules that depends on the value of the control variables in real-time. The main advantages of the rule-based control strategy are that it does not require any information regarding the type of drive cycle being used, and it is simple to implement.

The response of the laboratory size scale of the semi-active HESS prototype was investigated using the emulate of the real road electric vehicle (Veneri et al., 2018). The proposed HESS in this work was controlled by three different strategies of rule-based energy management. The responses of the proposed rule-based controllers were evaluated in terms of the effects on the battery peck current. This study discussed the harmful effect of the high discharging rate current for the urban driving cycles in terms of battery life-time and efficiency. Figure 2.14 depicts the scheme of the three control modes of HESS.

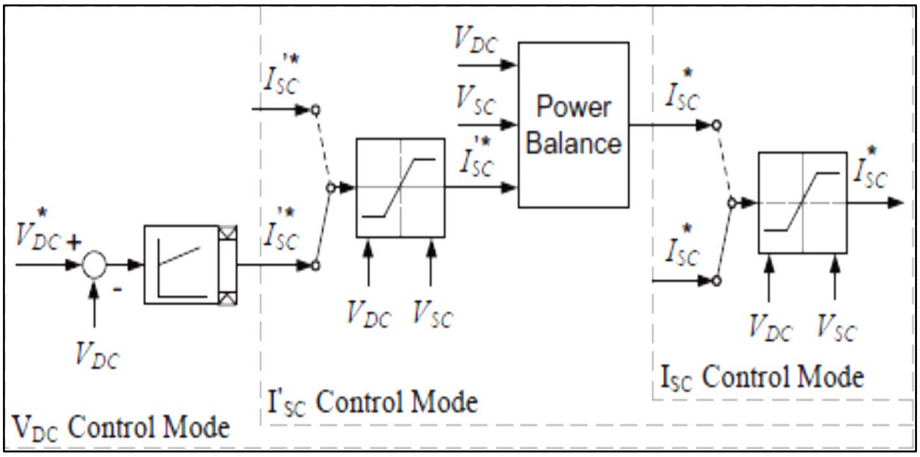

Figure 2.14 The scheme of the three control modes of HESS in (Veneri et al., 2018).

An adaptive power split strategy was used to split the load between the battery and the supercapacitor in the HESS for EVs in (Sun et al., 2017). The controller drove the interleaved DC-DC converter in the semi-active HESS, and the Zero Voltage Switching Method minimized the switching losses in the converter. The system was evaluated over four drive cycles in an EV.

A real-time rule-based power-split control strategy based on a Lyapunov-based nonlinear approach was proposed in (Zhang et al., 2020) for energy management of the battery-Supercapacitor HESS for EV. The proposed controller was tested to consider the speed of two standard drive cycles and the slope of a city road drive cycle.

The control strategy illustrated in Figure 2.15 was implemented to drive the switching bi-directional buck-boost converter for vehicles- to-grid systems (Liu et al., 2020). A state-space averaging approach was used to test the system stability. The controller considered the SOC of HESS to regulate the power flow in the system. The experimental results for laboratory prototypes were presented to verify the design.

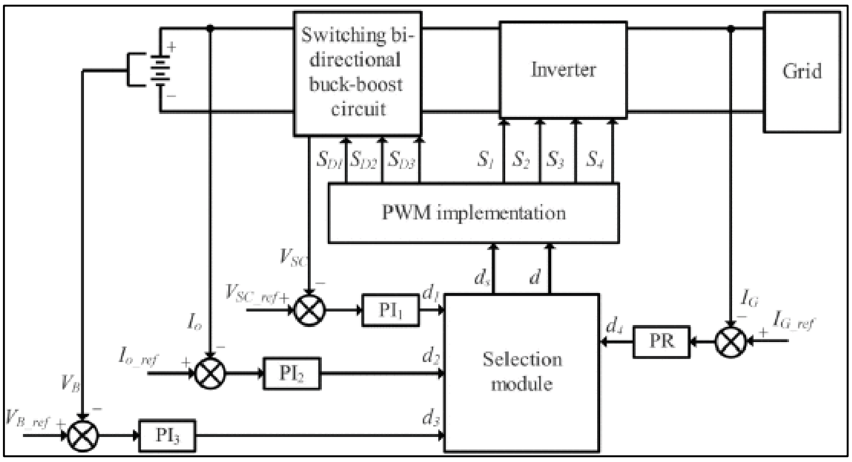

Figure 2.15 The diagram of the control strategy of HESS in (Liu et al., 2020).

A fuzzy logic controller was applied to control the HESS for EVs in (Sellali et al., 2019). The aim of the controller was to split the load power between the battery and supercapacitor, regulate the DC bus voltage, and monitor the SOC of the supercapacitor. The proposed control algorithm aimed to manage the power flow from HESS by the Fuzzy Logic Controller. Furthermore, the sliding mode controllers was implemented to control the vehicle traction. Figure 2.16 illustrates the flow chart of the proposed controller in this work. The results showed that the proposed controller improved the battery life by supplying the load energy from the battery at a steady state and from the supercapacitor during the transients.

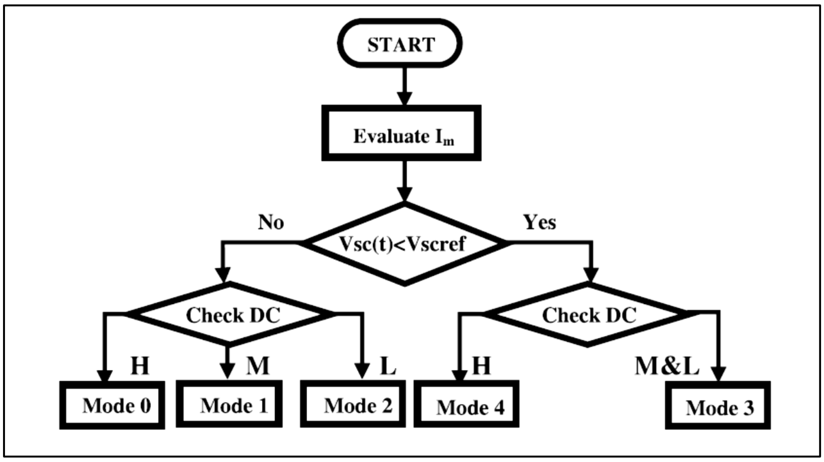

Figure 2.16 The flowchart of the Fuzzy Logic Controller in (Sellali et al., 2019).

The rule-based energy management strategy was proposed in (Armenta et al., 2015) to reduce the battery current peak and extend the driving time. The proposed EMS in this study aimed to control the power flow from the supercapacitor to enhance the ability of the supercapacitor to absorb all the regenerative energy during the braking. The efficiency of the EV increased by 8%–25% in terms of driving range when including the regenerative energy.

The rule-based fuzzy logic control approach was applied in (Wang et al., 2016) to manage the power flow in the HESS. The accuracy in measurement noise and adaptation of Fuzzy Logic was used as an energy management strategy. However, human experience was implemented to design the membership function and fuzzy rule. The proposed Fuzzy Logic Controller considered three inputs: the total power, the battery SOC, and the supercapacitor SOC. Figure 2.17 shows the structure of the proposed fuzzy controller.

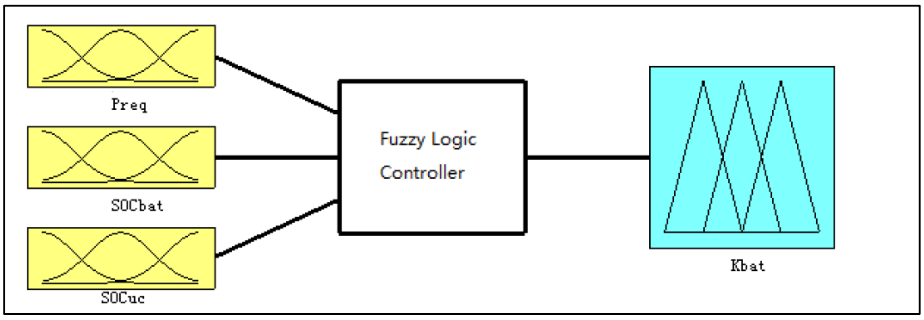

In (Bharath and Pandey, 2017), they designed a Fuzzy Logic Controller to manage the power distributed between the battery and the supercapacitor. The total vehicle load demand, supercapacitor SOC, and battery SOC were used as the controller's input. The ADVISOR platform was utilised to implement the model vehicle control strategy. In (Eckert et al., 2020), a genetic algorithm multi-objective optimization was applied to reduce the HESS sizing and extend the driving range of the EV. A fuzzy control strategy was used to split the power between the front and rear HESS to achieve better performance. The proposed configuration was tested in three standard drive cycles, and it succeeded to increase the driving range and reduce the HESS total weight. The architecture of the electric vehicle is shown in Figure 2.18.

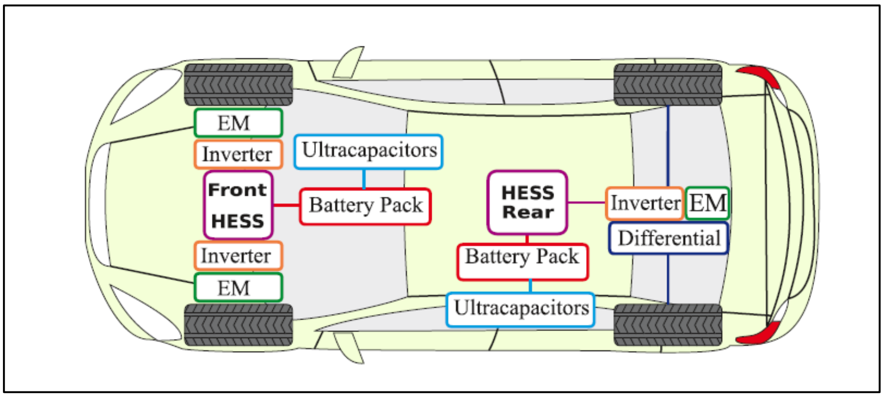

Figure 2.18 The configuration of the EV in (Eckert et al., 2020).

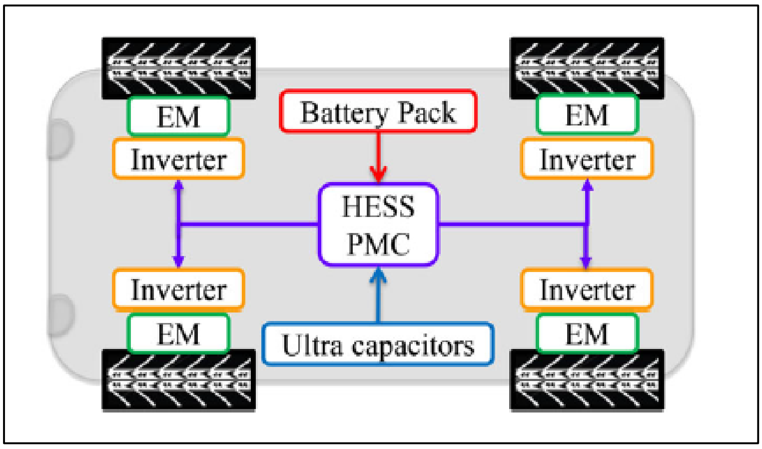

Figure 2.19 The configuration of the HESS in (Javorski Eckert et al., 2018).

2.5.3 Pattern recognition Energy Management Strategy

A different control strategy was applied in HESS for EV in (Alobeidli and Khadkikar, 2018). A two-stage neural network was used to control the SOC of the supercapacitor. This control strategy was used to extend the supercapacitor life and guarantee continuous hybridization. This concept was tested for three standard drive cycles and underwent both numerical and experimental investigations. The performance of a rule-based and a fuzzy adaptive controller was compared and the results showed improvements in the battery life.

Other researchers attempted to improve the HESS and battery life in the EVs by formulating real-time energy problems. This helped determine the optimal current split point between the battery and the supercapacitor. A cost objective function was derived to minimize the battery current variations and amplitude, and reduce the error between the supercapacitor current and the reference current. A neural network-based strategy was used to split the load current between the battery and the supercapacitor (Shen and Khaligh, 2016a).

Another work investigated a new energy management system for HESS for six standard drive cycles using a neural network (Zhang and Deng, 2016). The characteristic parameters were taken in real-time from the different drive cycles employing a slide time window to determine the load distributed components between the battery and the supercapacitor.

2.6 The Impact of the Topography on the Energy Consumption for Electric Vehicle

The Pontryagin's Minimum Principle was used to develop an algorithm for eco driving for electric vehicle (Shen et al., 2020). The real-world parameters such as traffic laws, road slope, safety concerns, and power train were used to adapt the proposed algorithm. The eco-driving algorithms were tested in three different scenarios and compared with human driving behaviours.

Other research was aimed to predict the energy consumption of the selected drive cycle for the battery electric vehicles (Wang et al., 2018a). The general effects of the weather conditions, road topography information, traffic condition, and driver behaviour are considered in the total energy estimation. The error between the results of the proposed prediction algorithm and the measured energy consumption within 5% for all tested trips.

In (Cheng et al., 2019) a driving control algorithm was proposed to improve the climbing performance of pure electric vehicles. The road slope, vehicle speed, rate of acceleration pedal, and battery state of charge were used to design the fuzzy controller. The proposed control method improved the dynamic and operation performance of the electric vehicle in terms of climbing conditions.

The energy estimation model for electric vehicle was proposed in (Wang et al., 2015). In this study Battery model, regenerative model, road load model, energy loss model, and auxiliary system model were used to predict the total energy consumption of electric vehicles for real routes.

Similar to the normal way to find the fastest way or shortest distance for the selected journey, a new design for route planner was presented in (Perger and Auer, 2020). The aim of this method is to find the driving path for the selected route which have less energy consumption. The multi-objective problem was identify based on energy consumption, driving time, and battery lifetime. The major impact of topography on the energy consumption of electric vehicle was validated.

Other research proposed an instant control energy strategy to improve the efficacy of electric vehicle depends on road slope and vehicle speed (Qu et al., 2019). The total energy consumption was decreased by including the kinetic energy of the electric vehicle in real-time. The proposed speed controller was saving 5.9% compared with driving with constant speed.

The effects of the road slope and traffic conditions on the total energy consumption of EV were investigated (Neaimeh et al., 2012). The presented data prove the impact of the topographical conditions of the selected route in terms of energy consumption.

2.7 Chapter Summary

This chapter presents a review of the architecture of the electric vehicle, the energy sources used commonly in the EVs, the main topologies implemented in the EVs, and the energy management system in the EVs. With a view to achieve the optimal energy management system for EVs, researchers should develop the optimization method of the rule-based energy management system.

The presented control strategies of the EVs in the literature have different characteristics. The Rule-based controller was implemented widely in mercantile vehicles due to the simplicity; however, the optimal solution is difficult to obtain. The review reveals a research gap in terms of the effect of road slopes and traffic information on the design of the energy storage system in EVs. Ignoring road topography informations can lead to incorrect estimation of the total energy demand in a drive cycle. An uphill drive consumes more energy when the vehicle accelerates while less energy is used when the vehicle goes downhill. There are several methods used to measure the road elevation and slopes such as DEM, GPS, and CPS (Han et al., 2012, Chew et al., 2014). Vehicle-to-vehicle communications can also be used to collect information regarding the slope of the road (Coelingh and Solyom, 2012).

CHAPTER 3

MODELLING THE HYBRID ENERGY STORAGE SYSTEM AND ELECTRIC VEHICLE

3.1 Introduction

This chapter presents the Hybrid Energy Storage System proposed topology for the Electric Vehicle and the system components mathematical models. Battery model, Supercapacitor model, DC-DC converter model and Electric Vehicle model are explained in details. Determining an accurate and precise hybrid energy storage system is required to design the energy management system with optimal electric vehicles performance. Also, the Contour Positioning System is discussed and explained. The purpose of obtaining the slope and angles of a road based on the road contour distance and elevation is clarified. The study considered several natural drive cycles with different characteristics and different speeds to validate the proposed system. At the same time, the design of the energy management system of the Hybrid Energy Storage System for Electric Vehicle is discussed in detail in the next chapter. Finally, the sizing method to select the proper size for the battery and supercapacitor of the Hybrid Energy Storage System for Electric Vehicles application is presented.

3.2 System Modelling and Configuration

This research implements the semi-active topology of HESS to deliver the required energy for EV. In this topology, the supercapacitor are connected to the DC bus through a bidirectional DC-DC converter in parallel with a battery to capitalise on the two systems advantages and mitigate their limitations.

The proposed energy management system is designed to split the demand energy between the battery and supercapacitor and limit the battery current. The battery provides low traction and steady-state EV load current whilst the supercapacitor supplies the peak demand EV load current and absorbs the regenerative energy during braking. The Rule-based adaptive controller is designed to manage the super capacitor energy flow by tuning the drive cycle of the DC-DC converter. Figure 3.1 shows the HESS architecture for the EV in this research.

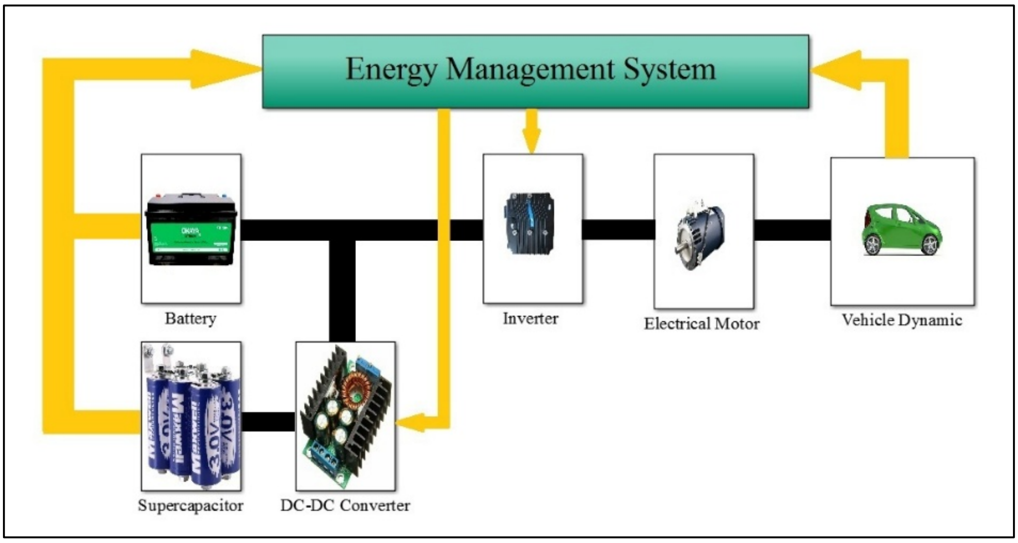

FIGURE 3.1 Architecture of HESS for Electric Vehicle in this research

3.2.1 Battery Model

As presented in the literature, many researchers focused on battery modelling. Battery models can be categorised based on the used modelling approaches. The major categories are mathematical models, electrochemical models, and electrical equivalent circuit networks. Usually, some empirical formulas or heuristic techniques are used to obtain the specific characteristics and mathematical models of batteries. One of the simplest and oldest analytical methods is the Peukert's equation which shows that battery capacity depends on the battery current discharge rate. The electrochemical models rely on the internal chemical reactions between the materials inside the battery.

Consequently, these models have high accuracy compared with other models since they simulate the cells at the microscopic scale. They often involve six-coupled non-linear differential equations. The complexity of the electrochemical models and limitations of the computers computing power in the past led researchers to investigate another modelling approach called equivalent circuit model. Generally, this model uses electrical components to model the behaviour of the battery. Batteries may be modelled with a constant voltage source in series with resistance in its simplest form. Adding more components to the capacitor can show different effects. Many examples of battery models can be found in literature and will not be reviewed in this chapter. Most of them are not directly applicable to the EV application. Instead, the focus will be on a group of works which involves the simplification of these battery models. The electrical equivalent circuit model for the battery will be considered in this research. There are many ways to represent the electrical equivalent circuit model for the battery. Most of these models fall under three main categories: Thevenin, impedance, and runtime-based models. Figure 3.2 illustrates the different electrical equivalent circuit models for the battery (Chen and Rincon-Mora, 2006, Shafiei et al., 2011, Fotouhi et al., 2016).

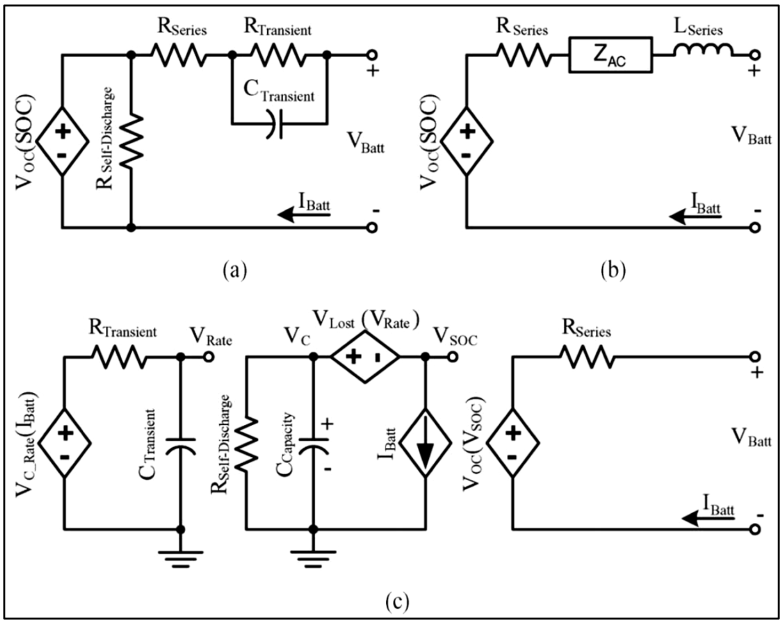

Figure 3.2 Different equivalent circuit model of the battery (a) Thevenin model, (b) impedance model, and (c) runtime-based electrical battery model(Chen and Rincon-Mora, 2006).

After choosing the electrical equivalent circuit model construction, the parameters or the values of the model components need to be determined. These parameters can be found using the real data for charging and discharging the battery. For EV application, a fast battery model that is accurate at different SOC levels subjected to various charge/discharge current amplitudes, a wide range of temperature, etc. is needed (Fotouhi et al., 2016). The electrochemical batteries, like Lead-acid battery, have complex and non-linear behaviour during charging and discharging depending on battery state-of-charge and electrolyte temperature. For those reasons, (Ceraolo, 2000, Barsali and Ceraolo, 2002) tried to find dynamic model to represent this nonlinearity. Furthermore, the equivalent electric model was used to estimate the values of this model parameters using two ways: a complete identification procedure involving extensive lab tests and a simplified one that combined information from lab tests and data supplied by the manufacturer. The accuracy of these models was acceptable, and the proposed models behaviour was validated via the comparison with lab tests data.

Some researchers used the system identification technique to estimate the parameters of the battery model (Fotouhi et al., 2015). The real-time model identification technique combined with an adaptive neuro-fuzzy inference system (ANFIS) was used to estimate the battery SOC in the real-world electric vehicle applications.

SOC, the average current, and the electrolyte temperature. The parameter estimation result constitutes the look-up tables for the parameter values of the equivalent circuit elements that represent the battery behaviour in a different SOC (Ahmed et al., 2015).

The battery model can be found in the MATLAB/Simulink/ SimPowerSystems library. This equivalent model contains a control voltage source and an internal resistance, as shown in Figure 3.3. The relationship between the time-varying parameters in the battery model is shown in Equation 3.1. Table 1.1 shows the main parameters of the battery model used in this study.

$$\begin{cases} V_b(t) = E_b(t) - r_b . i_b(t) \\ SOC(t) = 100\left(SOC(0) - \frac{1}{Q}\int_0^t i(t)dt \right) \end{cases} \quad (3.1)$$

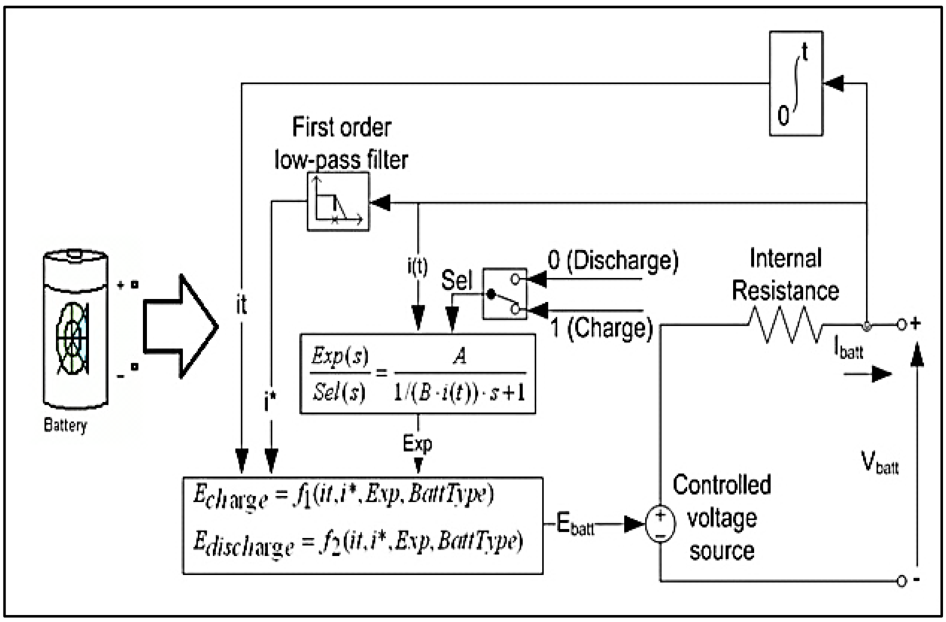

Figure 3.3 Equivalent model of the battery in SimPowerSystems library

Table 3.1 The parameters of battery model

Parameter	Value
Capacity (Ah)	100
Internal Resistance (Ohms)	0.125
Nominal voltage (V)	500
Stored energy (kWh)	50
Initial $\boldsymbol{SOC_b(0)}$	0.95

3.2.2 Supercapacitor Model

Supercapacitor have a widespread use in academia and the automotive industry due to their characteristics, high efficiency, low internal resistance high power density, long cycle life, fast charging, and wide operational temperature range. A model that can emulate supercapacitor dynamics with high precision and good robustness is of utmost importance for energy management design. The model should also avoid complexity to be easily incorporated into real-time controllers. Therefore, it is vital to strike a balance between the model accuracy, robustness, and model complexity (Zhang et al., 2015). Many supercapacitor models are presented in the literature (Faranda et al., 2007, Johansson and Andersson, 2008, Zubieta and Bonert, 2000, Sharma and Bhatti, 2010). The supercapacitor models can be generally categorised into three groups: electrochemical models, equivalent circuit models, and artificial-neural-network-based (ANN-based) models. This research will rely on the equivalent circuit model for the supercapacitor.

One of the practical models for the supercapacitor was proposed in (Zubieta and Bonert, 2000). The model consisting of three RC branches was suggested to achieve a better fit for the collected data. The capacitance of the branch with the fastest response was modelled as a voltage-dependent capacitor. The model parameters were determined from the terminal measurements of the charging and discharging of the supercapacitor. Figure 3.4 represents the different equivalent circuit models for the supercapacitor in the literature. This model was verified using MATLAB/Simulink as in (Shah et al., 2012).

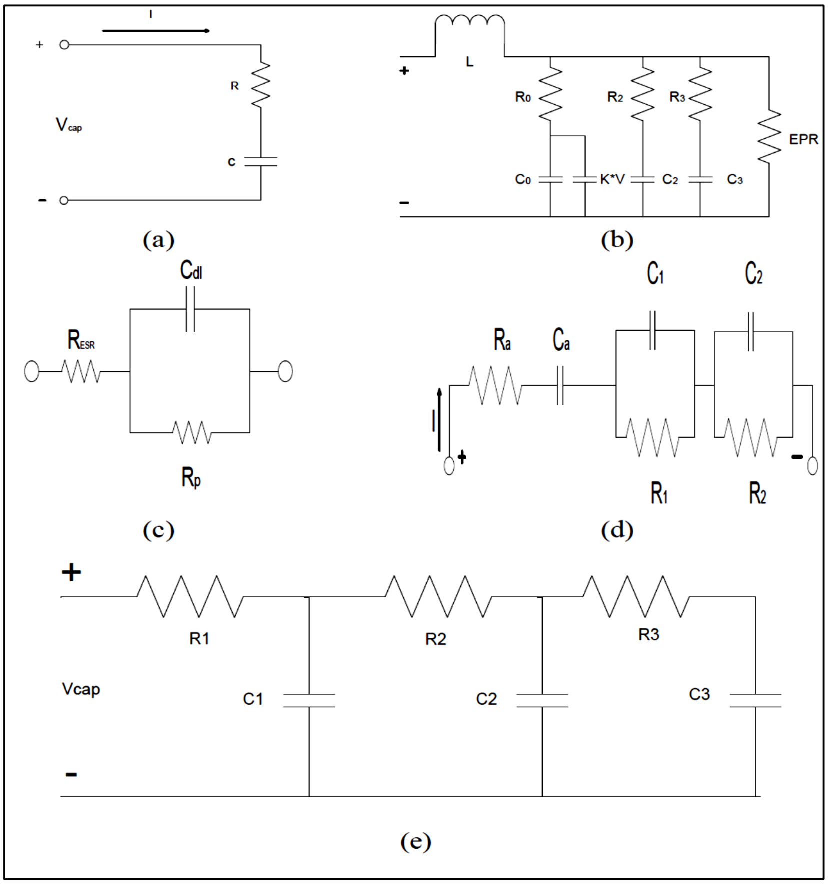

Figure 3.4 Equivalent circuit models for the supercapacitor in the literature.

Other researchers presented the two branches equivalent circuit model for the supercapacitor (Faranda et al., 2007). The process of identifying the model parameters was easier and faster than the previous model. Additionally, a dynamic model that describes the behaviour of supercapacitor can be used for the simulation and the analysis of the supercapacitor transient behaviour as mentioned in the literature. According to (Devillers et al., 2014), the model parameters are identified with adapted characterisation tests, such as charge and discharge test at constant current and Electrochemical Impedance Spectroscopy in environmental constraints.

Furthermore, other studies included the thermal effect to obtain an accurate model that represents the supercapacitor behaviour (Al Sakka et al., 2009, Rafik et al., 2007, Marie-Francoise et al., 2006). In (Rafik et al., 2007), an electrical model consisting of 14 RLC elements has been proposed to describe the supercapacitor behaviour. Electrochemical impedance spectroscopy was used to find the parameters values from the experimental data. The simulation and experimental results verified the accuracy of this method. Generally, the most common way to identify the parameters representing the dynamic behaviour of the supercapacitor is based on the impedance spectroscopy. However, it requires specialised instrumentation and cannot be easily implemented for model identification in a large frequency band. On the other hand, different researches tried to estimate the supercapacitor model parameters using the online identification method (Bertrand et al., 2010).

MATLAB/Simulink/SimPowerSystems elements are used to model the supercapacitor in this research. Table 2 lists the parameters of the supercapacitor module used in this study. The terminal voltage $\mathrm{V_{sc}}$ and the total capacity $\mathrm{C_{sc}}$ of the supercapacitor module can be calculated as per Equation 3.2.

$$\begin{cases} C_{sc} = \dfrac{C_{cell}.\, N_{parallel}}{N_{series}} \\ V_{sc} = V_{cell}.\, N_{series} \end{cases} \tag{3.2}$$

Table 3.2. The Parameters of Supercapacitor Model

Parameter	Value
Rated voltage (V)	300
Rated capacitance (F)	100
Resistance (mΩ)	2.1
Initial $\boldsymbol{SOC_{sc}(0)}$	0.9224

3.2.3 DC-DC converter Model

The model that describes the DC-DC converter behaviour is important for designing the HESS controller because the controller aims to drive the DC-DC converter to supply the required energy from the supercapacitor. The DC-DC converter output voltage and current are regulated by changing the duty cycle of the Pulse Width Modulation (PWM) which is applied to the IGBT of the DC-DC converter. In this research, a single layer bidirectional DC-DC converter is used to control the supercapacitor energy flow in both directions. The boost converter is used to discharge the supercapacitor, and the buck converter is utilised to charge the supercapacitor. Figure 3.5 represents the bidirectional DC-DC converter construction and main components (Machado et al., 2015).

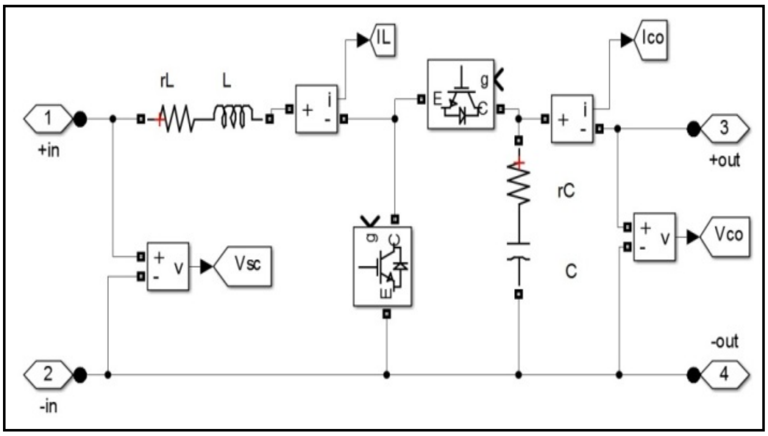

Figure 3.5 The main components of the DC-DC converter

The state-space average model is used to model the DC-DC converter in this research. This method approximates the DC-DC converter non-linear characteristics to the linear system (Abdullah et al., 2012) whereas the ON and OFF state of the IGBT is considered in modelling the DC-DC converter. The time averaging is performed as in Equation 3.3:

$$\dot{x} = [dA_{ON} + (1-d)A_{OFF}]X + [dB_{ON} + (1-d)B_{OFF}]V_{sc} \quad (3.3)$$

Where:

$$\begin{cases} d = the\_switching\_period \\ A_{on,off} = state\_matrices \\ B_{on,off} = control\_matrices \end{cases}$$

According to the main components of the bidirectional DC-DC converter in Figure 3.5, the following matrices represent the state and control matrices of the DC-DC converter in ON and OFF states:

$$X = [I_{\mathrm{L}} \quad V_c]^T = state\ vector$$

$$A_{\mathrm{ON}} = \begin{bmatrix} -\frac{r_L}{L} & 0 \\ 0 & \frac{-1}{C.(R + r_C)} \end{bmatrix}, \quad B_{\mathrm{ON}} = \begin{bmatrix} \frac{1}{L} \\ 0 \end{bmatrix}$$

$$A_{\text{OFF}}' = \begin{bmatrix} \frac{-R.r_C - R.r_L - r_C.r_L}{L(R+r_C)} & -\frac{R}{L(R+r_C)} \\ \frac{R}{C(R_o+R_c)} & -\frac{1}{C(R_o+R_c)} \end{bmatrix}, \quad B_{\text{OFF}} = \begin{bmatrix} \frac{1}{L} \\ 0 \end{bmatrix}$$

The state-space model of the DC-DC converter is represented by the following Equations (Wangsupphaphol et al., 2013):

$$\frac{d}{dt}\begin{bmatrix} i_L \\ V_c \end{bmatrix} = \begin{bmatrix} \frac{R.r_C.(d-1) - r_L(R+r_C)}{L(R+r_C)} & \frac{R.(d-1)}{L(R+r_C)} \\ \frac{R.(1-d)}{C(R+r_C)} & -\frac{1}{C(R+r_C)} \end{bmatrix} \begin{bmatrix} i_L \\ V_c \end{bmatrix} + \begin{bmatrix} \frac{1}{L} \\ 0 \end{bmatrix} V_{sc} \quad (3.4)$$

$$V_{co} = \begin{bmatrix} \frac{R.(d-1)}{(R+r_C)} & \frac{R}{(R+r_C)} \end{bmatrix} \begin{bmatrix} i_L \\ v_c \end{bmatrix} \quad (3.5)$$

$$\begin{cases} A_s = A = dA_{\text{ON}} + (1-d)A_{\text{OFF}} \\ B_d = (A_{\text{ON}} - A_{\text{OFF}})X - (B_{\text{ON}} - B_{\text{OFF}})V_{sc} \\ B_s = [B_d \quad B] \end{cases} \quad (3.6)$$

$$B_d = \begin{bmatrix} \frac{R.r_C}{L(R+r_C)}.i_L + \frac{R.r_C}{L(R+r_C)}.V_c \\ -\frac{R}{C.(R+r_C)}.i_L \end{bmatrix} \quad (3.7)$$

The parameters of the DC-DC converter are designed based on (Mohan and Undeland, 2007). The DC-DC converter model in Figure 3.5 is simplified by replacing the switching elements using a combination of controlled current and voltage sources as shown in Figure 3.6. This simplified model has good accuracy and a low computational time (Abdullah et al., 2014). Another method to estimate the discrete transfer function of the DC-DC converter using system identification technique is presented in (Sadeq and Wai, 2019). The state and control matrices of the state-space model of the DC-DC converter is used to design the linear quadratic regulator LQR controller to obtain the desired duty cycle of the PWM.

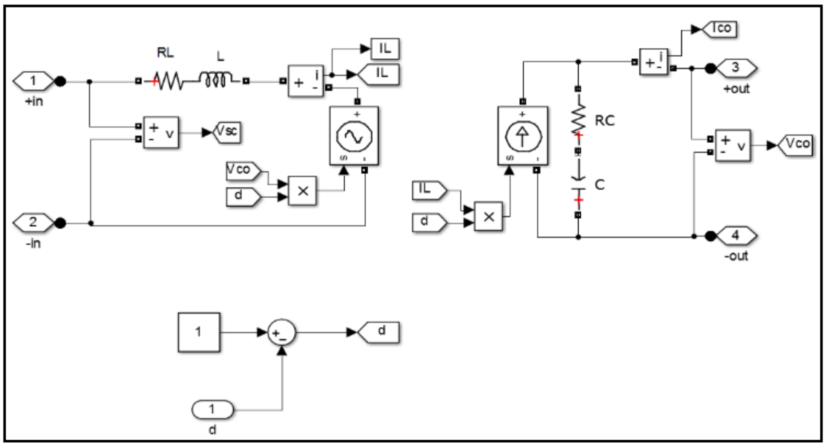

Figure 3.6 The equivalent model of the DC-DC converter

3.3 Electric Vehicle Model

A proper model representing the EV performance is required to obtain a better energy consumption. Many researchers used MATLAB/Simulink to develop the model for EVs whilst others used ADVISOR or other software to perform comprehensive performance analyses for a wide range of vehicles (Wipke et al., 1999, Fotouhi et al., 2015, Wai et al., 2015, Bampoulas et al., 2016, Kaloko et al., 2011, Mahmud and Town, 2016). The vehicle dynamic system was explained clearly in (Larminie and Lowry, 2003, Ehsani et al., 2010, Schaltz, 2011). In term of the fundamental of the vehicle dynamics and Newton's second law of motion, the total forces (F_{total}) affecting the vehicle momentum are aerodynamic force (F_{aero}), rolling force (F_{roll}), grading force

(F_{gr}), and acceleration force (F_{accel}) as presented in Equation 3.7. Figure 3.7 represents the main forces that affect the vehicle during movement.

$$\sum F_{Total} = F_{aero} + F_{roll} + F_{grad} + F_{accel} \qquad (3.7)$$

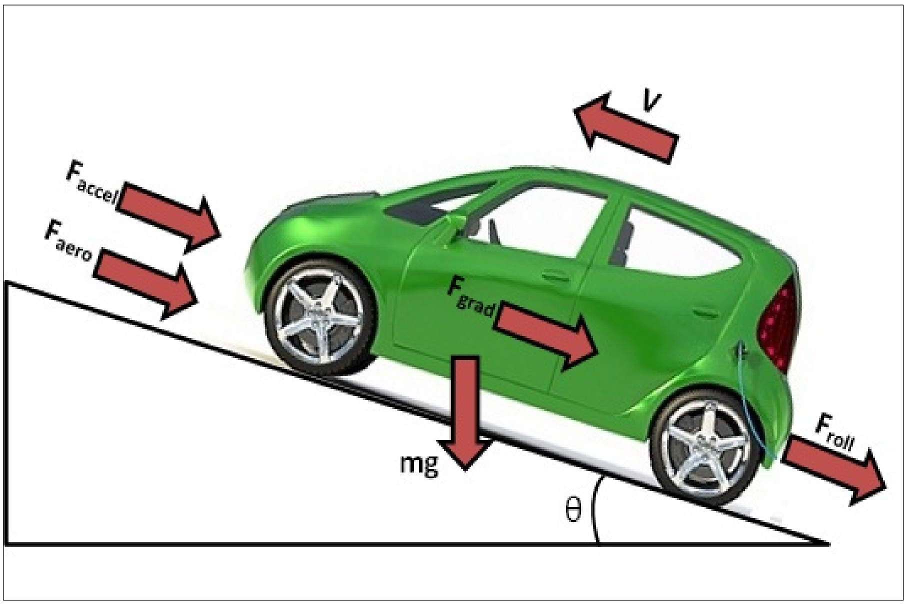

FIGURE 3.7 Forces affecting the vehicle during movement

The glutinous resistance that impedes movement of the vehicle body through air is called the aerodynamic resistance force. This force is a function of few factors such as the vehicle shape, the front area, the air passages, and the side mirrors. The aerodynamic resistance force depends on the following constants: air density ($\rho = 1.29$) (kg/m^3), the vehicle front area ($A_f = 2.57$ m^2), and the drag coefficient ($C_d = 0.26$). Equation 3.8 represents the aerodynamic resistance.

$$F_{aero} = 0.5.\rho.A_f.C_d.V^2 \qquad (3.8)$$

The force that arises from the contact between the vehicle tires and the road surface is called the Rolling force(F_{roll}). This force is proportional to the road slope angle and the total vehicle mass. The tire properties such as the structure, the material, the temperature, and the air pressure play a significant role in the rolling resistance coefficient (μ_{rr}). Furthermore, the road specifications such as the materials, the roughness, and the percentage of liquids on the road surface affect the value of the rolling resistance coefficient. In this research, the rolling resistance coefficient in Equation 3.9 is chosen as 0.0048. Equation 3.9 represents the rolling resistance force.

$$F_{roll} = \mu_{rr}.\, M_{V.}g.\cos\theta \qquad (3.9)$$

The effects of the road elevation and topography information in which the vehicle is moving are called the grading force. This force is of two types: downhill and uphill climbing. The grading resistance force of the movement in downhill helps the vehicle move forward while the movement in uphill impedes the vehicle movement. This force is equal to the parallel component effect of the road multiplied by the vehicle mass and gravity as shown in Equation 3.10.

$$F_{grad} = M_{V.}g.\sin\theta \qquad (3.10)$$

The vehicle acceleration force can be calculated based on Newton's laws of motion with friction forces. This force is equal to the sum of the tractive resistance force and the tractive effort. The acceleration force is given by Equation 3.11.

$$F_{accel} = M_{V.}\frac{\partial V}{\partial t} \qquad (3.11)$$

In the translational motion, the total torque applied to motor's shaft can be calculated by Equation (3.12).

$$\begin{cases} T_{eq}\omega_{m,max} = \frac{F_{tr}v_{V,max}}{\eta_{mech}} \\ T_{eq} = \frac{F_{tr}}{\eta_{mech}}\left(\frac{v_{V,max}}{\omega_{m,max}}\right) \end{cases} \tag{3.12}$$

In term of simplification, the transmission loss is neglected at the calculation of the total value of moment of inertia indicates to motor shaft, J_{eq}. So, the summation of kinetic energy of the different moving parts is equal to the kinetic energy due to the inertia's total moment. The value of J_{eq} can be calculated by Equation (3.13), where J_m is the total moment of inertia of the electrical motor.

$$\begin{cases} J_{eq} = J_m + M_V\left(\frac{v_{V,max}}{\omega_{m,max}}\right)^2 \\ \frac{1}{2} J_{eq}\omega_{m,max}^2 = \frac{1}{2} J_m\omega_{m,max}^2 + \frac{1}{2} M_V v_{V,max}^2 \end{cases} \tag{3.13}$$

MATLAB/Simulink/Vehicle Component library is used to model the behaviour of the EV. Table 3 shows the main coefficients of the EV model. Figure 4 shows the completed model of the EV's HESS using MATLAB/Simulink. The inverter and the induction motor use the inner loop intelligent controller (Tarbosh et al., 2020, Farah et al., 2019).

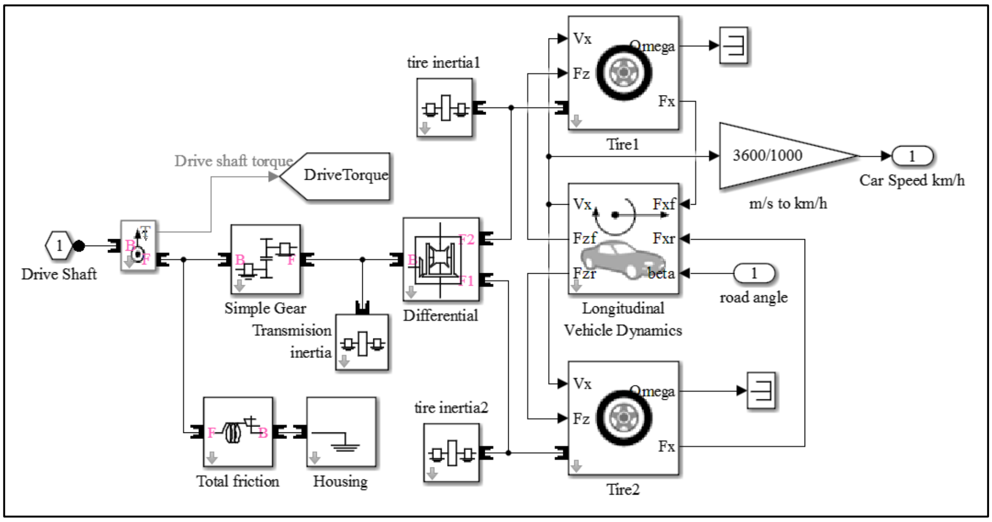

FIGURE 3.8 The dynamic model of vehicle in Matlab\Simulink

Table 3.3 The Parameters of Electric Vehicle Model.

Parameter	Value
M_v ≡ Vehicle Mass [kg]	1325
C_d ≡ Drag coefficient	0.26
A_f ≡ Frontal area [m^2]	2.57
Wheel radius [m]	0.3
μ_{rr} ≡ rolling resistance	0.0048
g ≡ Gravity acceleration (g) [ms^{-2}]	9.8
ρ ≡ Air density [kgm^{-3}]	1.29
θ ≡ Road angle [radian]	Variable
V ≡ Vehicle Speed [Km/h]	50, 60, 70

3.4 Contour Positioning System

Road elevation is an essential factor which affects the energy consumption in EVs. Total energy consumption in EVs is affected by 15% to 20% when road slopes are taken into account (Boriboonsomsin and Barth, 2009). The driving road information is available in many data sources such as Google Maps, Inter-map, and Google Earth. Contour Positioning System (CPS) is an algorithm designed to estimate the driving journey energy consumption for electric vehicles. The CPS depends on the contour lines to estimate how much energy is needed in the specific journey to reach the desired destination. This algorithm considers the road slope in the journey to identify the total energy consumption which does not take into account the conventional distance estimation system. CPS uses Python programming to extract the elevation from Google Earth and simulates the results in the MATLAB.

In this research, the driver needs to set the desired destination before starting the journey. The automated CPS obtains the road slope in terms of elevation and uses it to estimate the total energy consumption for the desired drive cycle. Google Earth is used as a source of topography information to obtain the road elevation. Three real routes, namely, uphill, downhill, and city tour are selected in this study to investigate the influence of slopes of the road on the EV energy consumption and validate the proposed HESS energy management system effectiveness. The CPS and vehicle speed are used to control and estimate the required energy consumption for each drive cycle. The three journeys elevation profiles are used to measure the road slope calculated by CPS using Equation 3.14.

$$\begin{cases} \angle\theta = \frac{|\Delta E|}{\Delta E} \times \sin^{-1}\frac{|\Delta E|}{\Delta D} \\ \Delta D(k) = D(k) - D(k-1) \\ \Delta E(k) = E(k) - E(k-1) \end{cases} \tag{3.14}$$

$$\text{Where: }\begin{cases} \mathrm{D(k)} = \text{Distance} \\ \mathrm{D(k-1)} = \text{Previous Distance} \\ \Delta \mathrm{D} = \text{Distance Difference} \\ \mathrm{E(k)} = \text{Elevation} \\ \mathrm{E(k-1)} = \text{Previous Elevation} \\ \Delta \mathrm{E} = \text{ElevationDifference} \end{cases}$$

The uphill data is obtained for the drive from Berinchang (4°29’30.16’’N 101°23’15.65’’E) to Equatorial Hotel (4°30’17.64”N 101°24’31.18”E) in Cameron Highlands, Malaysia. The distance covered is five kilometres, and the elevations at the starting and destination points measured every ten meters are 1496 m and 1627 m, respectively. CPS is used to obtain the data and calculate the road slope along the journey. Figure 3.9 shows the road elevation profile and the road slope against the distance based on the uphill drive cycle.

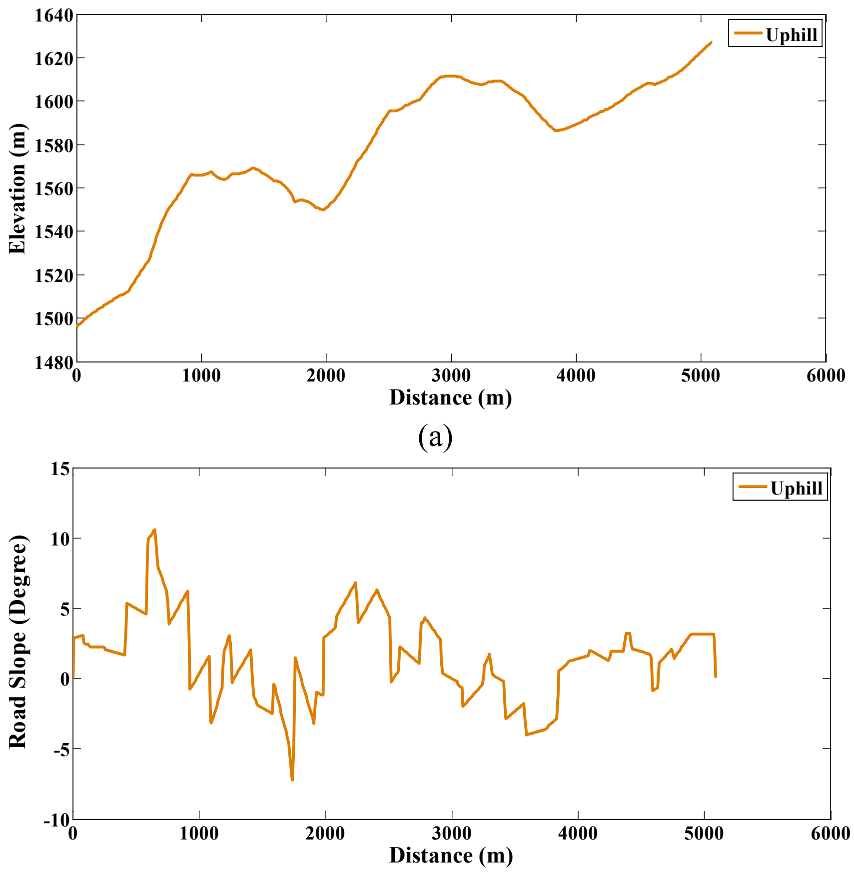

(a)

(b)

FIGURE 3.9 The uphill drive cycle (a) road elevation, (b) road slope.

Meanwhile, the downhill elevation starts from 1615 m and goes down to 1496m. The total distance travelled is five Kilometres, and the elevation is measured every ten meters. Figure 3.10 represents the road elevation profile and the road slope against the distance based on the downhill drive cycle.

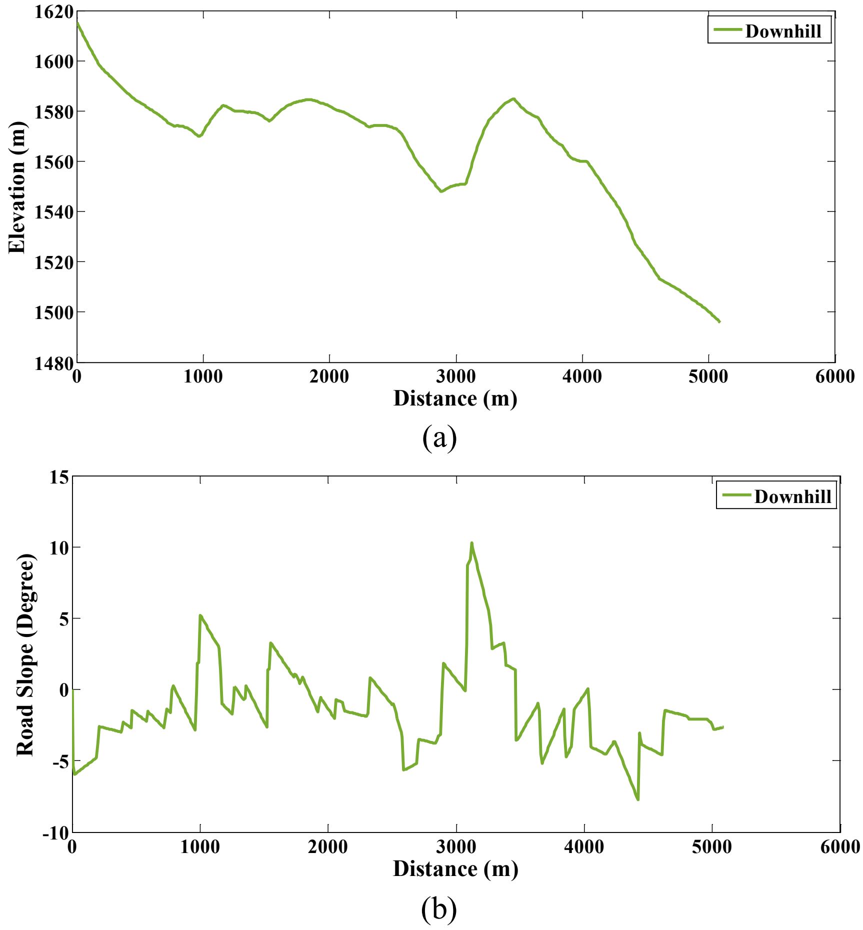

FIGURE 3.10 The downhill drive cycle (a) road elevation, (b) road slope.

Furthermore, the city tour involves travelling from University Tunku Abdul Rahman (UTAR) Old Campus in Setapak, Kuala Lumpur, to Technology Park Malaysia (TPM) in Bukit Jalil. The elevation levels at the starting and destination points are 61 m and 66 m, respectively. The city tour total distance is 15.85 Kilometres, and the elevation is measured every ten meters. The road elevation profile and the road slope against the distance based on the downhill drive cycle are represented in Figure 3.11.

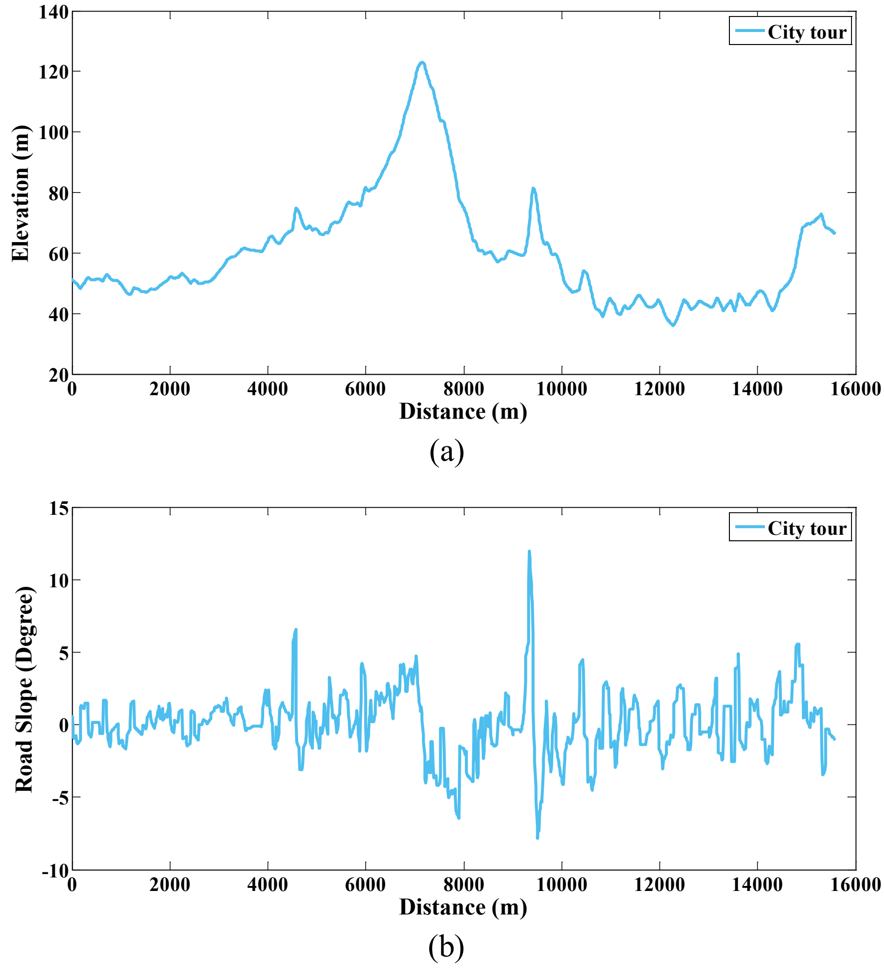

FIGURE 3.11 The city-tour drive cycle (a) road elevation, (b) road slope.

3.5 Standard drive cycles

The standard drive cycles are defined as a concatenation of data points simulating the vehicle speed against time. Driving cycles are issued by several organizations and countries to assess the performance of vehicles in various ways as for instance fuel consumption, electric vehicle autonomy, and polluting emissions (Ericsson, 2000). The drive cycles are used to estimate the fuel consumption in conventional vehicles and the energy consumption in electric vehicles. There are several types of standard drive cycles with different characteristics. In this research, three standard drive cycles represent the diversity of the driver's behaviour in different countries and are selected to validate the proposed controller performance. In the standard drive cycles, the road slope is ignored while the vehicle speed profile changes during the journey.

The Urban Dynamometer Driving Schedule (UDDS) represents an urban route with several traffic stops in Europe with a total distance of 12.07 km. The average and the maximum speeds in the UDDS drive cycle are 31.5 km/h and 91.25 km/h, respectively. The total duration of this drive cycle is 0.39 hours. Figure 3.12 depicts the speed profile based on the UDDS drive cycle.

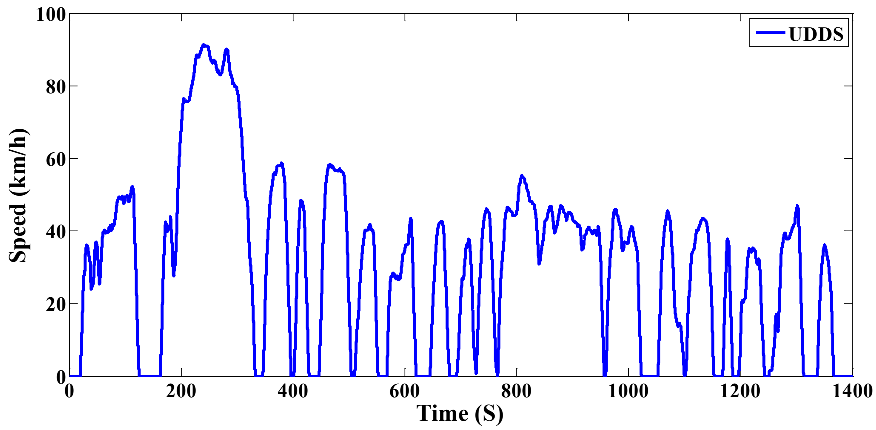

FIGURE 3.12 The UDDS speed profile

The New York City Cycle (NYCC) is a test drive cycle which includes the city traffic. This drive cycles is developed for chassis dynamometer testing of light vehicles. The total Distance of NYCC is 1.89km while the driving duration is 0.16 hour. The maximum speed in NYCC is 44.6km/h, and the average speed is 11.4km/h. Figure 3.13 represents the speed profile based on the NYCC drive cycle.

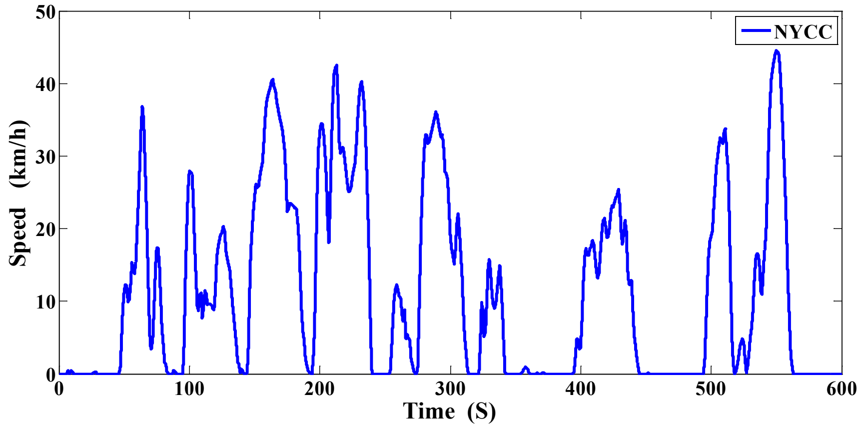

FIGURE 3.13 The NYCC speed profile

The Japan1015 drive cycle includes repeatable driving accelerations with several traffic stops. The total distance of the drive cycle is 4.16 km while the driving duration is 0.183 hours. The average and the maximum speed in Japan1015 drive cycle are 22.7 km/h and 70km/h, respectively. Figure 3.14 represents the speed profile based on Japan1015 drive cycle.

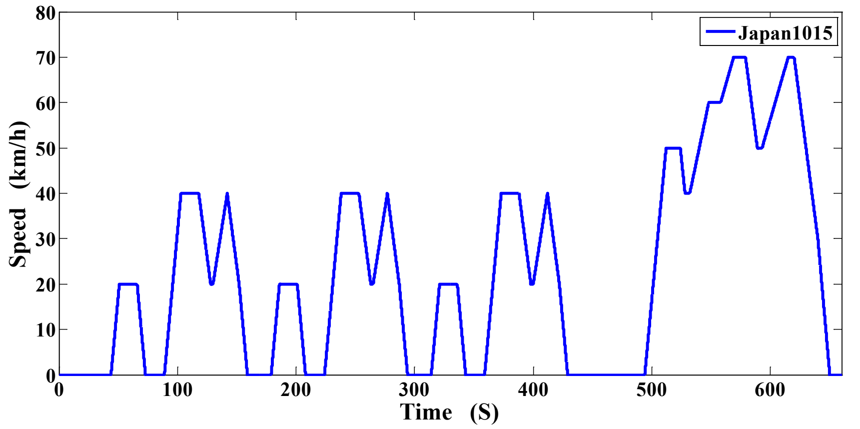

FIGURE 3.14 The Japan1015 speed profile

3.6 Sizing the Hybrid energy storage system

The energy requirement in electric vehicles applications depends on many factors such as the depth of discharge, the load current, the operation temperature, the charging time, and the longest distance. Due to the battery working principles, the current discharge rate is different compared with the charging rate. In most batteries, the discharge power density is higher than the charging power density. The most critical step in sizing the battery is obtaining the number of batteries in series (N_{bat_s}), and the number of batteries in parallel (N_{bat_p}). This number depends on many parameters such as the mission, the vehicle dynamics, and the energy management strategy. The mission includes the speed profile, the slope of the desired journey, the rate of power recovery during braking phases, and the depth of discharge of the battery. The operating range of the batteries in electric vehicle applications is around 80% of the total capacity (Sadoun et al., 2011, Wang et al., 2018b). Figure 3.15 illustrates the sizing step of electric vehicle application.

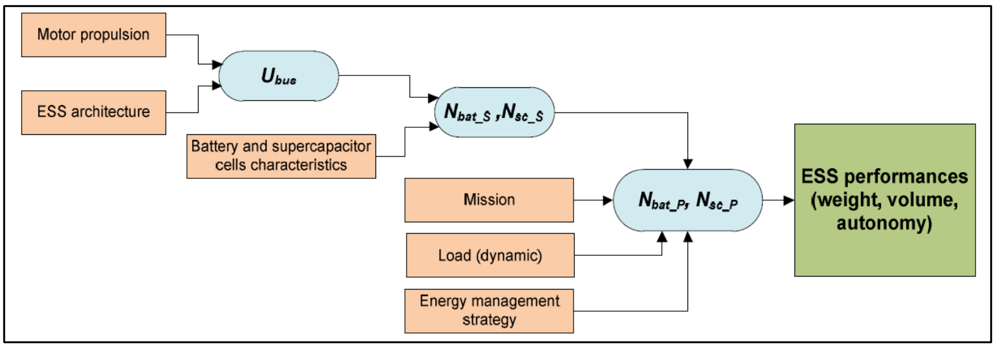

Figure 3.15 The sizing step for electric vehicle application (Sadoun et al., 2011)

In this research, the total power of electric vehicle (P_{EV}) equals the battery power (P_{bat}) and the supercapacitor power(P_{sc}). Equations (3.15-3.18) are used to size the EV battery.

$$P_{EV} = P_{bat} + P_{sc} \tag{3.15}$$

$$i_b = \frac{V_b - \sqrt{V_b^2 - 4 .R_b .P_b}}{2 .R_b} \tag{3.16}$$

$$N_{bat\_ser} = \frac{V_{bus}}{V_{cell}} \tag{3.17}$$

$$N_{bat\_p} = \frac{E_{cons}}{N_{bat\_s} .(E_{bat\_cell} - W_{bat\_cell})} \tag{3.18}$$

Based on (Roy and Rengarajan, 2015, Douglas and Pillay, 2005), the flowchart in Figure 3.16 summarises the procedure for selecting the supercapacitor module proper size for EV applications.

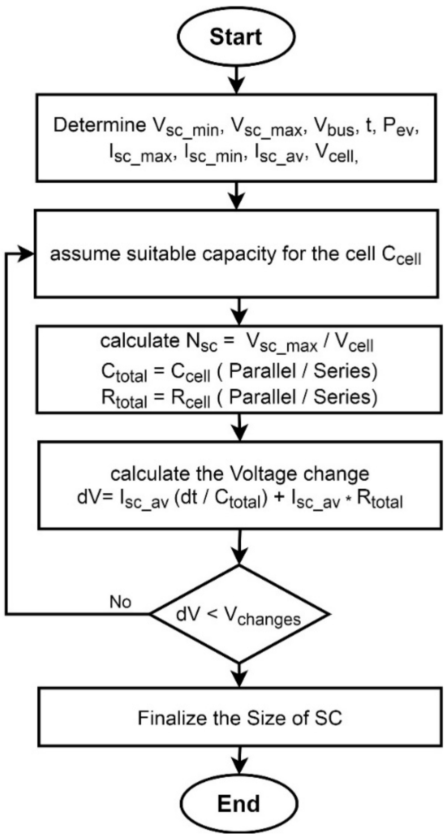

Figure 3.16 The steps to select the supercapacitor size for HESS

The proposed rule-based controller is used the estimated total current of the selected drive cycles to calculate the practical value of the maximum value of the battery current (I_{b_max}). The functions of the root-mean-square (RMS) and the mean value are implemented to estimate the maximum value of the battery current. Figure illustrates the algorithm of selected the (I_{b_max}). Equations 3.19 and 3.20 describe the root-mean-square (RMS) and the mean functions. Figure 3.17 shows the to select the maximum value of the battery current (I_{b_max}).

$$RMS = \sqrt{\left(\frac{1}{n}\sum_0^n X_n^2\right)} \qquad (3.19)$$

$$M = \frac{\sum_0^n X_n}{n} \qquad (3.20)$$

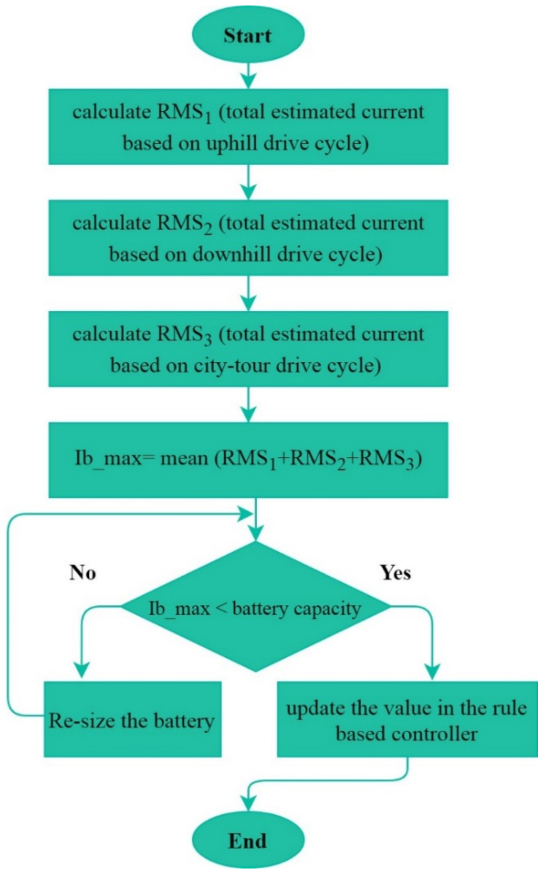

Figure 3.17 The steps to select the maximum value of the battery current (I_{b_max})

3.7 Chapter Summary

This chapter presented the models of the hybrid energy storage system of the electric vehicle. The model of batteries, supercapacitor and DC-DC converters are described in details. Furthermore, the dynamic model of the vehicle are discussed. In addition, the method to calculate the road slope using contour positioning system is also explained. The three different real driving cycles (uphill, downhill, and city-tour) used in this research are presented. Moreover, the characteristics of the standard drive cycles (UDDS, NYCC, and Japan1015 drive cycle) are summarised. Finally, the algorithms of sizing the HESS (battery and supercapacitor) are carried out.

CHAPTER 4

DESIGN THE ENERGY MANAGEMENT SYSTEM OF HYBRID ENERGY STORAGE SYSTEM

4.1 Introduction

One of the primary challenges in designing a battery–supercapacitor Hybrid Energy Storage System for Electric Vehicle is distributing the energy demand in real-time between the primary energy storage device and the auxiliary energy storage device. This Chapter presents the proposed energy management of the semi-active HESS for electric vehicles. The proposed control algorithm aimed to split the vehicle demand current between battery and supercapacitor optimally to extend battery life and ensure continuous HESS hybridization (Sadeq et al., 2020). The battery provides low traction current while the supercapacitor supplies the peak traction current and absorbs the regenerated current during braking. In this research, two different algorithms were designed to adapt the proposed rule-based controller to distribute the total operating current of an EV between the HESS battery and the supercapacitor. The adaptive rule-based controller controlled the DC-DC converter $\mathrm{I_{co}(t)}$ output current to manage the supercapacitor energy output in different operation conditions. The total electric vehicle load current $\mathrm{I_t(t)}$ is defined as per Equation 4.1.

$$\mathrm{I_t(t)} = \mathrm{I_b(t)} + \mathrm{I_{co}(t)} \qquad (4.1)$$

This research proposed energy management strategy contains three control layers to manage the power flow between the battery and the supercapacitor of the HESS. The first layer is an adaptive control to obtain the optimal energy sharing percentage (R) between the battery and the supercapacitor depending on the road slope and the vehicle speed. CPS was used to estimate the road slope for the selected drive journey. The second control layer is a rule-based controller to determine the optimal reference current for the supercapacitor online during the journey. The third control layer is the LQR control to drive the bidirectional DC-DC converter by changing the duty cycle of the PWM online.

4.2 The Rule-Based Controller of HESS

The proposed rule-based controllers allocate the HESS's current instantaneously for different drive cycles. The proposed controller is designed to limit the battery current $I_b(t)$ to the desired value (I_{b_max}) and split the vehicle load current between the battery and the supercapacitor during any drive cycle. The controller is designed to manage the HESS energy flow under various operation conditions accounting for the total demand load current ($I_t(t)$), the supercapacitor state of charge (SC_{soc}), and the energy flow direction. The controller working conditions are defined as per Equation 4.2.

$$\begin{cases} \textbf{If } (\mathbf{I_t} > \mathbf{0}) \textbf{ and } (\mathbf{I_t} < \mathbf{I_{b\_max}}) \textbf{ then } \quad \mathbf{I_{co}} = \mathbf{0} \\ \textbf{If } (\mathbf{I_t} > \mathbf{0}) \textbf{ and } \left(\mathbf{I_t} > \mathbf{I_{b\_max}}\right) \textbf{and } (\mathbf{SOC_{sc}} > \mathbf{SOC_{sc\_min}}) \textbf{ then } \quad \mathbf{I_{co}} = (\mathbf{I_t} - \mathbf{I_{b\_max}}) \\ \textbf{If } (\mathbf{I_t} < \mathbf{0}) \textbf{ and } (\mathbf{SOC_{sc}} < \mathbf{SOC_{sc\_max}}) \qquad \textbf{then } \quad \mathbf{I_{co}} = \mathbf{I_t} \end{cases} \tag{4.2}$$

The proposed rule-based controller allows the HESS to supply the EV with current from the battery when the EV total load current is less than the maximum value of the battery current (I_{b_max}). The proposed controller also limits the battery current to (I_{b_max}) during a high load drive cycle. On the other hand, the proposed rule-based controller is designed to use the supercapacitor to absorb all the regenerative energy during the drive cycle deceleration. The total regenerative energy absorbed by the supercapacitor from the initial voltage to the final voltage is defined as per Equation 4.3. The state of the charge condition for the supercapacitor in the proposed rule-based controller is defined as per Equation 4.4.

$$\Delta En_{SC} = \frac{C_0}{2}(V_{sc}(0) - V_{sc}(t)) \tag{4.3}$$

$$SOC_{sc\_max} \geq SOC_{sc} > SOC_{sc\_min} \tag{4.4}$$

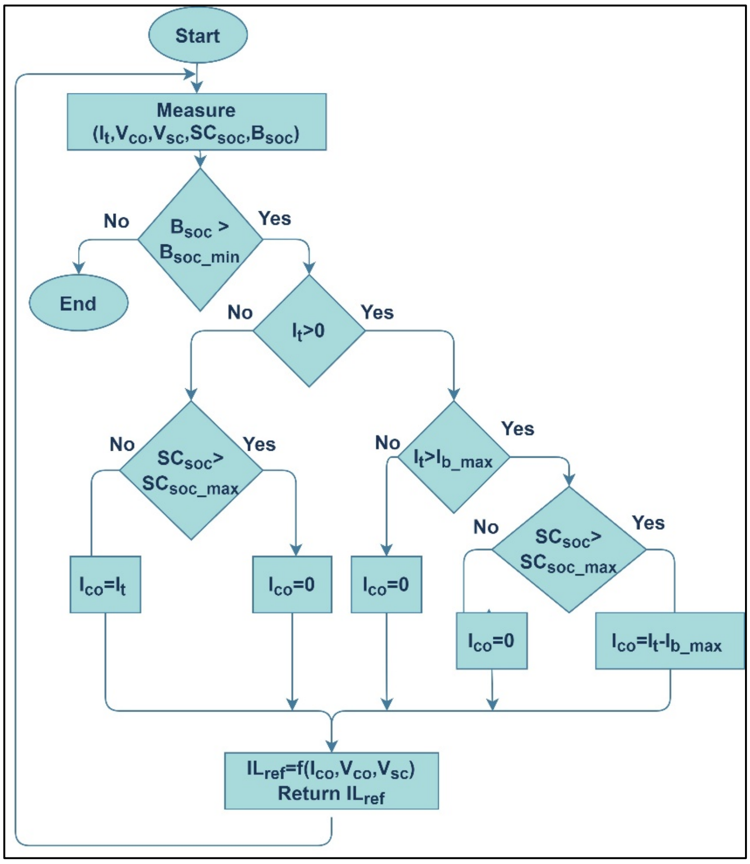

Figure 4.1 The flowchart of the proposed rule-based controller.

4.3 The Adaptive Rule-Based Controller of HESS

Adaptive control is a control approach implemented to achieve the optimal performance of the system by adapting and tuning the controller coefficients. In the proposed algorithm, the EV destination is selected before the journey initiated. The adaptive algorithm estimates the total current demand needed for the drive cycle and the regenerative current depending on the road slope, the vehicle speed, and the EV model parameters. The percentage of power split between the battery and the supercapacitor (R) in HESS can be determined independently. Two methods are investigated to adapt the rule-based controller in terms of energy split between the battery and the supercapacitor. The first method is called the optimal method which compares the total current demand and the electric vehicle regenerative current during the drive cycle. The second one is called the fuzzy adaptive rule-based controller using the concept of the fuzzy logic controller. The energy sharing percentage between the battery and the supercapacitor (R) is used to regulate the controller to save energy during the drive cycle. The adaptive rule-based controller is defined as per Equation 4.5.

$$\begin{cases} \textbf{If } (\mathbf{I_t} > \mathbf{0}) \textbf{ and } \left((\mathbf{1}-\mathbf{R})\mathbf{I_t} < \mathbf{I_{b_{max}}}\right) \textbf{and } (\mathbf{SOC_{sc}} > \mathrm{SOC_{sc\_min}}) \textbf{ then } \mathbf{I_{co}} = \mathbf{I_t} * \mathbf{R} \\ \textbf{If } (\mathbf{I_t} > \mathbf{0}) \textbf{ and } \left((\mathbf{1}-\mathbf{R})\mathbf{I_t} > \mathbf{I_{b_{max}}}\right) \textbf{and } (\mathbf{SOC_{sc}} > \mathrm{SOC_{sc_{min}}}) \textbf{ then } \mathbf{I_{co}} = (\mathbf{I_t} - \mathbf{I_{b\_max}}) \\ \textbf{If } (\mathbf{I_t} < \mathbf{0}) \textbf{ and } (\mathbf{SOC_{sc}} < \mathrm{SOC_{sc\_max}}) \textbf{ then } \mathbf{I_{co}} = \mathbf{I_t} \end{cases} \quad (4.5)$$

4.3.1 The Optimal Adaptive Rule-Base Controller of HESS

In this method, the percentage of energy sharing between the battery and the supercapacitor in HESS is tuned one time for the distance travelled during a specific drive cycle. After setting the destination and the road slope is calculated by CPS; the proposed energy management system then estimates the total energy required for the desired drive cycle. The road slope and the vehicle approximated speed are considered along the journey to the desired destination. The accumulation method for the total positive EV load supplied current (I_{tp}) and the regenerative EV current (I_{reg}) during the drive cycle is applied. The energy split percentage between the battery and the supercapacitor is set by comparing the total load current demand and the EV total regenerative current during the desired drive cycle. The total positive EV load supplied current (I_{tp}) and the total regenerative current (I_{reg}) are defined as in Equation 4.6.

$$\begin{cases} I_{reg} = \sum_{0}^{t} I_t(t) & I_t < 0 \\ I_{tp} = \sum_{0}^{t} I_t(t) & I_t > 0 \end{cases} \tag{4.6}$$

This proposed method reduces the battery stress and saves the energy inside the HESS. The proposed energy management system predicts the approximate amount of regenerative energy depending on the road slope. Then, the percentage of energy sharing between the battery and the supercapacitor (R) is set to ensure that the HESS is working properly. The supercapacitor can absorb all the regenerative energy during the desired drive cycle. Figure 4.2 presents the flowchart of the proposed optimal adaptive rule-based controller.

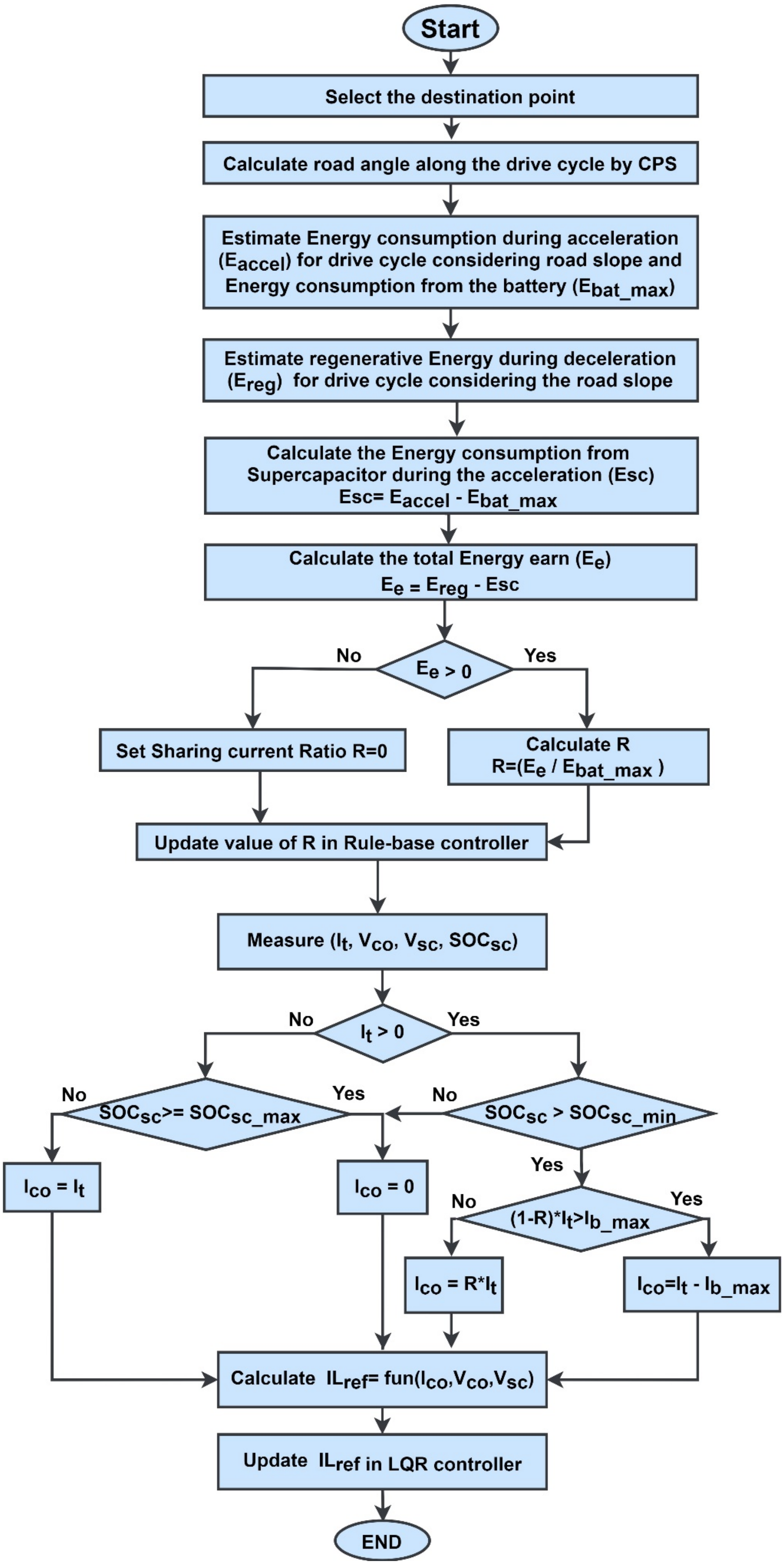

FIGURE 4.2. Flowchart of optimal adaptive rule-based controller

4.3.2 The Fuzzy Adaptive Rule-Base Controller of HESS

Most researches in the literature on terrain information take the instant effect of the road slope in the control action. In this method, the value of energy sharing percentage between the battery and the supercapacitor in HESS varies during the drive cycle. A fuzzy logic controller is used to manipulate the percentage of energy sharing between the battery and the supercapacitor online during the journey. The road slope and the vehicle speed are considered as inputs for the fuzzy logic controller in controlling the journey. Figure 4.3 shows the fuzzy logic controller surface plot which represents the relationship between the inputs (road slope and vehicle speed) and the percentage of energy sharing between the battery and the supercapacitor (R).

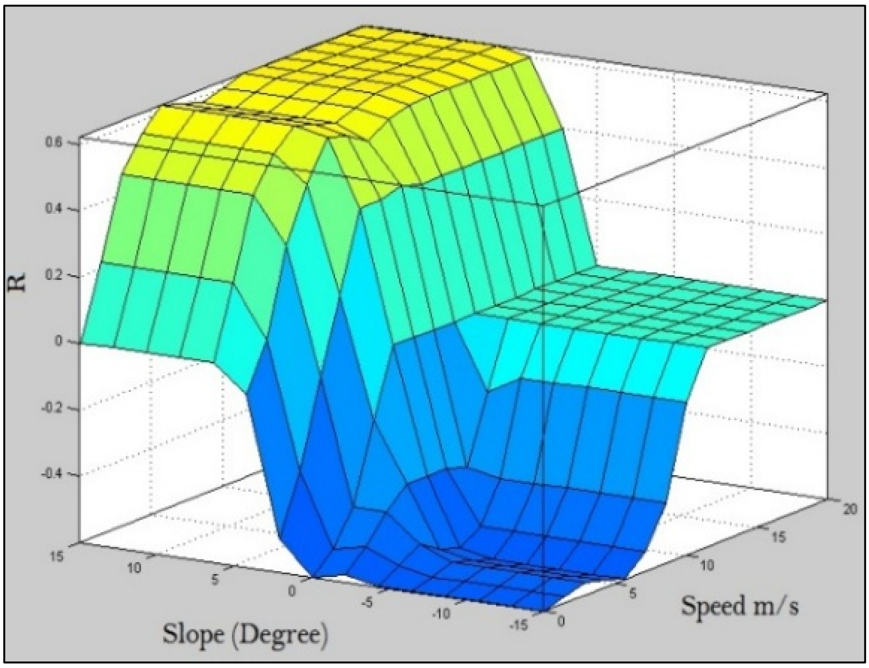

FIGURE 4.3. The fuzzy logic controller surface.

Here, the supercapacitor assist the battery in delivering the total EV load current continuously with different values of energy sharing percentages (R) along the drive cycle. The energy management system measures the actual total EV load current and the state of charge of the supercapacitor to consider the identified values of the energy sharing percentage between the battery and the supercapacitor in HESS. Furthermore, the operation effect of the fuzzy adaptive rule-based controller is shown in Figure 4.4.

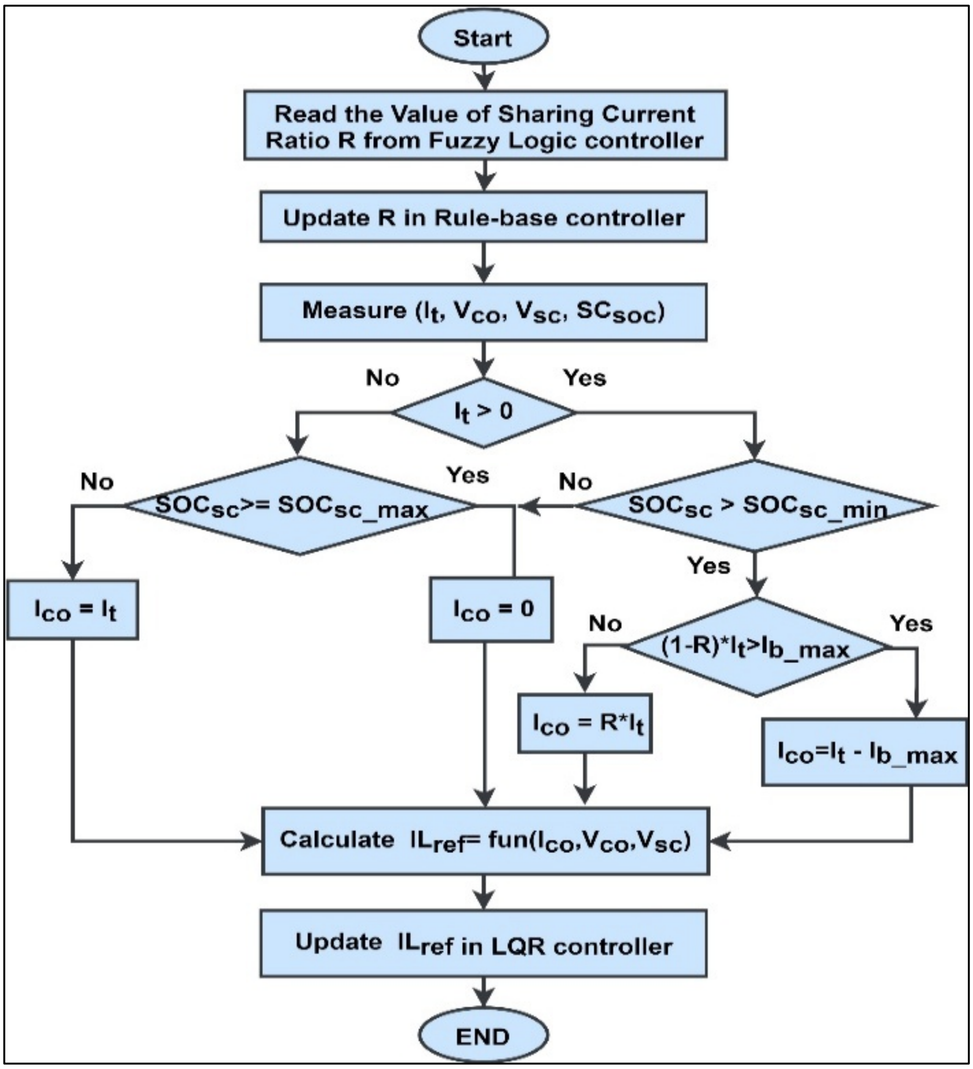

FIGURE 4.4. Flowchart of Fuzzy adaptive rule-based controller

4.4 The Linear Quadratic Regulator (LQR)

This section presents the linear quadratic regulator (LQR) controller to drive the interfacing DC-DC bidirectional converter in the proposed semi-active HESS. LQR is a control method that depends on generated feedback gains to improve the system response by controlling one state of the model. Equation 4.7 represents the cost function for a continuous-time linear.

$$J(u) = \int_0^{\infty} (x^T Q x + u^T R u + 2x^T N u) dt \qquad (4.7)$$

where Q is a symmetric positive definite matrix and R is a positive scalar.

LQR provides a systematic computing method that relies on the state feedback control gain matrix (Katshiko, 2010). Q and R are the weighting matrices and strongly affect the closed-loop poles positions (Abdullah et al., 2012, Sadeq and Wai, 2020). Depending on the chosen value of these matrices, the closed-loop system will exhibit a different response. The values of the weighting matrices can be selected depending on several optimization methods.

LQR returns the solution S of the associated Riccati equation presented in Equation 4.8. The closed-loop Eigenvalues are defined as in Equation 4.9.

$$A^T S + SA - (SB + N)R^{-1}(B^T S + N^T) + Q = 0 \qquad (4.8)$$

$$e = \mathrm{eig}(A - B \times K) \qquad (4.9)$$

where K is derived from variable S using Equation 4.10.

$$K = R^{-1}(B^T S + N^T) \qquad (4.10)$$

The purpose of designing LQR in the proposed algorithm is to drive the DC-DC converter to supply the desired current from the supercapacitor module. The DC-DC converter output current is controlled by varying the duty cycle of the Pulse Width Modulation (PWM). LQR is selected to be implemented in the EVs application due to its simplicity and ease of implementation. The feedback gains can be directly obtained from the matrices of the DC-DC converter model. Moreover, the closed-loop response of LQR is stable and insensitive to external disturbances (Sadeq and Wai, 2020).

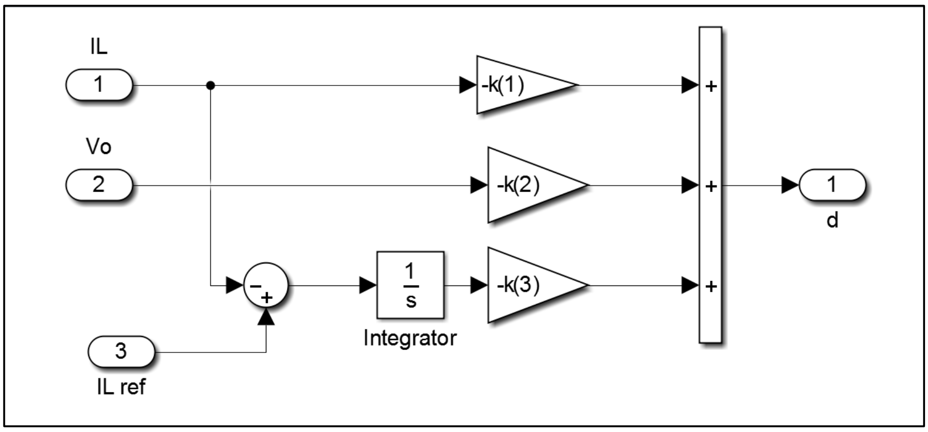

Figure 4.5 The feedback gains of the LQR controller.

To discover the response of the proposed LQR for semi-active HESS, the step current load profile is applied to the system. A simulation using MATLAB/Simulink is carried out for several values of Q and R. The close loop response results of the step function are plotted in Figure 4.6. In the first case, the weighting values of q are changed with three different values (10^6, 10^8, 10^{10}) while the value of R is fixed at 1. The battery current is measured in every value of q (I_{b1}, I_{b2}, I_{b3}), respectively.

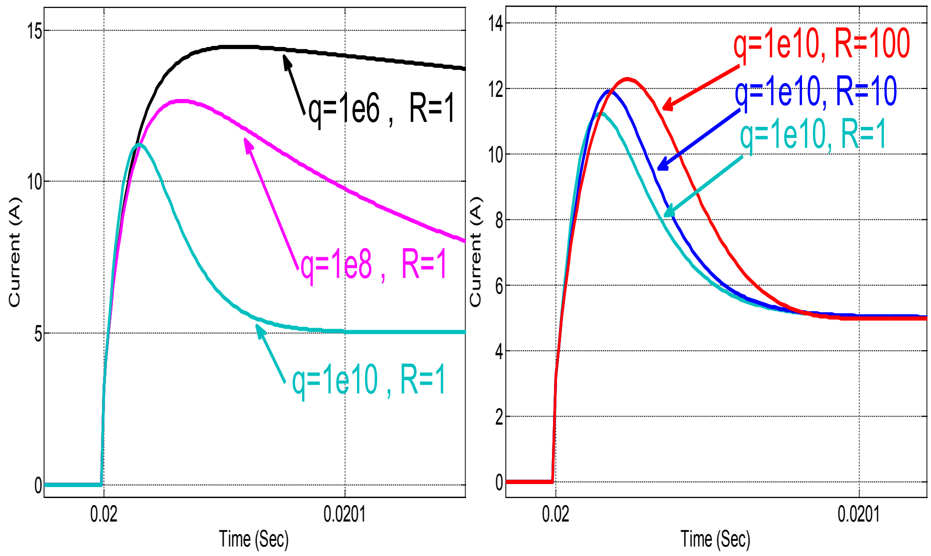

Figure 4.6 The transient responses of battery current with several values of q and R.

In the second case, R value is tested with three different values (1, 10, 100), and the weighting value of q is fixed at q= 10^{10}. The battery current is measured in every value of R (I_{b3}, I_{b4}, I_{b5}). The transient characteristics of these responses are represented in table 4.1.

Table 4.1 The transient time characteristics for different values of q and R.

Battery Current	I_{b1}	I_{b2}	I_{b3}	I_{b4}	I_{b5}
q	10^6	10^8	10^{10}	10^{10}	10^{10}
R	1	1	1	10	100
Rise Time	2.23×10^{-06}	2.24×10^{-06}	2.19×10^{-06}	2.25×10^{-06}	2.25×10^{-06}
Settling Time	0.0242	0.0205	0.0201	0.0201	0.0201
Overshoot	189%	153%	124%	138%	145%
SS_{error}	0.023	0.023	0.023	0.023	0.023

The results prove that an increment in q leads to a decreased settling time and overshoot of the battery current. On the other hand, the increment in the R value increases the overshoot of the battery current. In this research, the values of q and R are selected as 10^{10} and 1, respectively.

Furthermore, the DC-DC converter mathematical model is used to design the switching elements controller of the DC-DC converter (Sadeq and Wai, 2019). In this research, the proposed Rule-Based control primary task is to obtain the reference input current of the DC-DC converter. Simultaneously, the LQR controller aims to get the desired duty cycle to drive the DC-DC converter. The LQR function in MATLAB is used to obtain the desired closed-loop feedback gains while the steady-state errors are cancelled by adding an integration (Kedjar and Al-Haddad, 2009) as shown in Figure 4.5.

The feedback gains obtained using Matlab function K= lqr(As, Bs, Q, R); where A and B represent the matrices of the state-space model of the DC-DC converter presented in section 3.2.3. The results give the feedback gain matrix (K) as:

$$K = [1.49e - 01 \quad 2.37e - 03 \quad - 1.414e + 03]$$

For

R=1,

$$Q = \begin{bmatrix} 1 & 0 & 0 \\ 0 & 1 & 0 \\ 0 & 0 & 10^{10} \end{bmatrix}$$

4.5 The Proposed Hybrid Energy Storage System Model in Matlab

To validate the performance and the effectiveness of the proposed energy management system of HESS for the EV, a MATLAB/Simulink modelling is carried out. The performance of EV is tested with three real drive cycles and three standard drive cycles. The performances of the battery-supercapacitor HESS with adaptive rule-base controllers are compared with the performances of the battery-supercapacitor HESS with the rule-based controller and the single energy storage battery. Figure 4.7 depicts the MATLAB/Simulink model of the EV using the single energy storage battery based on the real drive cycles, uphill, downhill, and city tour. Figure 4.8 illustrates the model of EV using the single energy storage battery based on the standard drive cycles.

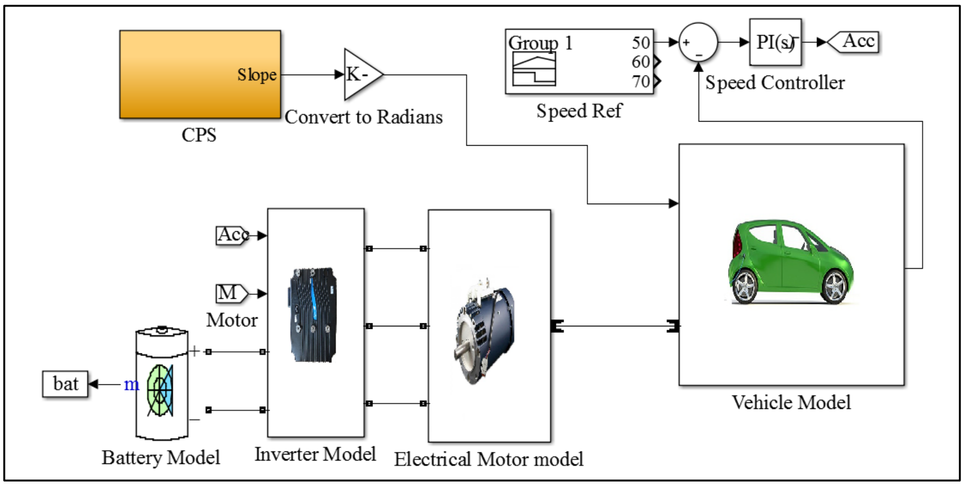

Figure 4.7 MATLAB/Simulink model of the EV using the single energy storage battery based on the real drive cycles

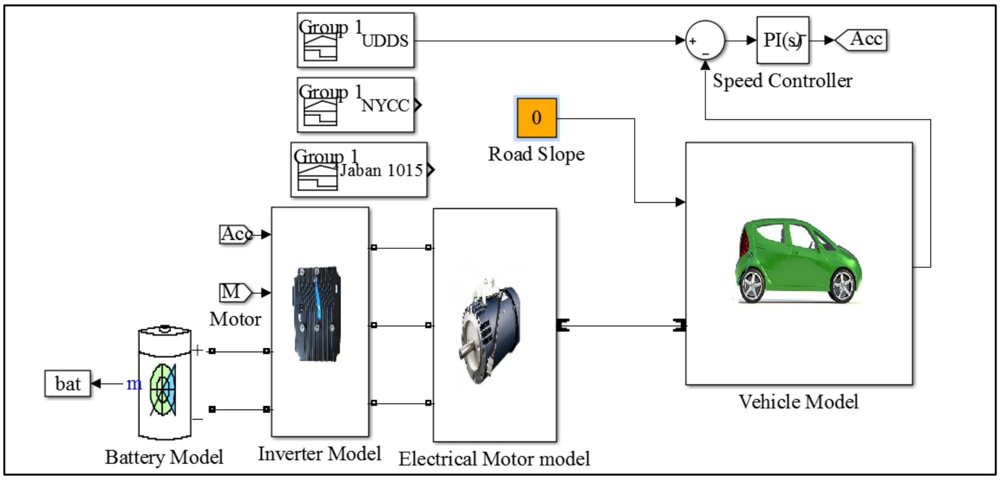

Figure 4.8 MATLAB/Simulink model of the EV using the single energy storage battery based on the standard drive cycles

To verify the effect of the road slope in the total energy consumption for any real drive cycle, the energy variance between the drive cycles total energy consumption is calculated by Equation 4.11; where, $SOC_b(0)$ is the initial state of charge for the battery, $SOC_b(t)_{slope=CPS}$ is the final state of charge for the battery considering the road slope, and $SOC_b(t)_{slope=0}$ is the final state of charge for the battery without the road slope.

$$EnVar = \frac{(SOC_b(0)-SOC_b(t)_{slope=CPS})-(SOC_b(0)-SOC_b(t)_{slope=0})}{SOC_b(0)} \times 100 \qquad (4.11)$$

The MATLAB/Simulink models of the rule-base controller of HESS for the EV based on the real drive cycles and the standard drive cycles are presented in Figures 4.9 and 4.10, respectively. These models are used to measure the performance of the HESS in the selected drive cycle.

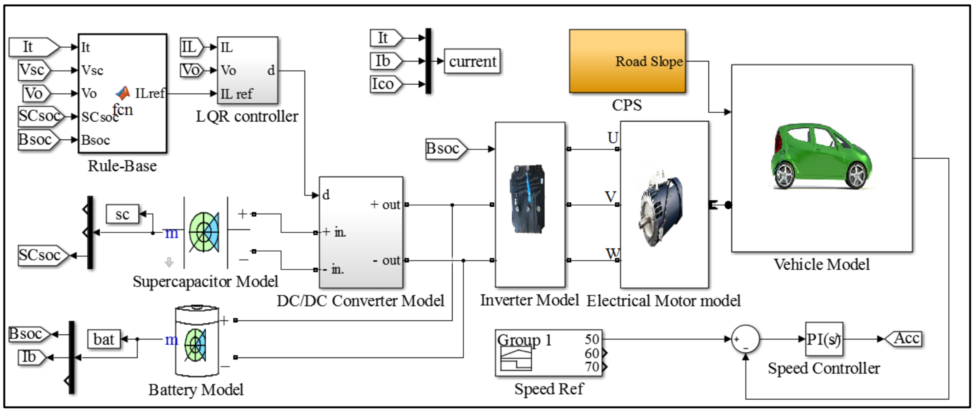

Figure 4.9 MATLAB/Simulink model of the HESS using the rule-based controller based on the real drive cycles

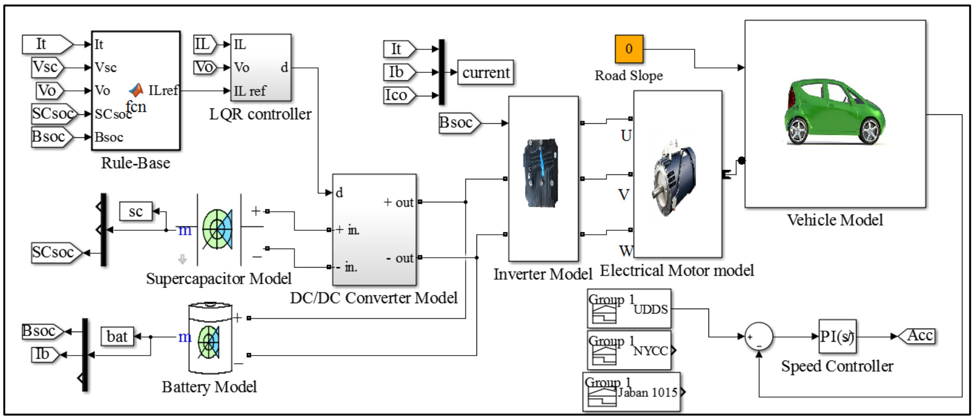

Figure 4.10 MATLAB/Simulink model of the HESS using the rule-based controller based on the standard drive cycles

To validate the improvement in the energy consumption of HESS, the final value of the state of charge for the battery ($SOC_b(t)_{CPS}$) and the supercapacitor ($SOC_{SC}(t)_{CPS}$) are measured at the end of the journey and compared with the different proposed controllers. The percentage of the total energy consumption for the battery and the supercapacitor are given by Equation 4.12.

$$\begin{cases} \text{Battery Consumption} = \dfrac{SOC_b(0) - SOC_b(t)_{CPS}}{SOC_b(0)} x100 \\ \text{Supercapacitor Consumption} = \dfrac{SOC_{SC}(0) - SOC_{SC}(t)_{CPS}}{SOC_{SC}(0)} x100 \end{cases} \quad (4.12)$$

Figure 4.11 shows the completed MATLAB/Simulink model of the proposed HESS, the optimal adaptive rule-based controller, and the fuzzy adaptive rule-based controller for the EV based on the real drive cycles. Figure 4.12 shows the completed MATLAB/Simulink model based on the standard drive cycles.

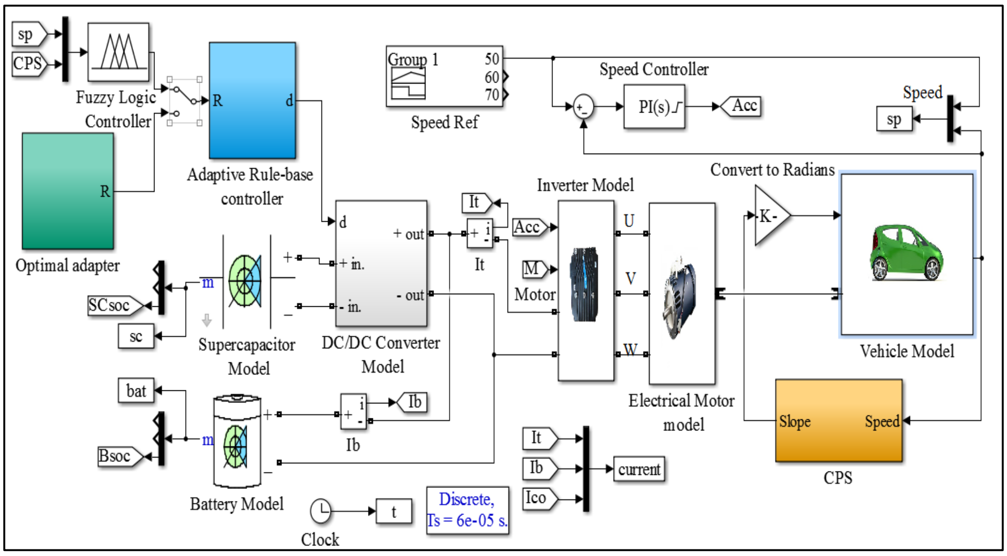

Figure 4.11 MATLAB/Simulink model of the HESS using the adaptive rule-based controller based on the real drive cycles

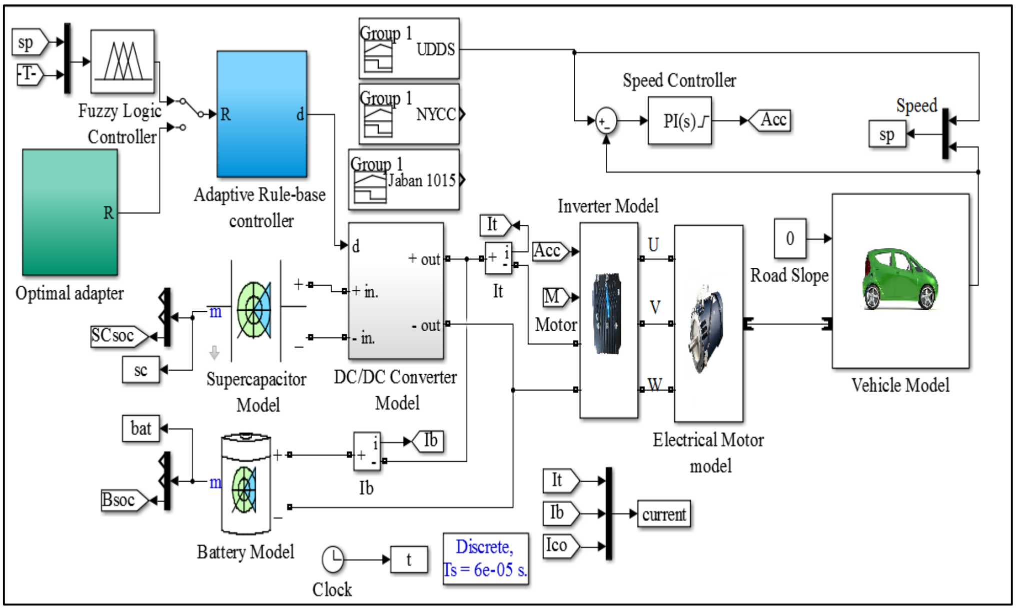

Figure 4.12 MATLAB/Simulink model of the HESS using the adaptive rule-based controller based on the standard drive cycles

4.6 Chapter Summary

In this chapter, the new energy management systems have been proposed. The design of the proposed rule-based controller for the HESS is presented in detail. Furthermore, two adaptive methods are proposed for the rule-based controller named the optimal adaptive and the fuzzy adaptive. The algorithms of the optimal adaptive rule-based controller and the fuzzy adaptive rule-based are described clearly. In addition, the design steps of the linear quadratic regulator are explained. Finally, the Matlab\Simulink model for the proposed controllers, the models of HESS components, and the EV model are presented.

CHAPTER 5

RESULTS AND DISCUSSION

5.1 Introduction

This chapter presents the electric vehicle performance results with a single energy storage battery system and with HESS for several types of drive cycles. Firstly, the results of the energy variance between an electric vehicle performances with and without the road slope are presented. The performance evaluated by comparing the final value of the battery state of charge for the single energy storage battery system in different drive cycles. Furthermore, the proposed HESS results with the energy management systems rule-based controller, the optimal adaptive rule-based controller, and the fuzzy adaptive rule-based controller are presented. The proposed control algorithms are tested in three real drive cycles (uphill, downhill, and city-tour) at three different speeds (50, 60, and 70 Kilometres per hour) and in three different standard drive cycles (UDDS, NYCC, and Japan1015). The state of charge for the HESS components (battery and supercapacitor) are measured at the end of the drive cycles to obtain the total energy consumption in HESS and calculate the maximum number of drive cycles that can be achieved by HESS. All the results are discussed and analyzed in detail to prove the contributions of this research.

5.2 The Results of the Single Energy Storage Battery System

In this section, the effect of the road slope in a single energy storage battery system is investigated. The comparison is presented between the battery states of charge with and without the road slope (measured using CPS).

5.2.1 Uphill Drive Cycle

The first tested real drive cycle is 5 Km uphill, and the road elevation and slope for the uphill drive cycle are illustrated in Figure 3.9. In this case, the total load current is supplied from the battery and no regenerated energy is absorbed during the braking. Figure 5.1 presents the EV total load currents based on the uphill drive cycle in different driving velocities (50, 60, and 70 Kilometres per hour). The load current rises by increasing the road slope. The total times to reach the desired destination by driving velocities (50, 60, and 70 Kilometres per hour) are 370, 305, and 265 seconds, respectively.

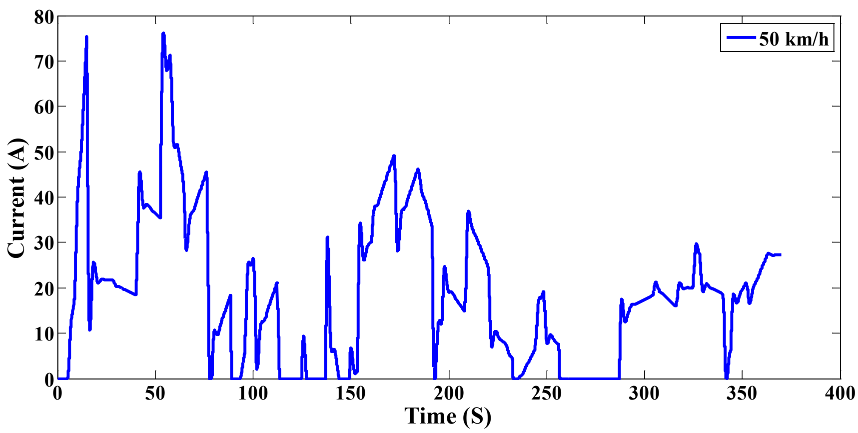

(a)

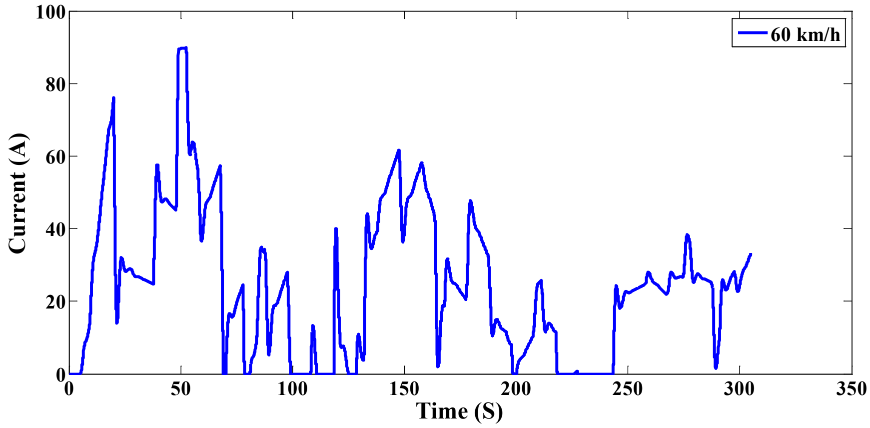

(b)

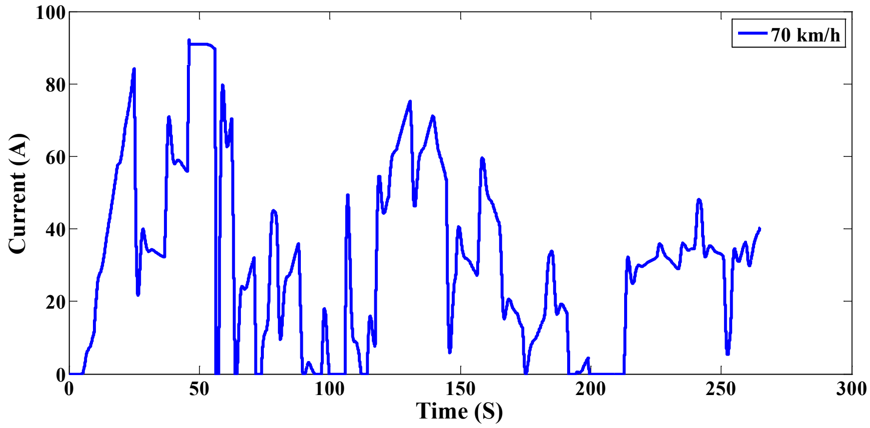

(c)

Figure 5.1 Total EV load currents based on an uphill drive cycle for a single energy storage battery system (a) 50km/h, (b) 60km/h, and (c) 70km/h

The changes of battery states of charge during the uphill drive cycle are illustrated in Figure 5.2. According to these results, the energy consumption of the uphill drive cycle increases with the increase of the vehicle speed.

Table 5.1 summarizes the initial values of the state of charge for battery $\mathrm{SOC_b}(0)$, the final values of state of charge for battery without the road slope $\mathrm{SOC_b}(t)_{\mathrm{slope}=0}$, the final values of state of charge for battery with the road slope $\mathrm{SOC_b}(t)_{\mathrm{slope}=\mathrm{CPS}}$, and the energy variance EnVar for uphill drive cycles for three speeds.

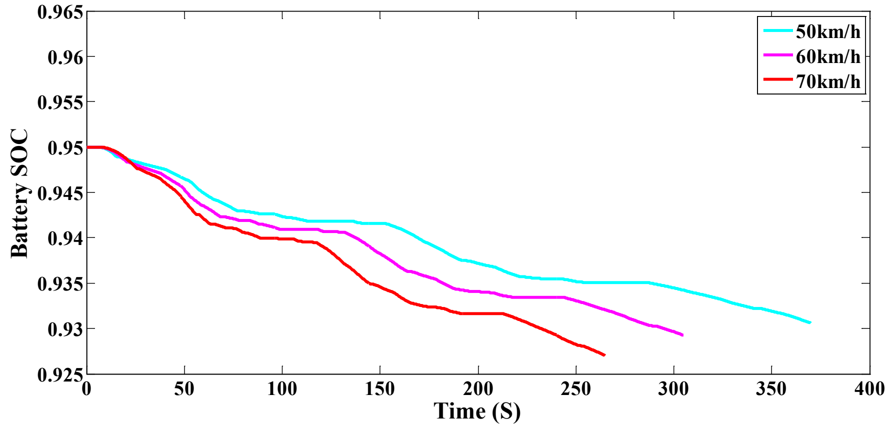

Figure 5.2 The battery states of charge in an uphill drive cycle for a single energy storage battery system

The energy variance represents the difference between the battery energy consumption with and without the road slope and are calculated using Equation 4.11. The results demonstrate that the EV using CPS consumes more energy going uphill taking up to 1% of the total energy.

Table 5.1 The effect of considering road slope in the uphill drive cycle.

Speed	$SOC_b(0)$	$SOC_b(t)_{slope=0}$	$SOC_b(t)_{slope=CPS}$	*EnVar*	*Energy consumption*
50km/h	0.95	0.9407	0.9306	1%	2.04%
60km/h	0.95	0.9385	0.9292	1%	2.19%
70km/h	0.95	0.9360	0.9270	1%	2.42%

5.2.2 Downhill Drive Cycle

The second tested real drive cycle is 5 Km downhill, the road elevation and slope for this drive cycle presented in Figure 3.10. In this case, the battery's total load is supplied during the acceleration, and no regenerated energy is absorbed during the braking. Figure 5.3 presents EV's total load currents based on the downhill drive cycle in different driving velocities (50, 60, and 70 Kilometres per hour). The load current rise by increasing the road slopes. The total time to reach the desired destination by driving velocities (50, 60, and 70 Kilometres per hour) is 370, 305, and 265 seconds.

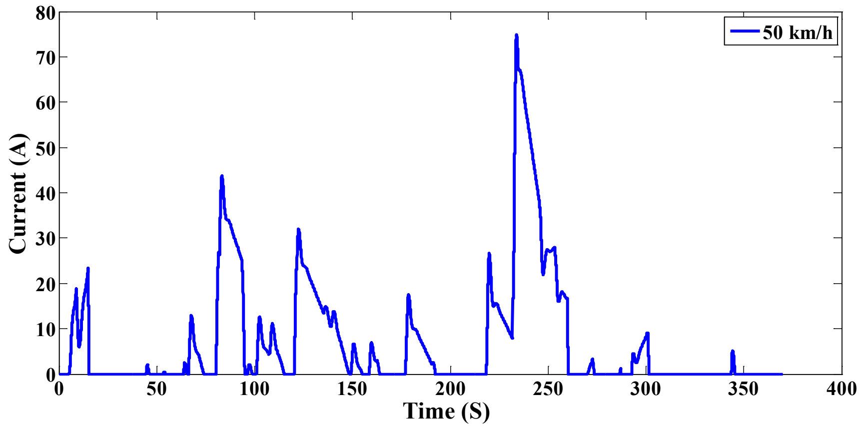

(a)

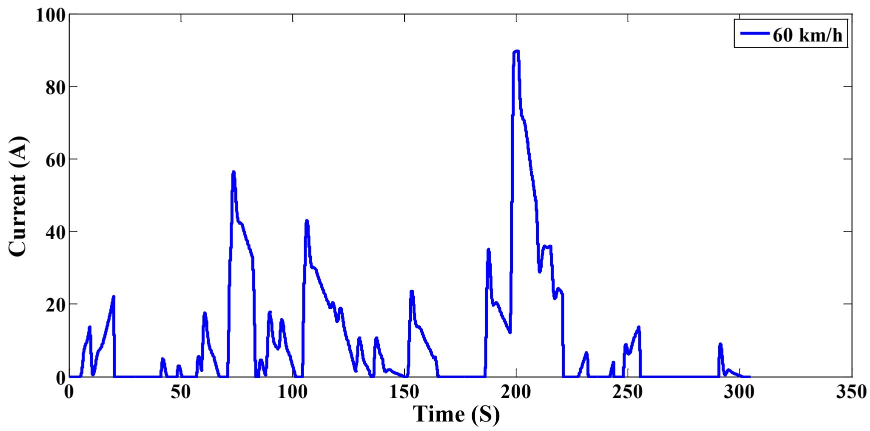

(b)

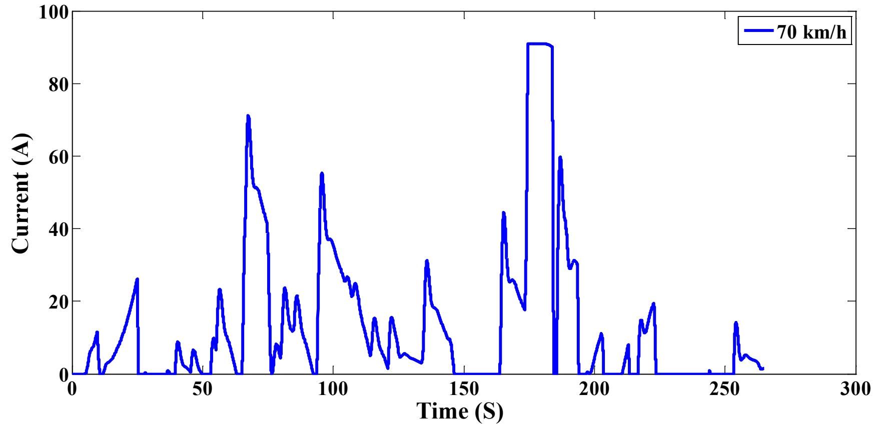

(c)

Figure 5.3 Total EV load currents based on a downhill drive cycle for a single energy storage battery system (a) 50km/h, (b) 60km/h, and (c) 70km/h

The diversity of battery states of charge during the downhill drive cycle are illustrated in Figure 5.4. These results prove the energy consumptions of the downhill drive cycle increased by increasing the vehicle speed. The final battery states of charge for driving velocities (50, 60, and 70 Kilometres per hour) are 0.9428, 0.9418, and 0.9401.

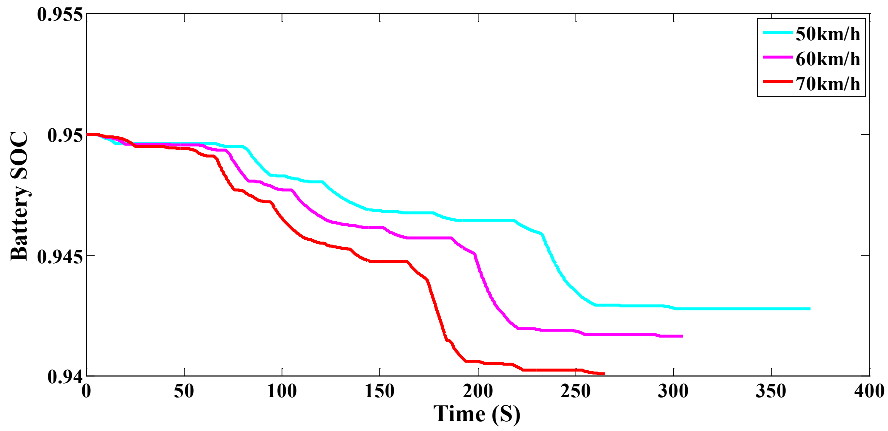

Figure 5.4 The battery states of charge in a downhill drive cycle for a single energy storage battery system

Table 5.2 summarises the road's effect based on the downhill drive cycle in terms of total energy consumptions. The results proved that the EV (using CPS) earned more energy going downhill, taking up to 0.22%, 0.35%, and 0.43% of the total energy for the driving velocities (50, 60, and 70 Kilometres per hour) respectively.

Table 5.2 The effect of considering road slope in the downhill drive cycle.

Speed	$SOC_b(0)$	$SOC_b(t)_{slope=0}$	$SOC_b(t)_{slope=CPS}$	$EnVar$	***Energy consumption***
50km/h	0.95	0.9407	0.9428	-0.22%	0.76%
60km/h	0.95	0.9385	0.9418	-0.35%	0.86%
70km/h	0.95	0.9360	0.9401	-0.43%	1.04%

5.2.3 City-tour Drive Cycle

The Third tested real drive cycle is a 15.85 Km city-tour, the road elevation and slope for this drive cycle presented in Figure 3.11. In this drive cycle, the battery's total load is supplied during the acceleration and no regenerated energy is absorbed during the braking. Figure 5.5 shows EV's total load currents based on the city-tour drive cycle in different driving velocities (50, 60, and 70 Kilometres per hour). The load current rise by increasing the road slopes. The total time to reach the desired destination by driving velocities (50, 60, and 70 Kilometres per hour) is 1100, 910, and 775 seconds.

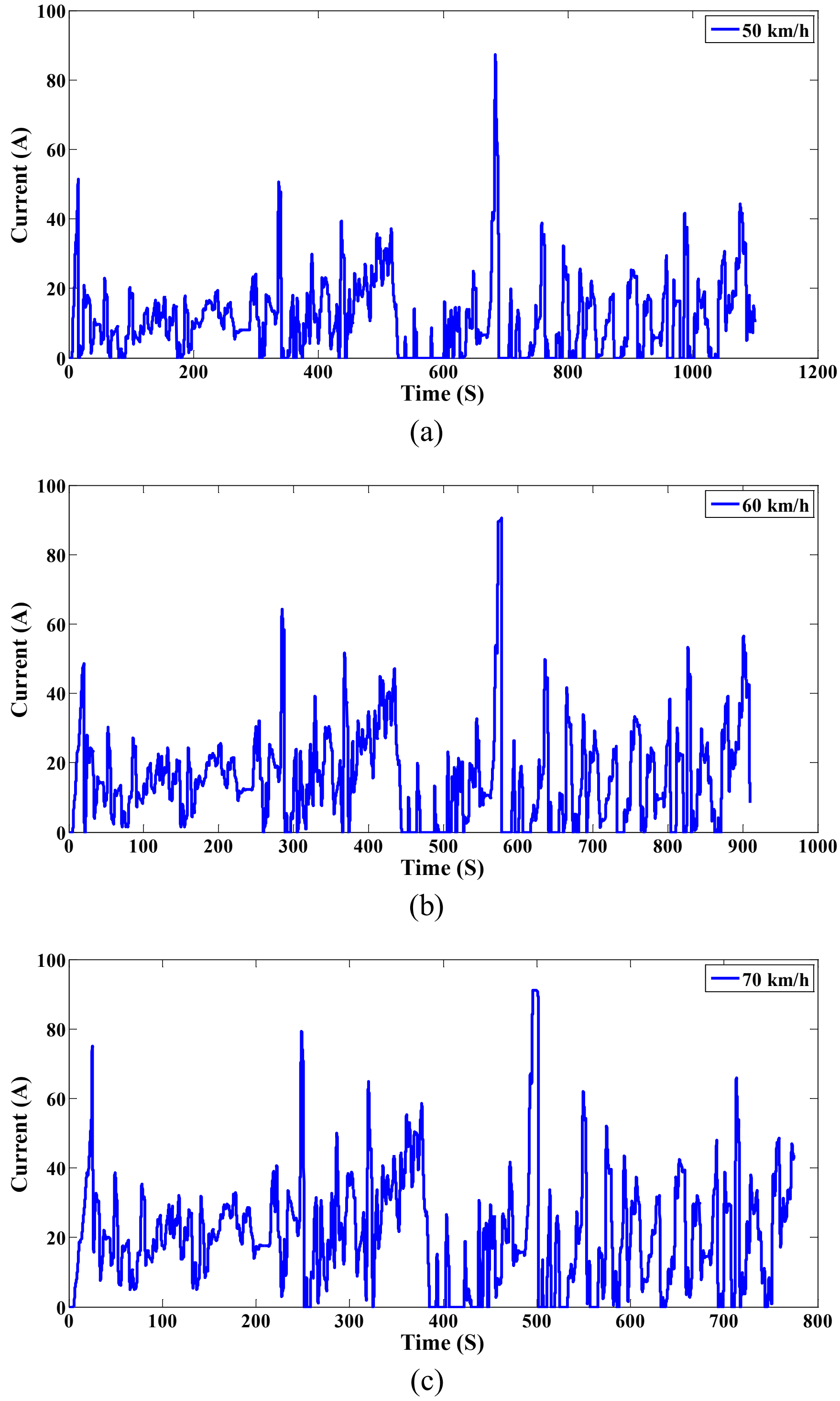

Figure 5.5 Total EV load currents based on a city-tour drive cycle for a single energy storage battery system (a) 50km/h, (b) 60km/h, and (c) 70km/h

The alterations of battery states of charge in the city-tour drive cycle are illustrated in Figure 5.6. These results prove the energy consumptions of the city-tour drive cycle increased by increasing the vehicle speed. The final battery states of charge for driving velocities (50, 60, and 70 Kilometres per hour) are 0.9165, 0.9106, and 0.9055 respectively

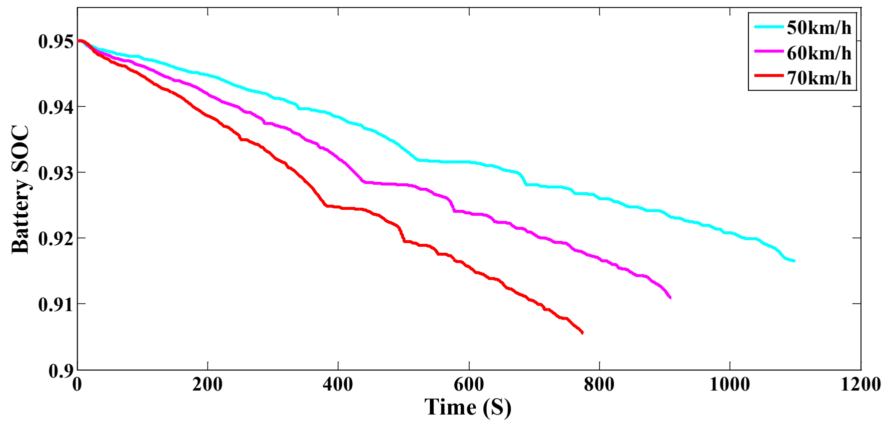

Figure 5.6 The battery states of charge in city-tour drive cycle for a single energy storage battery system

The results in Table 5.2 proved the effect of the road based on the city-tour drive cycle in terms of total energy consumptions. The EV (using CPS) consumed more energy taking up to 0.7%, 0.6%, and 0.4% of the total energy for the driving velocities (50, 60, and 70 Kilometres per hour) respectively.

Table 5.3 The effect of considering road slope in the city-tour drive cycle.

Speed	$SOC_b(0)$	$SOC_b(t)_{slope=0}$	$SOC_b(t)_{slope=CPS}$	$EnVar$	***Energy consumption***
50km/h	0.95	0.9231	0.9165	0.7%	3.53%
60km/h	0.95	0.9165	0.9106	0.6%	4.15%
70km/h	0.95	0.9095	0.9055	0.4%	4.68%

5.2.4 Standard Drive Cycles

The dynamic responses of three standard drive cycles, namely, UDDS Urban Dynamometer Driving Schedule, NYCC New York City Cycle, and Japan1015 drive cycle for EV with a single energy battery system were investigated. The road slope is ignored in the standard drive cycles, and the vehicle speed profile is variable. The battery supplies the total load current while no regenerative energy absorbed by the battery in this case. The speed profiles of the standard drive cycles (UDDS, NYCC, and Japan1015 drive cycle) are presented in Figures 3.12, 3.13, and 3.14, respectively. Figure 5.7 shows EV's total load currents based on three standard drive cycles selected in this research (UDDS, NYCC, and Japan1015 drive cycle). The total load current rises by increasing vehicle speed. The total time of the Urban Dynamometer Driving Schedule is 1400 seconds, the total time of the New York City Cycle is 600 seconds, and the total time of the Japan1015 drive cycle is 660 seconds.

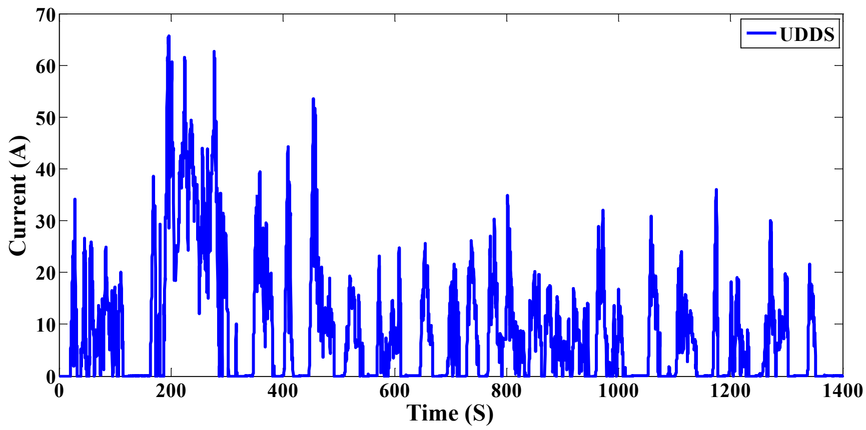

(a)

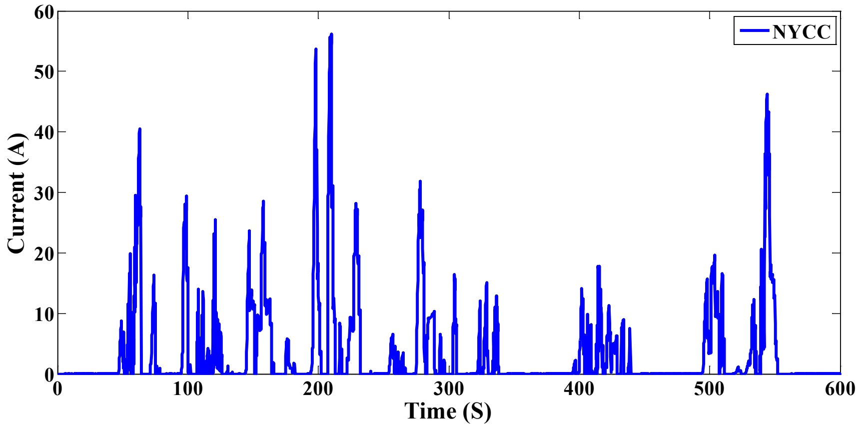

(b)

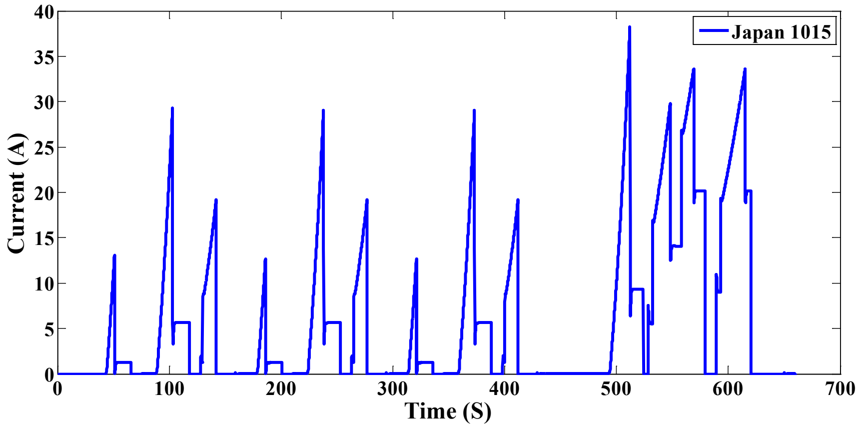

(c)

Figure 5.7 Total EV load currents for a single energy storage battery system based on (a) UDDS, (b) NYCC, and (c) Japan1015 drive cycles

The changes in the battery states of charge for UDDS, NYCC, and Japan1015 drive cycle are presented in Figure 5.8. The final battery states of charge for UDDS, NYCC, and Japan1015 drive cycles are 0.9171, 0.9446, and 0.9398.

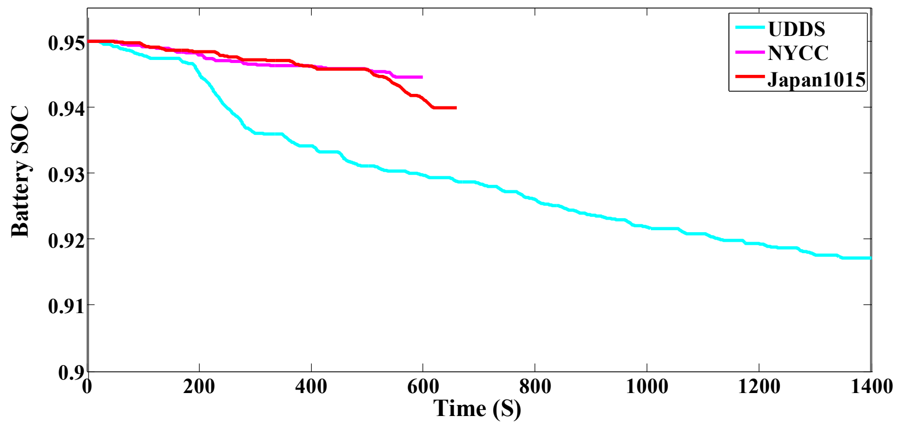

Figure 5.8 The battery states of charge in UDDS, NYCC and Japan1015 drive cycles for a single energy storage battery system

Table 5.4 presents the energy consumption of the standard drive cycles. The total energy consumption for a single cycle of the Urban Dynamometer Driving Schedule, New York City Cycle and Japan1015 drive cycle are 3.4%, 0.57% and 1.07%, respectively from the total energy.

Table 5.4 The total energy consumption in a standard drive cycle.

Speed	*UDDS*	*NYCC*	*Japan1015*
$\boldsymbol{SOC_b(0)}$	0.95	0.95	0.95
$\boldsymbol{SOC_b(t)}$	0.9171	0.9446	0.9398
Energy Consumption	3.46%	0.57%	1.07%

5.3 The Results of the Rule-Based Controller for HESS

This section represent the results of the rule-based controller for the real drive cycles and the standard cycles. The total current of the EV, the battery current, and the supercapacitor current of HESS are presented. The state of charge for the battery and the supercapacitor were measured at the end of the drive cycle. The total percentage of energy consumptions for the battery and supercapacitor were calculated by using Equation 4.12. The main aim of the rule-based controller is to limit the battery current $I_b(t)$ to the desired value I_{b_max}.

5.3.1 Uphill Drive Cycle

In the rule-based controller the battery and the supercapacitor supply the total load current and the supercapacitor absorbs the regenerated energy. Figure 5.9 shows the HESS current based on the rule-based controller on an uphill drive cycle in different driving velocities (50, 60, and 70 Kilometres per hour). The presented results the total load currents of the EV, the battery current and the supercapacitor current proved that the rule-based controller success to reduce the battery stress and limit the battery current to (I_{b_max}).

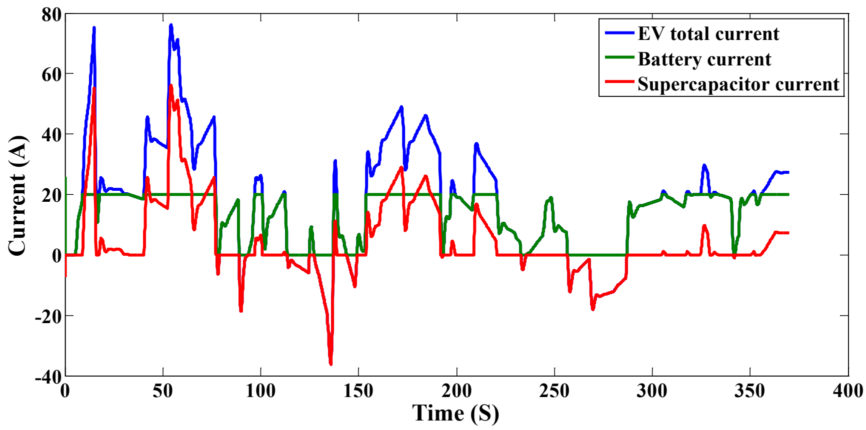

(a)

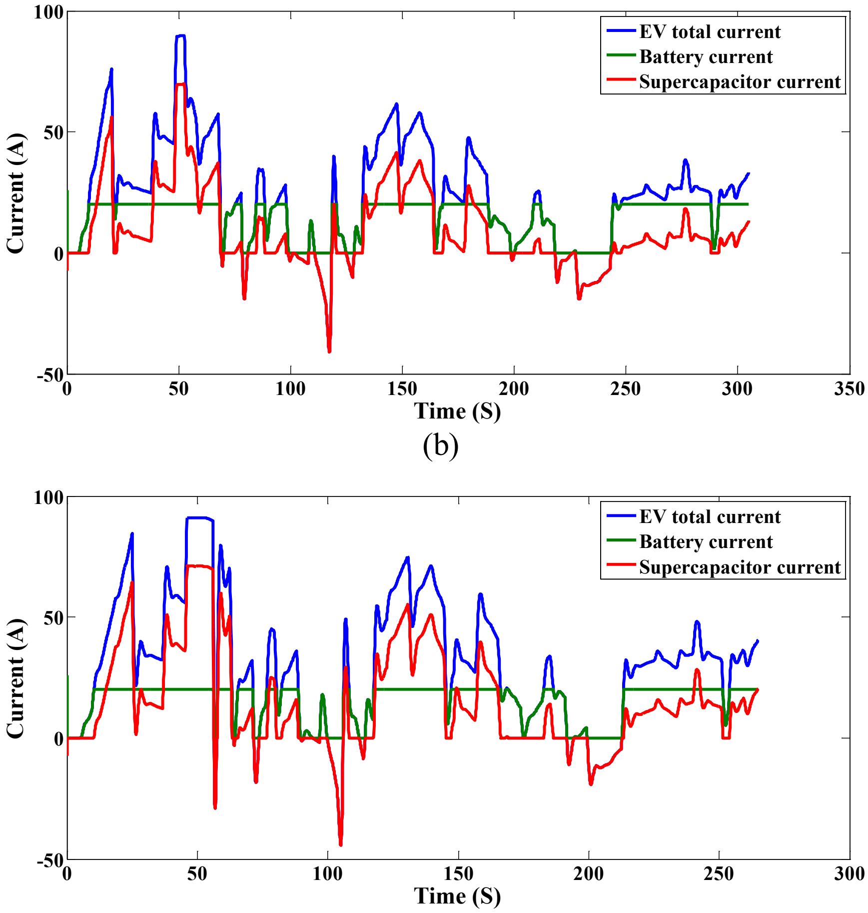

(b)

(c)

Figure 5.9 Total HESS currents based on uphill drive cycle using the rule-based controller (a) 50km/h, (b) 60km/h and (c) 70km/h

The changes of battery states of charge during the uphill drive cycle are illustrated in Figure 5.10. The final battery states of charge for the driving velocities (50, 60, and 70 Kilometres per hour) are 0.9364, 0.9379, and 0.9390 respectively while the total energy consumptions from the battery are 1.43%, 1.27%, and 1.16% for the driving velocities (50, 60, and 70 Kilometres per hour) respectively. The rule-based controller was decreased the battery consumptions in the uphill drive cycle compare with the single energy storage battery system in all driving velocities.

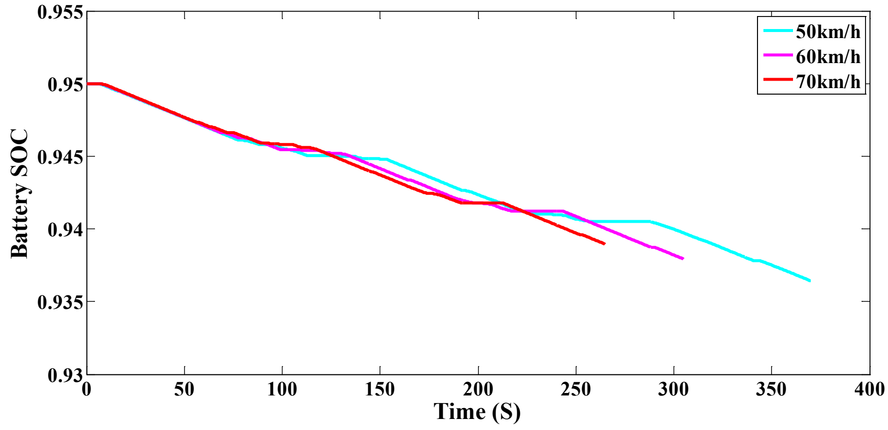

Figure 5.10 The battery states of charge in an uphill drive cycle using the rule-based controller

On the other hand, the variation of the states of charge for supercapacitor during the uphill drive cycle are presented in Figure 5.11. The supercapacitor supplying the high load current and it charges by absorbing the regenerative energy during the braking. The final supercapacitor states of charge are 0.8177, 0.7309, and 0.6246 for different driving velocities (50, 60, and 70 Kilometres per hour). These results prove the energy consumptions of the supercapacitor are increased by increasing the vehicle speed.

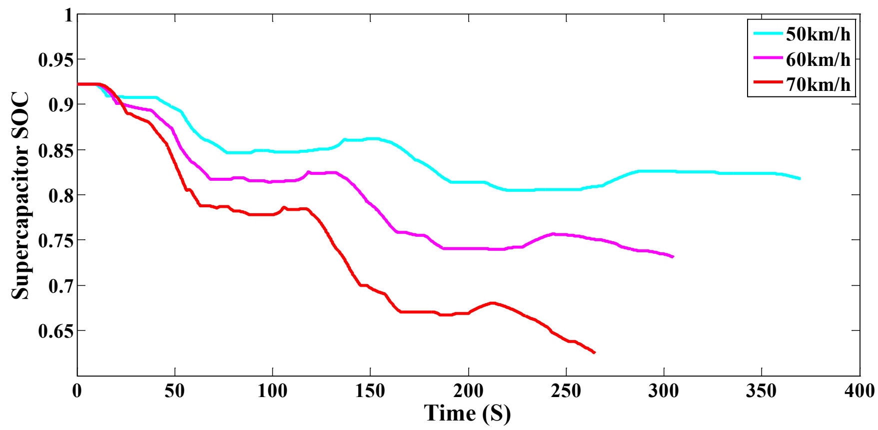

Figure 5.11 The supercapacitor states of charge in an uphill drive cycle using the rule-based controller

Table 5.5 presents the total energy consumption for battery and supercapacitor during the uphill drive cycles for the driving velocities (50, 60, and 70 Kilometres per hour). These results prove the rule-based controller success to reduce the battery energy consumption compared with the single energy storage battery system for the uphill drive cycle. The number of possible uphill drive cycles for HESS by using the rule-based controller are 6.6, 3.6, and 2.3 for the driving velocities (50, 60, and 70 Kilometres per hour) respectively.

Table 5.5 The HESS details in uphill drive cycle using the rule-based controller

	50km/h	*60km/h*	*70km/h*
$SOC_b(t)_{CPS}$	0.9364	0.9379	0.9390
$SOC_{sc}(t)_{CPS}$	0.8177	0.7309	0.6246
Battery Consumption	1.43%	1.27%	1.16%
Supercapacitor Consumption	11.35%	20.76%	32.29%
Cycles No.	6.6	3.6	2.3

5.3.2 Downhill Drive Cycle

The rule-based controller was designed to manage the energy flow of the HESS for the downhill drive cycle. The low load current is supplied from the battery while the high peak load current is supplied from the supercapacitor. The regenerated energy absorbed by the supercapacitor. Figure 5.12 presents the total load currents of the EV, the battery current, and the supercapacitor current based on the downhill drive cycle in different driving velocities (50, 60, and 70 Kilometres per hour). In the downhill drive cycle the amount of the regenerative energy is high compared with the regenerative energy in the uphill drive cycle. The presented results of HESS currents proved the rule-based controller success to limit the battery current to (I_{b_max}) and reduce the peak current compared with the results of the single energy storage battery system.

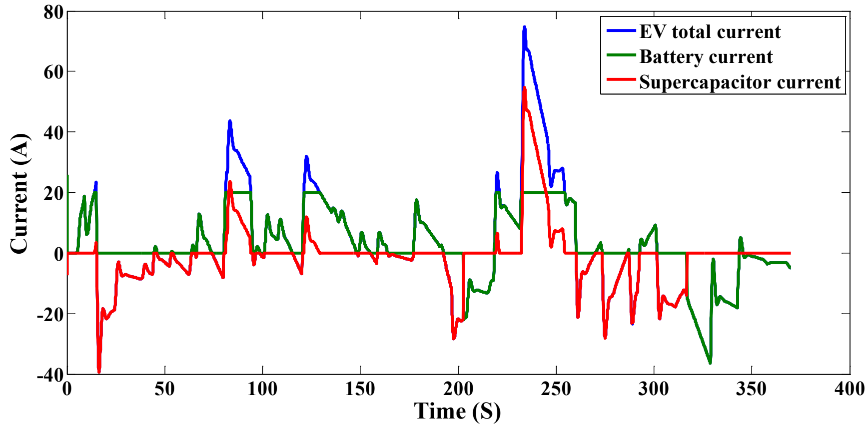

(a)

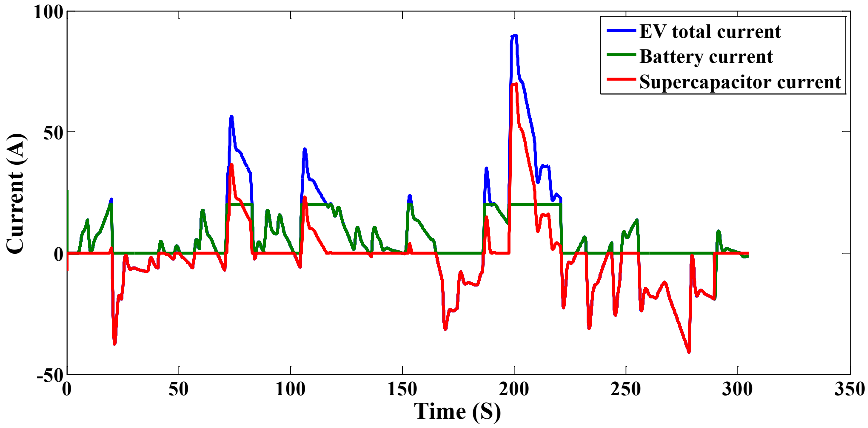

(b)

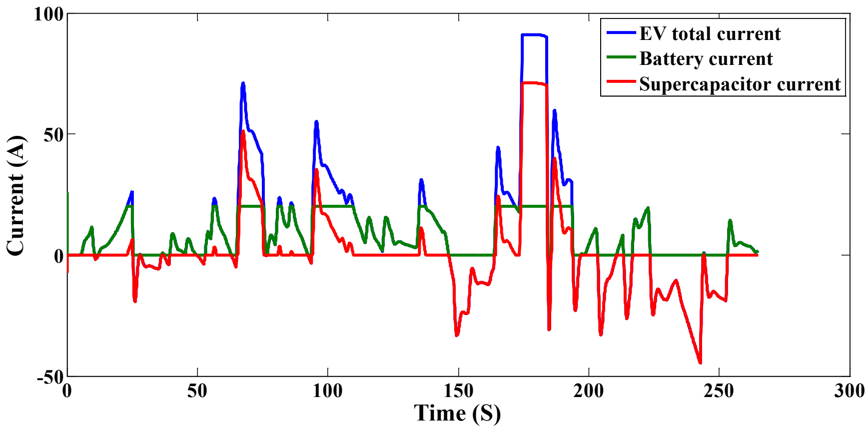

(c)

Figure 5.12 Total HESS currents based on downhill drive cycle using the rule-based controller (a) 50km/h, (b) 60km/h and (c) 70km/h

The changes of battery states of charge during the downhill drive cycle are illustrated in Figure 5.13. The final battery states of charge are 0.9471, 0.9446, and 0.9441 for the driving velocities (50, 60, and 70 Kilometres per hour). Moreover, the total energy consumptions from the battery for the driving velocities (50, 60, and 70 Kilometres per hour) are 0.31%, 0.57%, and 0.62% respectively. The results show the battery energy consumptions have a proportional relation to the vehicle speed.

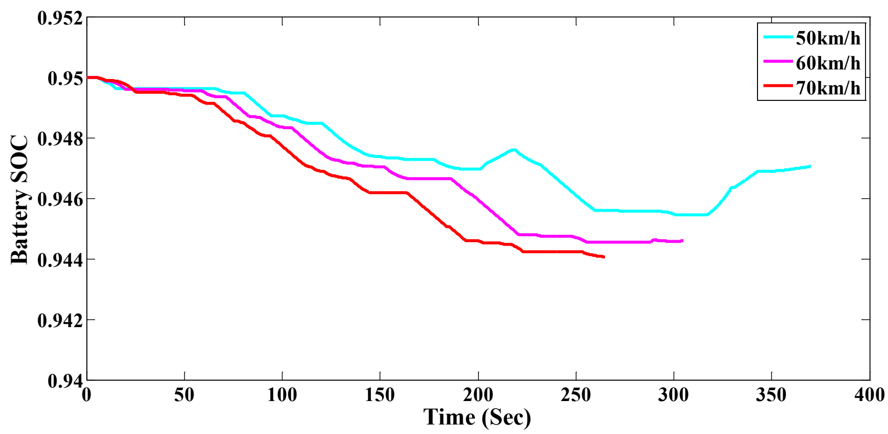

Figure 5.13 The battery states of charge in a downhill drive cycle using the rule-based controller

Furthermore, the changes in the states for the supercapacitor during the downhill drive cycle are illustrated in Figure 5.14. The supercapacitor discharges to supply the high load current while it is charged by absorbing the regenerative energy. The final supercapacitor state of charge is the maximum value of the state of charge which is 0.95 for the driving velocities 50km/h and 60km/h, while the supercapacitor state of charge for a driving velocities of 70km/h is 0.9028. These results prove the HESS earns more energy during the downhill drive cycle.

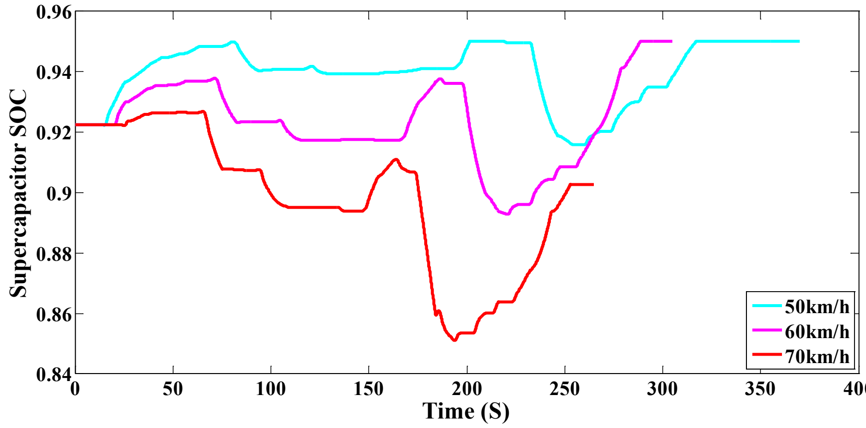

Figure 5.14 The supercapacitor states of charge in a downhill drive cycle using the rule-based controller

Table 5.6 summarize the total energy consumption of the battery and the supercapacitor during the downhill drive cycles at the driving velocities (50, 60, and 70 Kilometres per hour). These results demonstrate the rule-based controller success in reducing battery energy consumption compared with the single energy storage battery system for the downhill drive cycle. For example, the battery energy consumption at 50 km/h in a downhill drive cycle using a single energy storage battery system is 0.76%. It decreased to 0.31% by using HESS with the rule-based controller. The number of possible downhill drive cycles for HESS using the rule-based controller for the driving velocities (50, 60, and 70 Kilometres per hour) are 242, 132, and 35 respectively.

Table 5.6 The HESS details in downhill drive cycle using the rule-based controller

	50km/h	***60km/h***	***70km/h***
$SOC_b(t)_{CPS}$	0.9471	0.9446	0.9441
$SOC_{sc}(t)_{CPS}$	0.95	0.95	0.9028
Battery Consumption	0.31%	0.57%	0.62%
Supercapacitor Consumption	-3%	-3%	2.13%
Cycles No.	242	132	35

5.3.3 City-tour Drive Cycle

This section discusses the performance of HESS for EV by using the rule-based controller in the city-tour drive cycle. The EV performance has a minor effect by the road slope in the city-tour drive cycle. Figure 5.15 illustrated the total load currents of the EV, the battery current, and the supercapacitor current based on the city-tour drive cycle in different driving velocities (50, 60, and 70 Kilometres per hour). In this drive cycle, the presented results of HESS currents are proved the rule-based controller success to limit the battery current to (I_{b_max}) during the journey while the supercapacitor supplies the high peak load EV current and absorbs the regenerative energy during the braking.

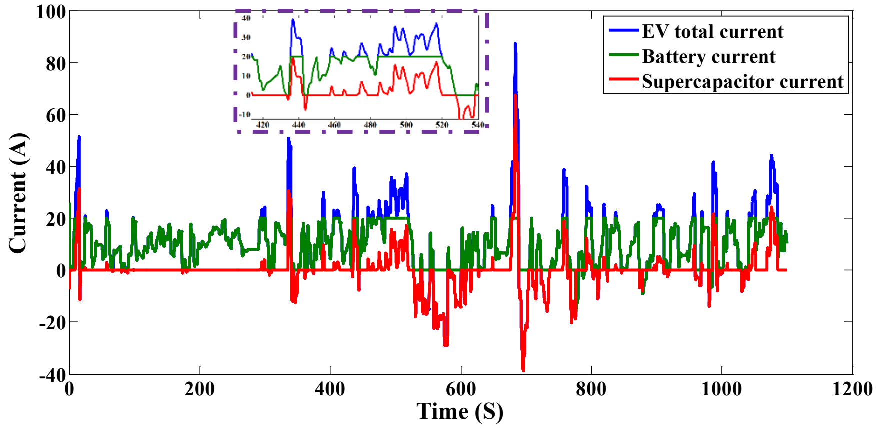

(a)

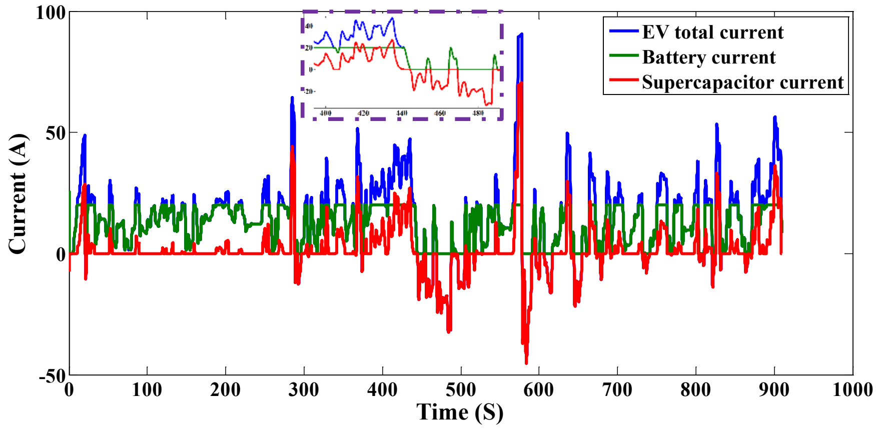

(b)

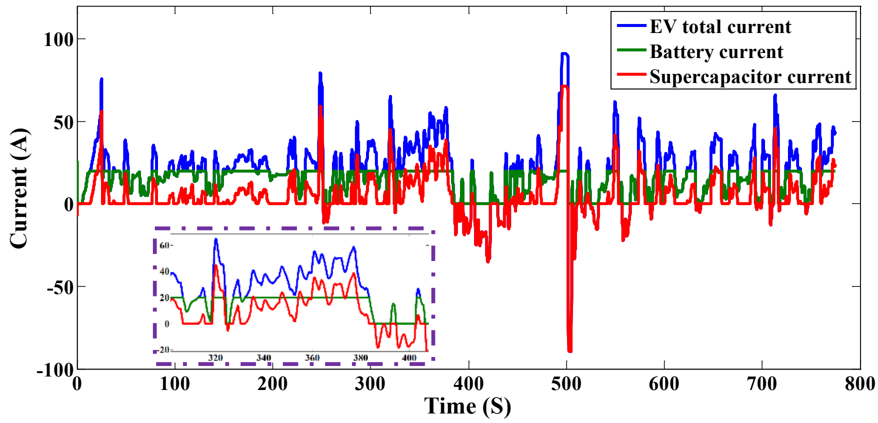

(c)

Figure 5.15 Total HESS currents based on city-tour drive cycle using the rule-based controller (a) 50km/h, (b) 60km/h and (c) 70km/h

The battery states of charge during the city-tour drive cycle are presented in Figure 5.16. The final battery states of charge are 0.9200, 0.9193, and 0.9191 for the driving velocities (50, 60, and 70 Kilometres per hour). The battery energy consumptions are increased by increasing the driving velocities. The total battery energy consumptions are 3.16%, 3.23%, and 3.25% for the driving velocities (50, 60, and 70 Kilometres per hour) respectively.

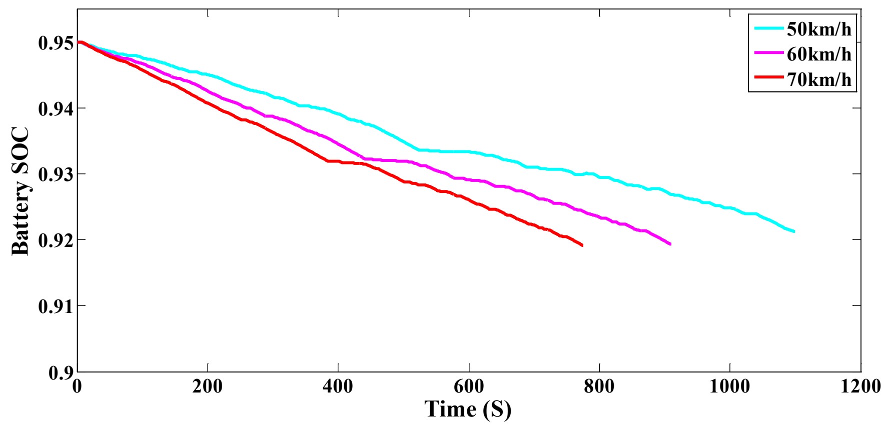

Figure 5.16 The battery states of charge in city-tour drive cycle using the rule-based controller

Moreover, the changes in the supercapacitor states during the city-tour drive cycle are presented in Figure 5.17. The supercapacitor is discharged to supply the high load current while it is charged by absorbing the regenerative energy. The final supercapacitor states of charge are 0.9312, 0.8211, and 0.6537 at the driving velocities (50, 60, and 70 Kilometres per hour). These results prove the energy consumptions of the supercapacitor are increased by increasing the vehicle speed.

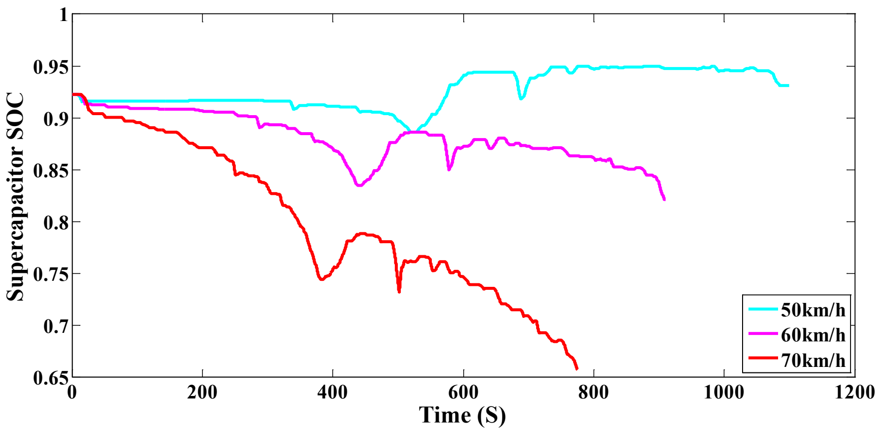

Figure 5.17 The supercapacitor states of charge in city-tour drive cycle using the rule-based controller

Table 5.7 presents the total energy consumption for the battery and the supercapacitor of HESS during the city-tour drive cycles at different driving velocities (50, 60, and 70 Kilometres per hour). These results prove the rule-based controller successes to reduce the battery energy consumption compared with the single energy storage battery system for the city-tour drive cycle. In the 50km/h the HESS with the rule-based controller is decreased the battery energy consumption to 3.17% compared with 3.53% in the single energy storage battery system. Furthermore, the number of possible city-tour drive cycles of the HESS using the rule-based controller at the driving velocities (50, 60, and 70 Kilometres per hour) are 24.7, 6.7, and 2.5 respectively.

Table 5.7 The HESS details in city-tour drive cycle using the rule-based controller

	50km/h	*60km/h*	*70km/h*
$SOC_b(t)_{CPS}$	0.9200	0.9193	0.9191
$SOC_{sc}(t)_{CPS}$	0.9312	0.8211	0.6537
Battery Consumption	3.16%	3.23%	3.25%
Supercapacitor Consumption	-1%	11%	29%
Cycles No.	23.7	6.8	2.6

5.3.4 Standard Drive Cycles

This section discusses the response of the rule-based controller of thr HESS based on three different standard drive cycles UDDS, NYCC, and Japan1015 drive cycle for the EV. The total EV current is changing depends on the vehicle speed profile. In this case, the battery is supplying the low load current while the supercapacitor is supplying the peak load current. The supercapacitor absorbs the regenerative energy during the deceleration. Figure 5.18 shows the total EV load current, the battery current, and the supercapacitor current during the drive cycles (UDDS, NYCC, and Japan1015). These results are proved the HESS implementation with the rule-based leads to a reduction in battery stress compared with the single energy storage battery system. The rule-based controller limits the battery current to (I_{b_max}) during the journey while the supercapacitor supply the high peak load EV current and absorb the regenerative energy.

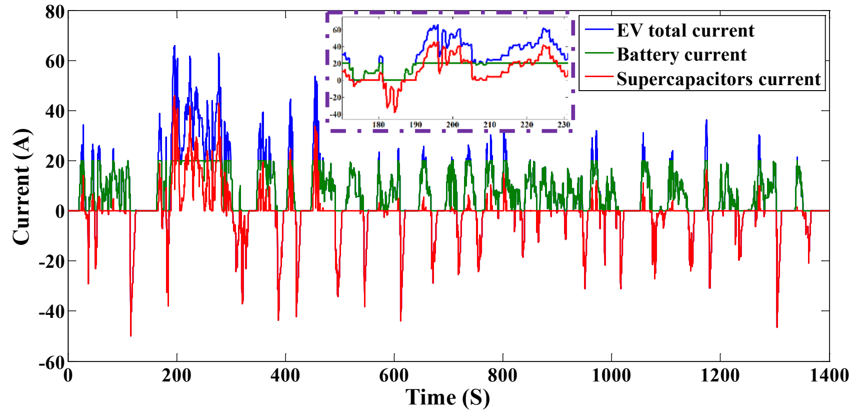

(a)

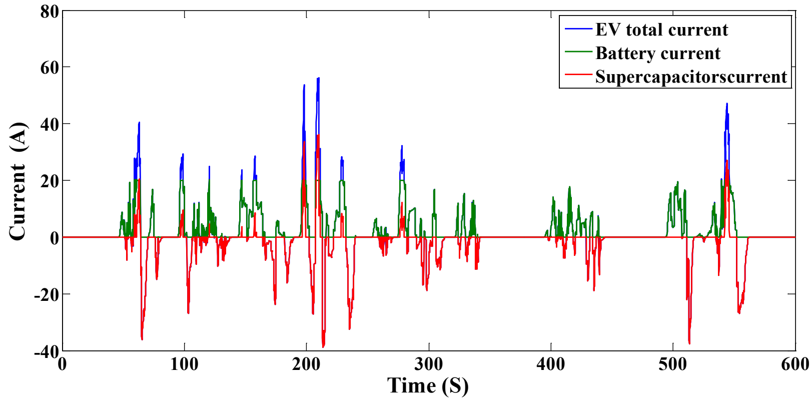

(b)

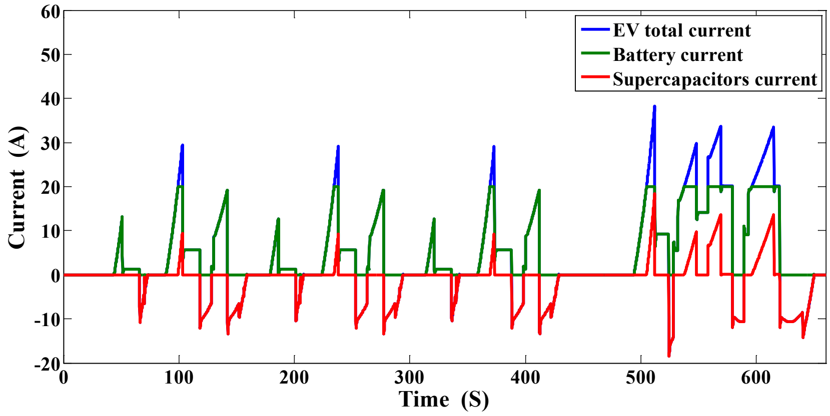

(c)

Figure 5.18 Total HESS currents based on standard drive cycle using the rule-based controller (a) UDDS, (b) NYCC and (c) Japan1015

Also, the changes of the battery states of charge during (UDDS, NYCC, and Japan1015) drive cycles are illustrated in Figure 5.19. After a single drive cycle the final battery state of charge is 0.9255, 0.9379, and 0.9419 for the UDDS, NYCC, and Japan1015 drive cycles respectively.

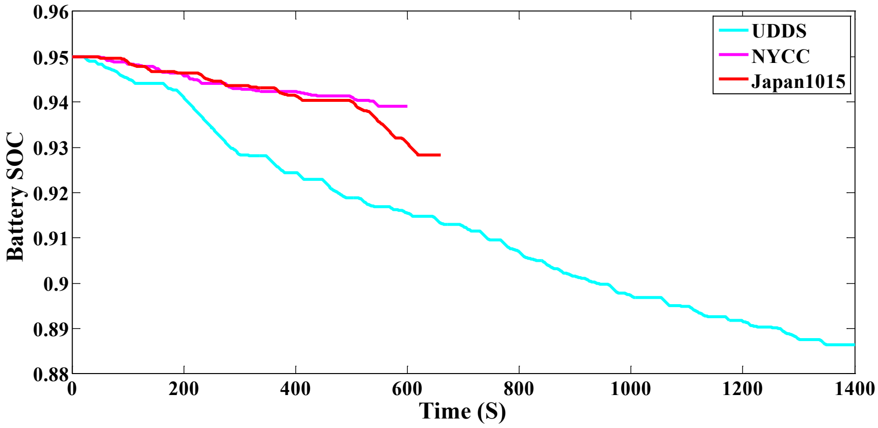

Figure 5.19 The battery states of charge in UDDS, NYCC, and Japan1015 drive cycles using the rule-based controller

Otherwise, the changes in states of charge for the supercapacitor during UDDS, NYCC, and Japan1015 drive cycles are presented in Figure 5.20. The supercapacitor discharges to supply the high load current while it charges by absorbing the regenerative energy. The final supercapacitor states of charge are the maximum value which is 0.95 for UDDS, NYCC, and Japan1015 drive cycles. These results are proved the supercapacitor of HESS with the rule-based controller earns energy during the tested drive cycles.

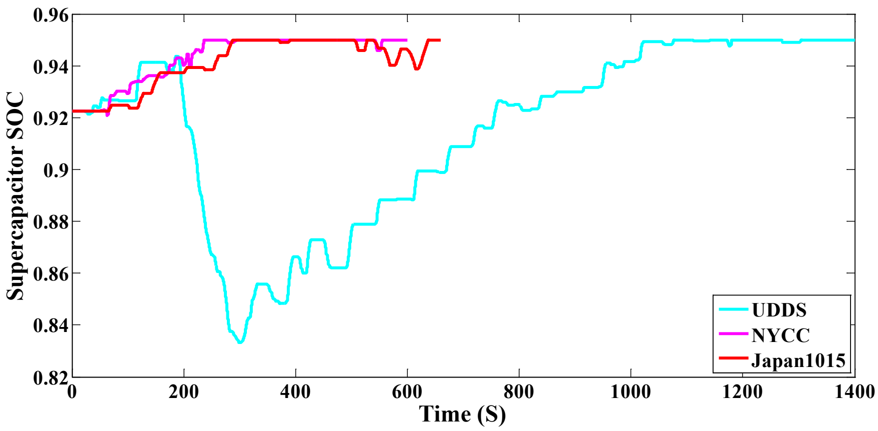

Figure 5.20 The supercapacitor states of charge in UDDS, NYCC, and Japan1015 drive cycles using the rule-based controller

Table 5.8 summarize the total energy consumption for the battery and the supercapacitor of the HESS with the rule-based controller during UDDS, NYCC, and Japan1015 drive cycles. The battery consumptions for UDDS, NYCC, and Japan1015 drive cycles are 2.58%, 0.33%, and 0.85% respectively. The results are proved the rule-based controller successes in reducing battery consumption compared with the single energy storage battery system in all drive cycles. The battery consumption of the UDDS by using the HESS with the rule-based controller is decreased to 2.58% compared with 3.46% in the single energy storage battery system. And the battery consumption of NYCC is decreased to 0.33% compared with 0.57% in the single energy storage battery system. Also, the battery consumption of the Japan1015 drive cycle is decreased to 0.85% compared with 1.07% in the single energy storage battery system. Furthermore, the number of possible drive cycles of the HESS with the rule-based controller are 29 drive cycles for UDDS, 227 drive cycles for NYCC, and 88 drive cycles for Japan1015.

Table 5.8 The HESS details in UDDS, NYCC, and Japan1015 drive cycles using the rule-based controller

	UDDS	***NYCC***	***Japan1015***
$\mathrm{SOC_b(t)_{CPS}}$	0.9255	0.9469	0.9419
$\mathrm{SOC_{sc}(t)_{CPS}}$	0.95	0.95	0.95
Battery Consumption	2.58%	0.33%	0.85%
Supercapacitor Consumption	-3%	-3%	-3%
Cycles No.	29	227	88

Table 5.9 summarizes the comparison between the energy consumption on the single energy storage battery system ($\boldsymbol{EngCons_{BVE}}$) and the battery energy consumption on the HESS using the rule-based controller($\boldsymbol{EngCons_{HESS}}$). The energy variance (*EngVar*) and the *Battery Energy Reduction Ratio* demonstrate the effectiveness of the HESS using the rule-based controller in terms of decrease the battery stress and prolong the battery aging.

Table 5.9 The battery energy reduction ratio using the rule-based controller

Drive cycle	***Speed***	$\boldsymbol{EngCons_{BVE}}$	$\boldsymbol{EngCons_{HESS}}$ ***Rule-Based***	***EngVar***	***Battery Energy Reduction Ratio***
Uphill	50Km/h	2.04%	1.43%	0.61%	29.9%
	60Km/h	2.19%	1.27%	0.92%	42%
	70Km/h	2.42%	1.16%	1.26%	52%
Downhill	50Km/h	0.76%	0.31%	0.45%	59%
	60Km/h	0.86%	0.57%	0.29%	33.7%
	70Km/h	1.04%	0.62%	0.42%	40%
City tour	50Km/h	3.53%	3.16%	0.37%	10.5%
	60Km/h	4.15%	3.23%	0.92%	22.2%
	70Km/h	4.68%	3.25%	1.43%	30.6%
Standard drive cycles	UDDS	3.46%	2.58%	0.88%	25.4%
	NYCC	0.57%	0.33%	0.24%	42.1%
	Japan1015	1.07%	0.85%	0.22%	20.6%

5.4 The Results of the Optimal Adaptive Rule-Based Controller for HESS

This section presents the results of the optimal adaptive rule-based controller for the real drive cycles and the standard cycles. The investigation of the proposed optimal adaptive rule-based controller, the total current of EV, the battery current, and the supercapacitor current of the HESS are presented. The state of charge for the battery and the supercapacitor are measured at the end of the drive cycles. The total percentage of energy consumptions for the battery and the supercapacitor were calculated using Equation 4.12. The optimal adaptive rule-based controller aims to limit the battery current $I_b(t)$ to a maximum value I_{b_max} and to obtain the optimal value of energy sharing between the battery and the supercapacitor during the selected journey. Section 3.3.1 described the design and the working principles of the optimal adaptive rule-based controller in detail. This controller is estimated a fixed value of the energy sharing percentage R for the entire journey.

5.4.1 Uphill Drive Cycle

In this drive cycle, the total load current is supplied by the battery and the supercapacitor with the optimal adaptive rule-based controller while the supercapacitor absorbed the regenerated energy. Figure 5.21 shows the total load currents of the EV, the battery current, and the supercapacitor current based on the uphill drive cycle in different driving velocities (50, 60, and 70 Kilometres per hour). The battery is supplied the low load current while the supercapacitor is supplied the peak load current. The energy sharing percentage between the battery and the supercapacitor (R) was estimated before the journey start depends on the road slope and it is equal to zero at all driving velocities.

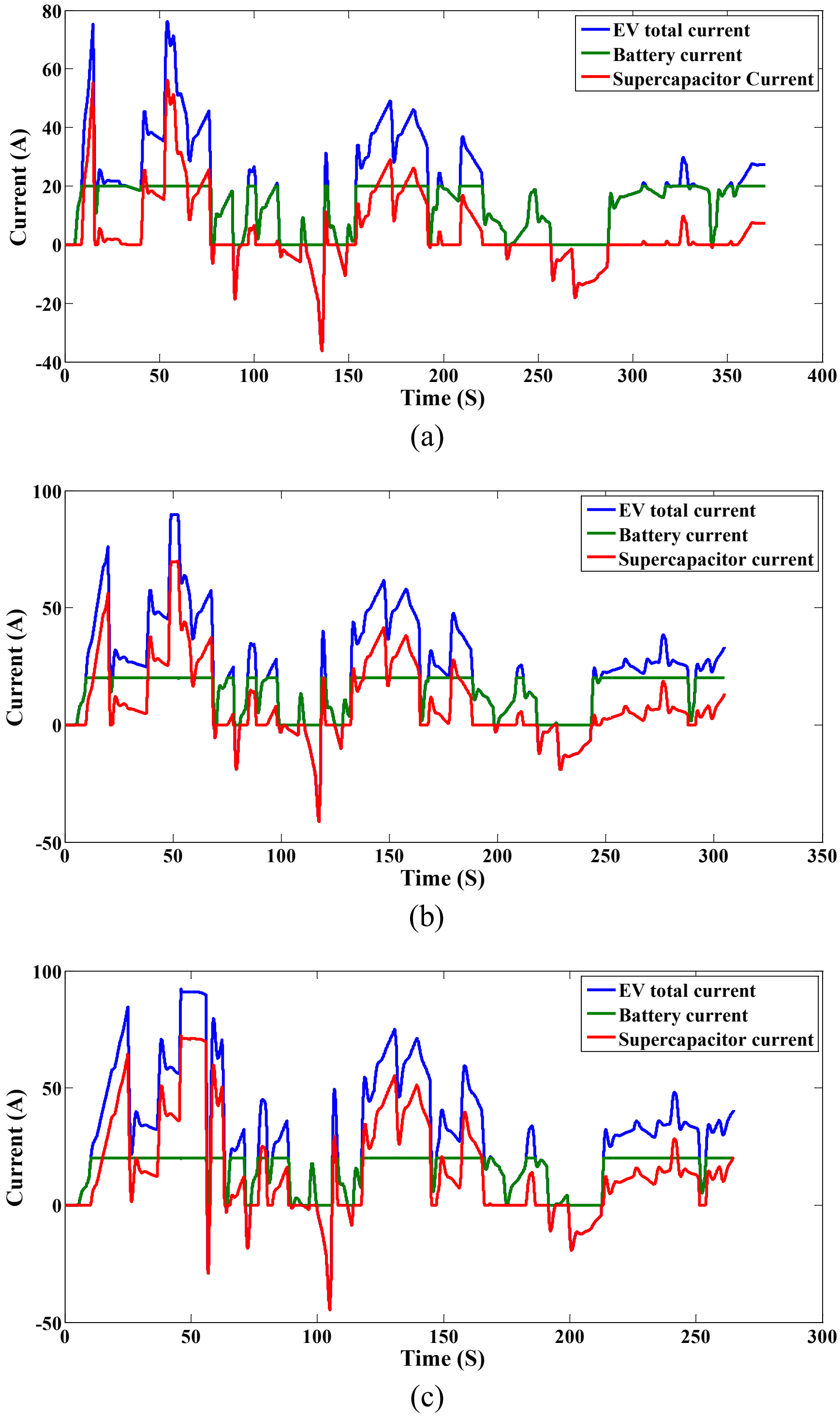

Figure 5.21 Total HESS currents based on uphill drive cycle using optimal adaptive rule-based controller (a) 50km/h, (b) 60km/h and (c) 70km/h

The changes of the battery states of charge during the uphill drive cycle are illustrated in Figure 5.22. The final value of the battery states of charge for the driving velocities (50, 60, and 70 Kilometres per hour) are 0.9364, 0.9379, and 0.9390 respectively. The optimal adaptive rule-based controller is succeed to reduce the battery stress and limit the battery current to (I_{b_max}). In this drive cycle the optimal adaptive controller acts like the rule-based controller due to the road slope characteristics which required a high peak load current compared with the regenerative energy.

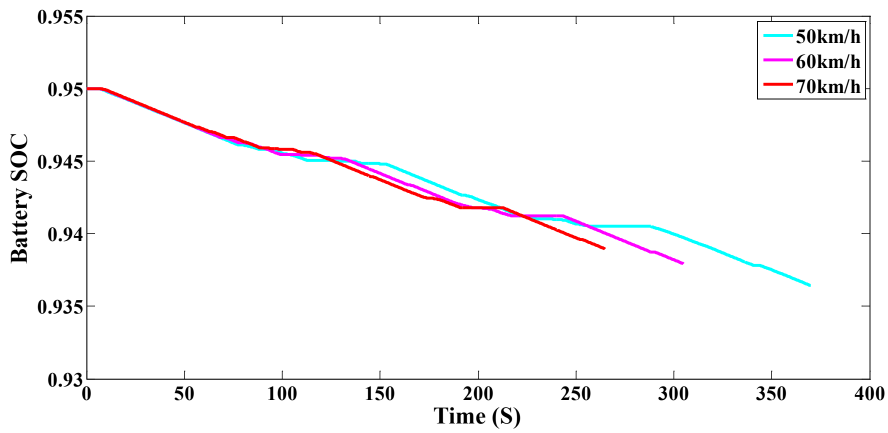

Figure 5.22 The battery states of charge in an uphill drive cycle using the optimal adaptive rule-based controller

The changes in the states of charge of the supercapacitor during the uphill drive cycle are presented in Figure 5.23. The supercapacitor discharges to supply the high peak load current while it charges by absorbing the regenerative energy. The final values of the supercapacitor states of charge are 0.8177, 0.7309, and 0.6246 for the driving velocities (50, 60, and 70 Kilometres per hour). These results are proved that the energy consumption of the supercapacitor is increased by increasing the vehicle speed.

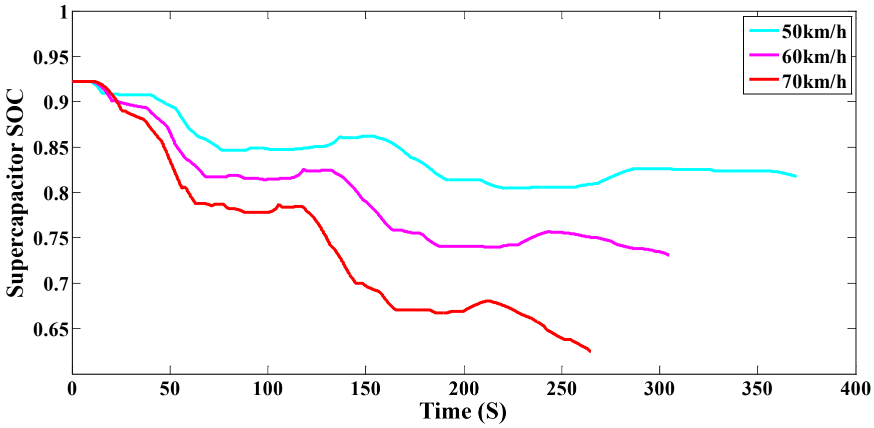

Figure 5.23 The supercapacitor states of charge in an uphill drive cycle using the optimal adaptive rule-based controller

Table 5.10 presents the total energy consumption of the HESS based on the optimal adaptive rule-based controller during the uphill drive cycles for the driving velocities (50, 60, and 70 Kilometres per hour). These results are proved the optimal adaptive rule-based controller is succeed to reduce the battery energy consumption compared with the single energy storage battery system for the uphill drive cycle. Furthermore, the number of possible uphill drive cycles for the HESS using the optimal adaptive rule-based controller are 6.6, 3.6, and 2.3 for the driving velocities (50, 60, and 70 Kilometres per hour) respectively.

Table 5.10 The HESS details in uphill drive cycle using the optimal adaptive rule-based controller

	50km/h	*60km/h*	*70km/h*
$\mathrm{SOC_b(t)_{CPS}}$	0.9364	0.9379	0.9390
$\mathrm{SOC_{sc}(t)_{CPS}}$	0.8177	0.7309	0.6246
Battery Consumption	1.43%	1.27%	1.16%
Supercapacitor Consumption	11.35%	20.76%	32.29%
Cycles No.	6.6	3.6	2.3

5.4.2 Downhill Drive Cycle

In this drive cycle the load current was supplied by the battery and supercapacitor using the optimal adaptive controller. The supercapacitor is absorbed the regenerated energy. Figure 5.24 shows the HESS currents of EV based on the downhill drive cycle in different driving velocities (50, 60, and 70 Kilometres per hour). The battery and the supercapacitor are supplied the low load current while the supercapacitor is supplied the peak current. The values of the energy sharing percentage between the battery and the supercapacitor (R) is estimated before the journey start by using the CPS and are equal 0.67, 0.23, and zero for driving velocities 50km/h, 60km/h, and 70km/h respectively. These results prove this controller improve the performance of the HESS in the downhill drive cycle compared with the single energy storage battery system.

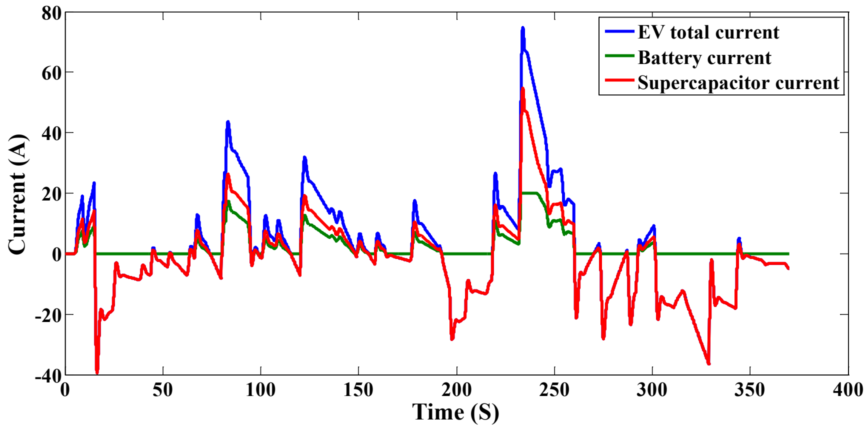

(a)

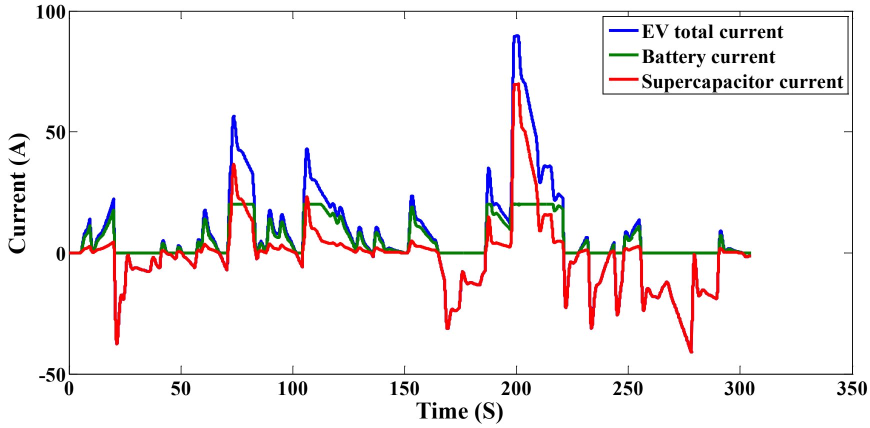

(b)

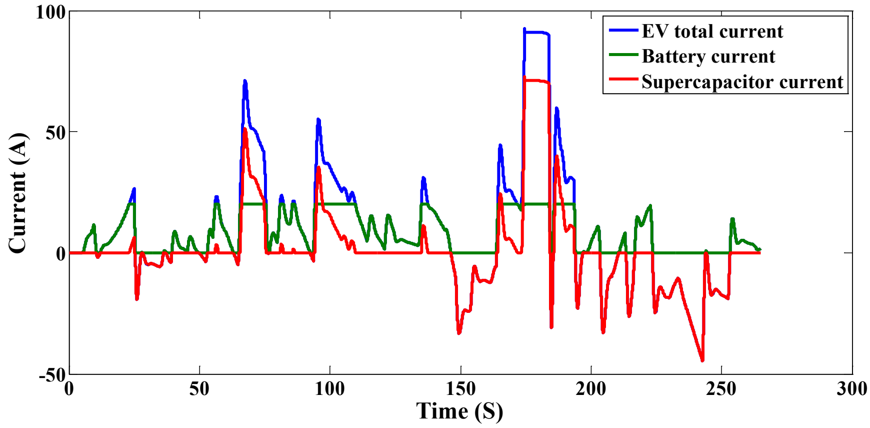

(c)

Figure 5.24 Total HESS currents based on downhill drive cycle using optimal adaptive rule-based controller (a) 50km/h, (b) 60km/h and (c) 70km/h

The changes of the battery states of charge during the downhill drive cycle are illustrated in Figure 5.25. The final values of the battery states of charge are 0.94720, 0.9451, and 0.9441 for the driving velocities (50, 60, and 70 Kilometres per hour). Moreover, in the downhill drive cycle the HESS with the optimal adaptive rule-based controller is reduced the battery energy consumptions for the driving velocities 50km/h and 60km/h compared with the rule-based controller from 0.31% to 0.3% in 50km/h and from 0.57% to 0.52% in 60km/h. The battery energy consumption is maintained in both controllers at 0.62% for the driving velocities 70km/h.

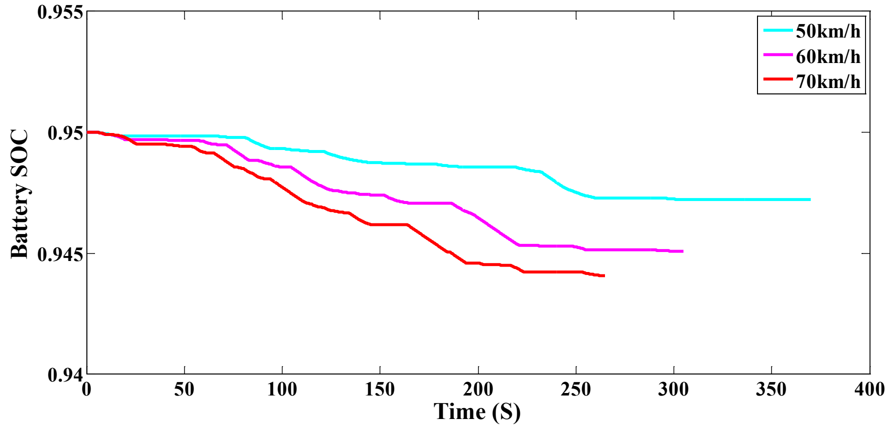

Figure 5.25 The battery states of charge in a downhill drive cycle using the optimal adaptive rule-based controller

Moreover, the supercapacitor discharged to supply the high peak load current and assisted the battery in providing low load current. The regenerative energy charged the supercapacitor. The final supercapacitor states of charge are 0.9464, 0.9386, and 0.9028 for the driving velocities 50km/h, 60km/h, and 70km/h. These results prove the HESS earns more energy during the downhill drive cycle. The changes in the states of charge for the supercapacitor during the downhill drive cycle are illustrated in Figure 5.26.

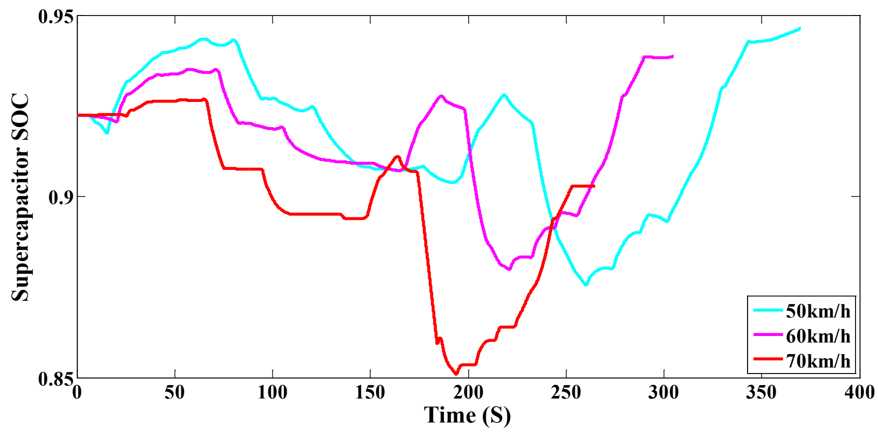

Figure 5.26 The supercapacitor states of charge in a downhill drive cycle using the optimal adaptive rule-based controller

Table 5.11 summarizes the total energy consumption for the battery and the supercapacitor during the downhill drive cycles for the driving velocities (50, 60, and 70 Kilometres per hour) by using the optimal adaptive rule-based controller. These results demonstrate that the HESS with optimal adaptive rule-based controller is increased the number of possible downhill drive cycles compared with the rule-based controller from 242 to 250 drive cycles in the driving velocities 50km/h, from 132 to 144 drive cycles in the driving velocities 60km/h and maintained the number of possible downhill drive cycles in driving velocities 70km/h with 35 drive cycles in both controllers.

Table 5.11 The HESS details in downhill drive cycle using the optimal adaptive rule-based controller

	50km/h	***60km/h***	***70km/h***
$\mathrm{SOC_b(t)_{CPS}}$	0.9472	0.9451	0.9441
$\mathrm{SOC_{sc}(t)_{CPS}}$	0.9464	0.9386	0.9028
Battery Consumption	0.3%	0.52%	0.62%
Supercapacitor Consumption	-2.6%	-1.47%	2.13%
Cycles No.	250	144	35

5.4.3 City-tour Drive Cycle

In the city-tour drive cycle the HESS with optimal adaptive rule-based controller is supplied the load current from the battery and the supercapacitor. The supercapacitor absorbed the regenerated energy. Figure 5.27 shows the total load currents of the EV, the battery current, and the supercapacitor current based on the city-tour drive cycle in different driving velocities (50, 60, and 70

Kilometres per hour). The low load current is supplied by the battery and the supercapacitor while the peak load current is supplied by the supercapacitor. The value of the energy sharing percentage between the battery and supercapacitor R is equal 0.02 in the driving velocities 50km/h, while R is equal zero in 60km/h and 70km/h. The performance of the HESS in this drive cycle is proved the HESS with optimal rule-based controller limit the battery current to (I_{b_max}) and reduced the battery stress compared with the single energy storage battery system.

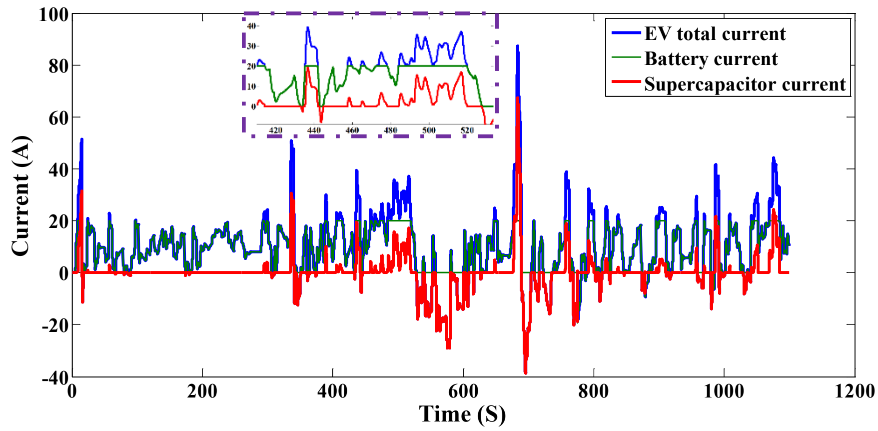

(a)

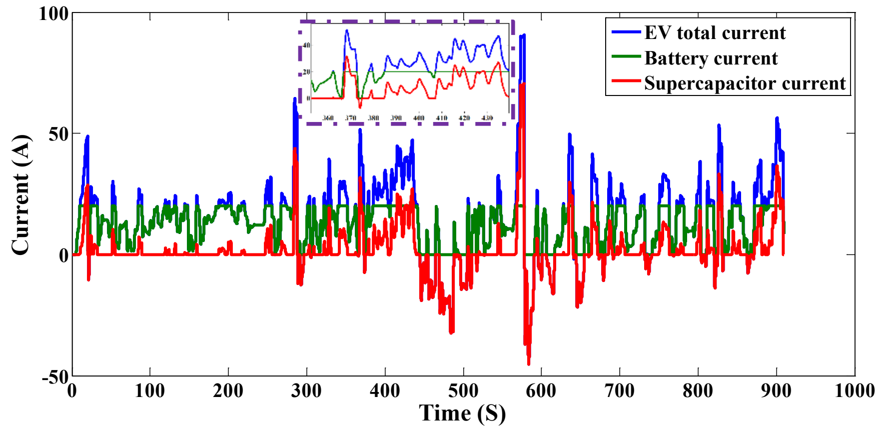

(b)

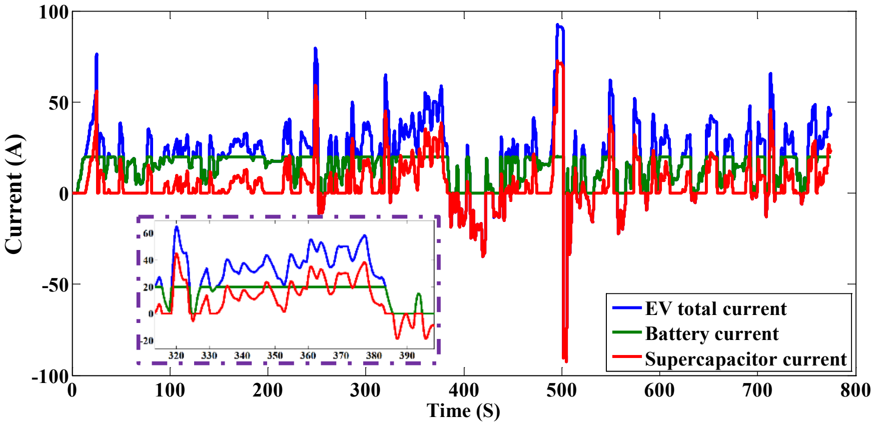

(c)

Figure 5.27 Total HESS currents based on city-tour drive cycle using optimal adaptive rule-based controller (a) 50km/h, (b) 60km/h and (c) 70km/h

The battery states of charge during the city-tour drive cycle are presented in Figure 5.28. The final battery states of charge are 0.9212, 0.9193and 0.9191 for the driving velocities (50, 60, and 70 Kilometres per hour). Furthermore, the battery energy consumption was increased by increasing the driving velocities. In the driving velocities 50km/h the HESS with optimal adaptive rule-based controller reduced the battery energy consumptions compared with the rule-based controller from 3.16% to 3.03%. At the same time the battery energy consumptions in both controllers were the same in driving velocities 60km/h and 70km/h.

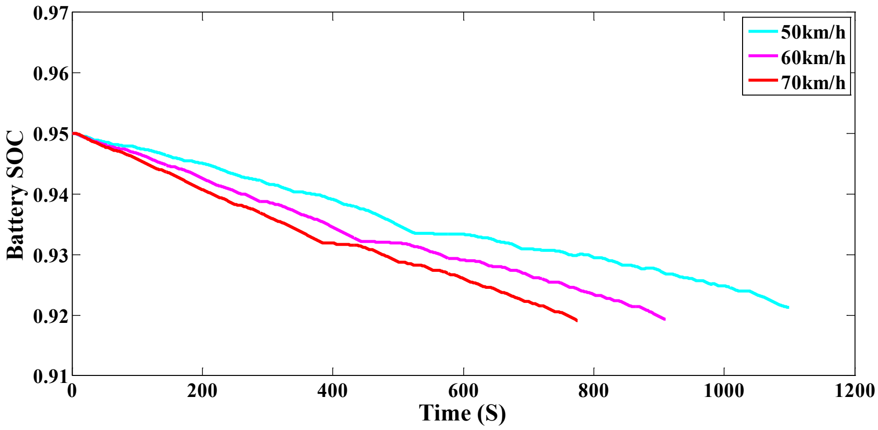

Figure 5.28 The battery states of charge in city-tour drive cycle using the optimal adaptive rule-based controller

Moreover, the HESS with the optimal adaptive rule-based controller manages the supercapacitor to supply the high load peak current and assist the battery to supply low load current in the driving velocities of 50km/h while the regenerated energy was used to charge the supercapacitor. On the other hand, in the driving velocities 60km/h and 70km/h the supercapacitor is supplied the high load peak current only and absorb regenerative energy. The final values of the supercapacitor states of charge for the driving velocities 50km/h, 60km/h, and 70km/h are 0.9312, 0.8211, and 0.6573. The changes in the states of charge for the supercapacitor during the city-tour drive cycle are presented in Figure 5.29.

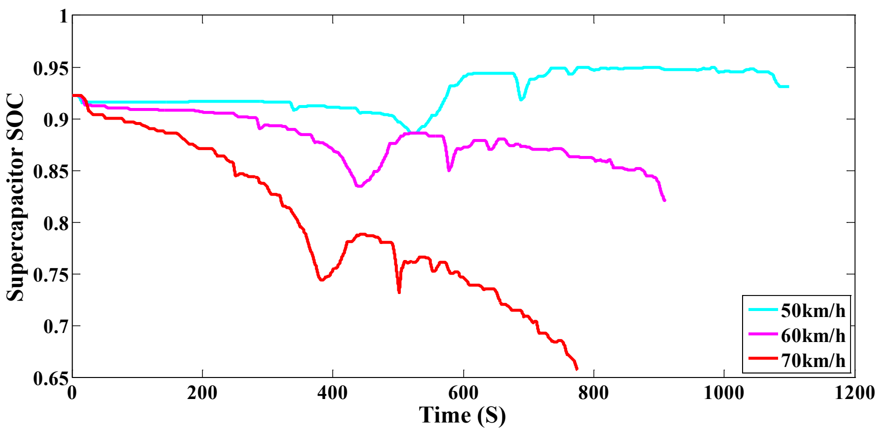

Figure 5.29 The supercapacitor states of charge in city-tour drive cycle using the optimal adaptive rule-based controller

Table 5.12 summarizes the total energy consumption of the battery and the supercapacitor during the city-tour drive cycles for the driving velocities (50, 60, and 70 Kilometres per hour) using the optimal adaptive rule-based controller. These results proved that the HESS with the optimal adaptive rule-based controller succeed in increasing the number of possible downhill drive cycles compared to the rule-based controller from 23.7 to 24.5 drive cycles in the driving velocities 50km/h and maintains the number of possible city-tour drive cycles in driving velocities 60km/h and 70km/h with 6.8 and 2.6 drive cycles.

Table 5.12 The HESS details in city-tour drive cycle using the optimal adaptive rule-based controller

	50km/h	***60km/h***	***70km/h***
$SOC_b(t)_{CPS}$	0.9212	0.9193	0.9191
$SOC_{sc}(t)_{CPS}$	0.9312	0.8211	0.6573
Battery Consumption	3.03%	3.23%	3.25%
Supercapacitor Consumption	-0.95%	10.98%	28.74%
No. Cycles	24.8	6.8	2.6

5.4.4 Standard Drive Cycles

This section presents the response of the HESS by using the optimal adaptive rule-based controller based on three different standard drive cycles, UDDS, NYCC, and Japan1015 drive cycle for the EV. The low load current is supplied by the battery and the supercapacitor while the supercapacitor supplied the peak load current and absorbed the regenerative energy during the deceleration. The values of the percentage of energy sharing between the battery and the supercapacitor are current are 0.22, 0.6, and 0.26 for UDDS, NYCC, and Japan1015 drive cycle respectively. The results of the HESS with the optimal adaptive rule-based controller for the EV are proved that the controller reduces the battery stress compared to single energy storage battery system and limit the battery current to (I_{b_max}) during the journey. Figure 5.30 illustrates the total EV load current, the battery current, and the supercapacitor current during the drive cycles (UDDS, NYCC, and Japan1015).

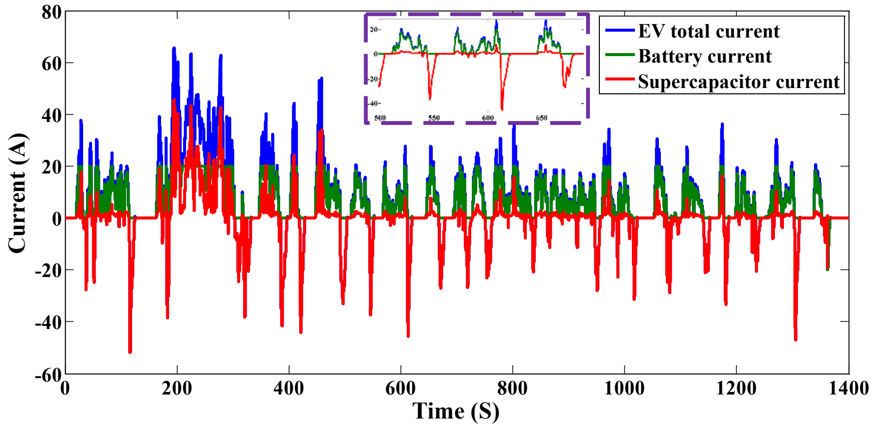

(a)

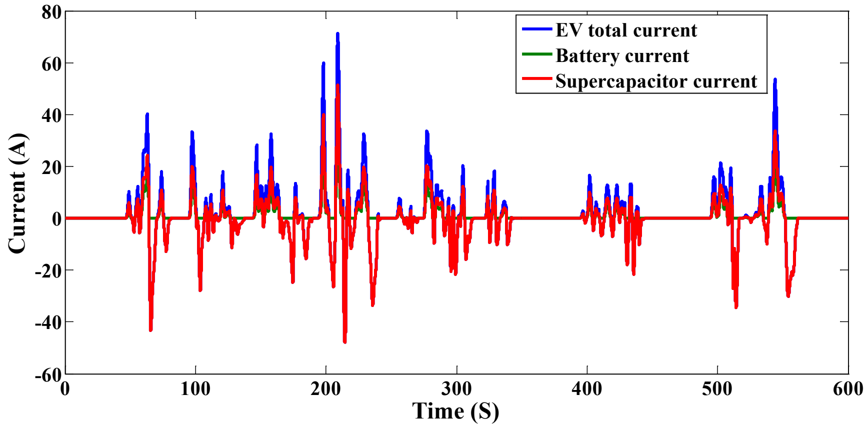

(b)

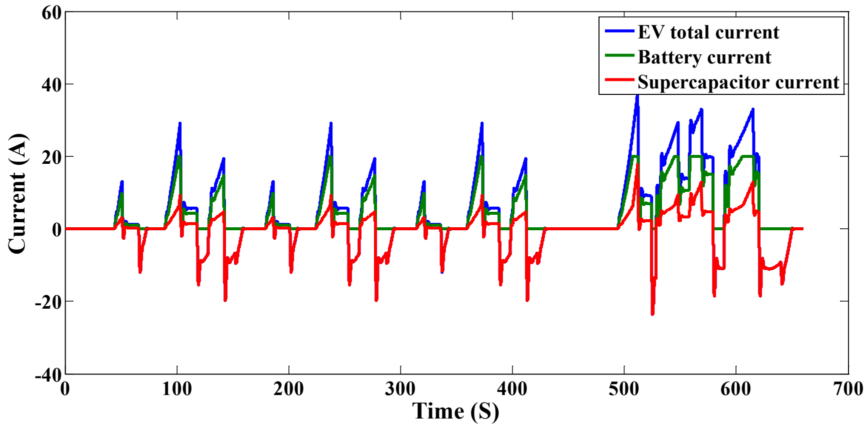

(c)

Figure 5.30 Total HESS currents based on standard drive cycle using the optimal adaptive rule-based controller (a) UDDS, (b) NYCC and (c) Japan1015

The changes of battery states of charge during (UDDS, NYCC, and Japan1015) drive cycles are presented in Figure 5.31. After a single drive cycle, the final battery states of charge are 0.9284, 0.9480, and 0.9431 for UDDS, NYCC, and Japan1015 drive cycles respectively. Furthermore, the battery energy consumption was decreased using the optimal rule-based controller compared with the rule-based controller and the single energy storage battery system in the three standard drive cycles.

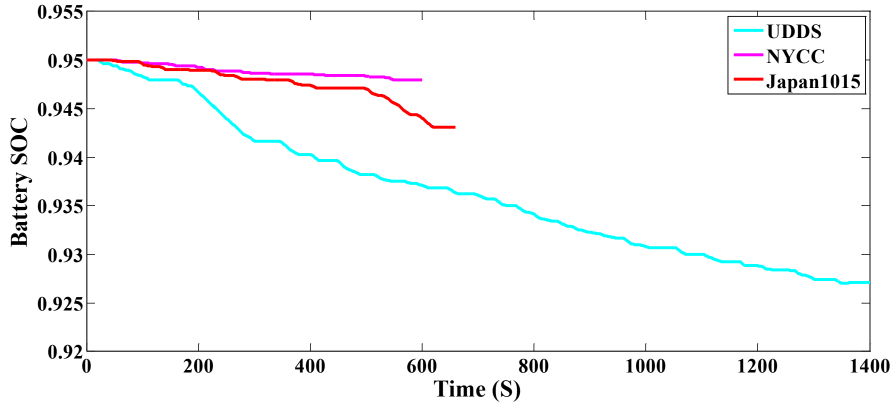

Figure 5.31 The battery states of charge in UDDS, NYCC, and Japan1015 drive cycles using the optimal adaptive rule-based controller

On the other hand, the final supercapacitor states of charge are 0.9214, 0.9289, and 0.9345 for UDDS, NYCC, and Japan1015 drive cycles, respectively. These results are proved the supercapacitor of the HESS with optimal adaptive rule-based controller earns energy during the Japan1015 drive cycles. The changes in the supercapacitor states during UDDS, NYCC, and Japan1015 drive cycles are presented in Figure 5.32.

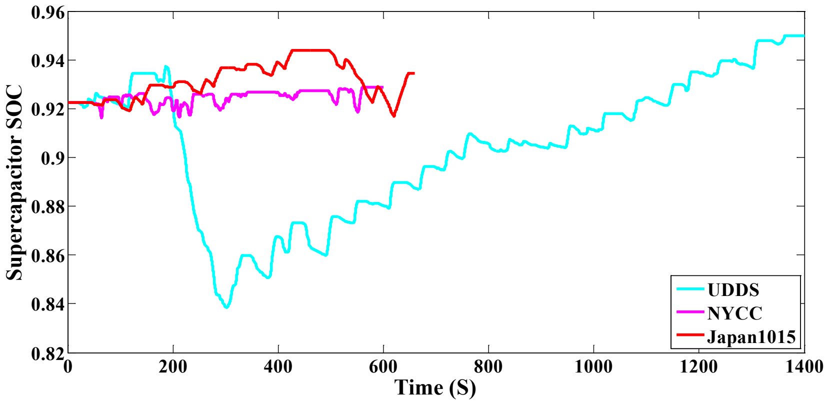

Figure 5.32 The supercapacitor states of charge in UDDS, NYCC, and Japan1015 drive cycles using the optimal adaptive rule-based controller

Table 5.13 summarizes the total energy consumption for the battery and the supercapacitor of the HESS by using the optimal adaptive rule-based controller. The battery energy consumptions for UDDS, NYCC, and Japan1015 drive cycles are 2.27%, 0.21%, and 0.73%. The presented results are proved the optimal adaptive rule-based controller succeed to reduce the battery energy consumption compared with the rule-based controller and the single energy storage battery system for all drive cycles. Furthermore, in UDDS, the number of drive cycles are increased by using the optimal adaptive rule-based to 33 compared with 29 in the rule-based controller. Likewise, in the NYCC, the number of drive cycles are increased by using the optimal adaptive rule-based to 357 compared with 227 in the rule-based controller. Also, in Japan1015 drive cycle, the number of drive cycles are increased by using the optimal adaptive rule-based to 102.7 compared with 95 in the rule-based controller.

Table 5.14 summarizes the comparison between the energy consumption on the single energy storage battery system ($\boldsymbol{EngCons_{BVE}}$) and the battery energy consumption on the HESS using the optimal adaptive rule-based controller($\boldsymbol{EngCons_{HESS}}$).

Table 5.13 The HESS details in UDDS, NYCC, and Japan1015 drive cycles using the optimal adaptive rule-based controller

	UDDS	***NYCC***	***Japan1015***
$\mathrm{SOC_b(t)_{CPS}}$	0.9284	0.9480	0.9431
$\mathrm{SOC_{sc}(t)_{CPS}}$	0.9214	0.9289	0.9345
Battery Consumption	2.27%	0.21%	0.73%
Supercapacitor Consumption	0.1%	-0.7%	-1.3%
Cycles No.	33	357	102.7

The energy variance (*EngVar*) and the *Battery Energy Reduction Ratio* demonstrate the effectiveness of the HESS using the optimal adaptive rule-based controller in terms of decrease the battery stress and prolong the battery aging.

Table 5.14 The battery energy reduction ratio using the optimal adaptive rule-based controller

Drive cycle	***Speed***	$\boldsymbol{EngCons_{BVE}}$	$\boldsymbol{EngCons_{HESS}}$ ***Optimal adaptive***	***EngVar***	***Battery Energy Reduction Ratio***
Uphill	50Km/h	2.04%	1.43%	0.61%	29.9%
	60Km/h	2.19%	1.27%	0.92%	42%
	70Km/h	2.42%	1.16%	1.26%	52%
Downhill	50Km/h	0.76%	0.3%	0.46%	60.5%
	60Km/h	0.86%	0.52%	0.34%	39.5%
	70Km/h	1.04%	0.62%	0.42%	40.4%
City tour	50Km/h	3.53%	3.03%	0.5%	15.2%
	60Km/h	4.15%	3.23%	0.92%	22.2%
	70Km/h	4.68%	3.25%	1.43%	30.6%
Standard drive cycles	UDDS	3.46%	2.27%	1.19%	34.4%
	NYCC	0.57%	0.21%	0.36%	63.2%
	Japan1015	1.07%	0.73%	0.34%	31.8%

5.5 The Results of the Fuzzy Adaptive Rule-Based Controller for HESS

The results of the HESS with the Fuzzy adaptive rule-based controller for the real drive cycles and the standard cycles are presented in this section. The total current of EV, the battery current, and the supercapacitor current are investigated. The state of charge for the battery and the supercapacitor were measured at the end of the drive cycles. The total percentage of the battery and the supercapacitor energy consumption were calculated using Equation 4.12. The main tasks of the fuzzy adaptive rule-based controller are to limit the battery current $I_b(t)$ to a maximum value I_{b_max} and obtain the energy sharing percentage R between the battery and the supercapacitor online during the selected journey. Section 3.3.2 described the design and the working principles of the fuzzy adaptive rule-based controller in detail.

5.5.1 Uphill Drive Cycle

In this drive cycle, the HESS with the fuzzy adaptive rule-based controller supplied the total load current from the battery and the supercapacitor while the supercapacitor absorbed the regenerated energy. Figure 5.33 shows the total load currents of the EV, the battery current, and the supercapacitor current based on the uphill drive cycle in different driving velocities (50, 60, and 70 Kilometres per hour). The battery and the supercapacitor are sharing to supply the low load current while the supercapacitor is supplying the peak load current. The energy sharing percentage between battery and supercapacitor R in this drive cycle was calculated instantly during the journey. The sharing percentage is a variable value which depends on the road slope and vehicle speed.

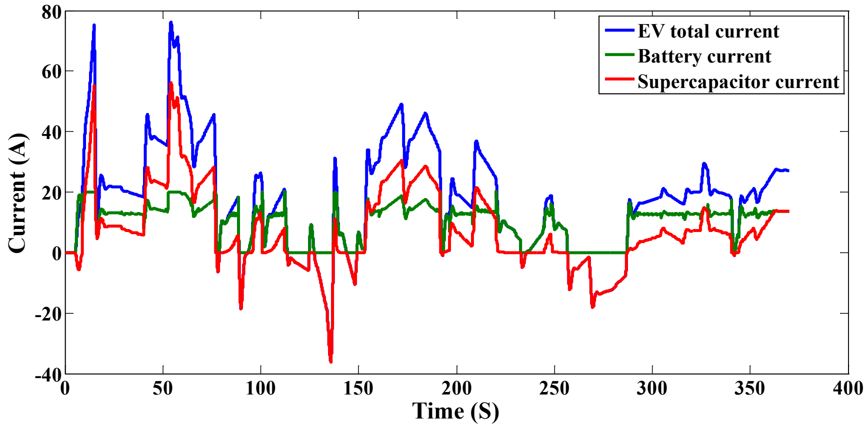

(a)

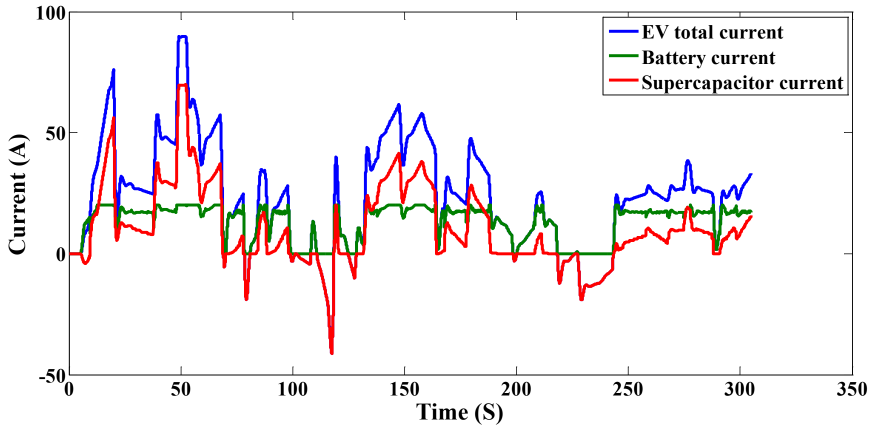

(b)

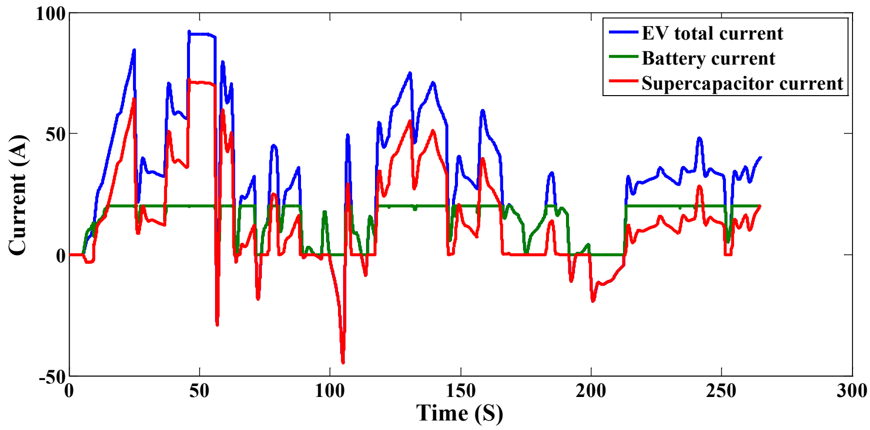

(c)

Figure 5.33 Total HESS currents based on uphill drive cycle using the fuzzy adaptive rule-based controller (a) 50km/h, (b) 60km/h and (c) 70km/h

Figure 5.34 represents the changes of the battery states of charge during the uphill drive cycle based on the fuzzy adaptive rule-based controller. The final battery states of charge are 0.9396, 0.9390, and 0.9391 for the driving velocities (50, 60, and 70 Kilometres per hour). The fuzzy adaptive rule-based controller is succeed to limit the battery current to (I_{b_max}). In this drive cycle, the battery energy consumption is decreased compared with the optimal adaptive rule-based controller and the rule-based controller.

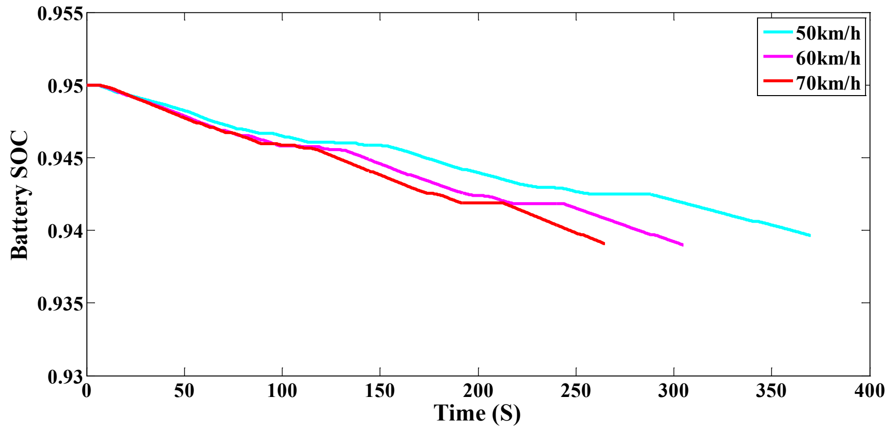

Figure 5.34 The battery states of charge in an uphill drive cycle using the fuzzy adaptive rule-based controller

Furthermore, Figure 5.35 presents the changes in the states of charge for the supercapacitor during the uphill drive cycle at the different velocities. The supercapacitor discharges to supply the load current together with the battery while the supercapacitor charges by absorbing the regenerative energy during the braking. The final values of the supercapacitor states of charge for the driving velocities (50, 60, and 70 Kilometres per hour) are 0.7315, 0.7005, and 0.6209 respectively. These results are proved the energy consumptions of the supercapacitor is increased by increasing the vehicle speed.

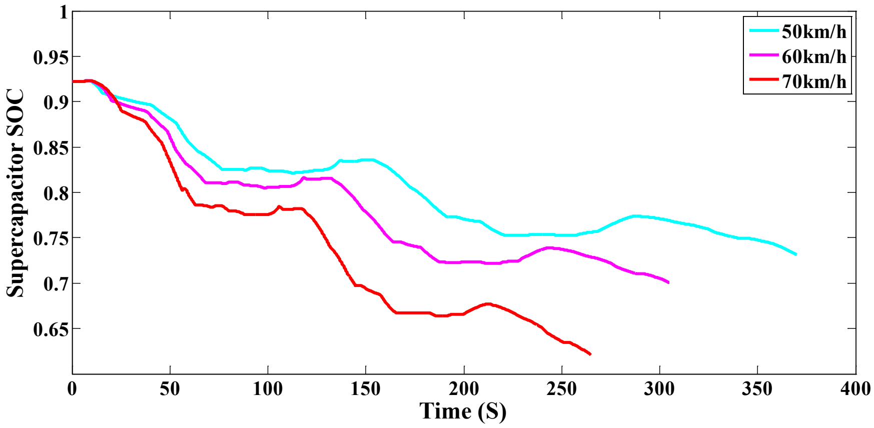

Figure 5.35 The supercapacitor states of charge in an uphill drive cycle using the fuzzy adaptive rule-based controller

Table 5.15 presents the total energy consumption of HESS with the fuzzy adaptive rule-based controller during the uphill drive cycles for the driving velocities (50, 60, and 70 Kilometres per hour). These results prove that the fuzzy adaptive rule-based controller is consuming more energy from the supercapacitor than the optimal adaptive rule-based controller for the uphill drive cycle. Furthermore, the number of possible uphill drive cycles of HESS using the fuzzy adaptive rule-based controller were 3.6, 3.1, and 2.3 for the driving velocities (50, 60, and 70 Kilometres per hour) respectively.

Table 5.15 The HESS details in uphill drive cycle using the fuzzy adaptive rule-based controller

	50km/h	***60km/h***	***70km/h***
$SOC_b(t)_{CPS}$	0.9396	0.9390	0.9391
$SOC_{sc}(t)_{CPS}$	0.7315	0.7005	0.6209
Battery Consumption	1.09%	1.16%	1.15%
Supercapacitor Consumption	20.70%	24.06%	32.69%
Cycles No.	3.6	3.1	2.3

5.5.2 Downhill Drive Cycle

The HESS currents of the EV based on the downhill drive cycle in different driving velocities (50, 60, and 70 Kilometres per hour) were presented in Figure 5.36. The battery and the supercapacitor are supplied the low load current while the supercapacitor supplies the peak load current. The energy sharing percentage between the battery and supercapacitor is estimated instantly during the journey. These results are proved the fuzzy adaptive controller is succeed to limit the battery current to (I_{b_max}).

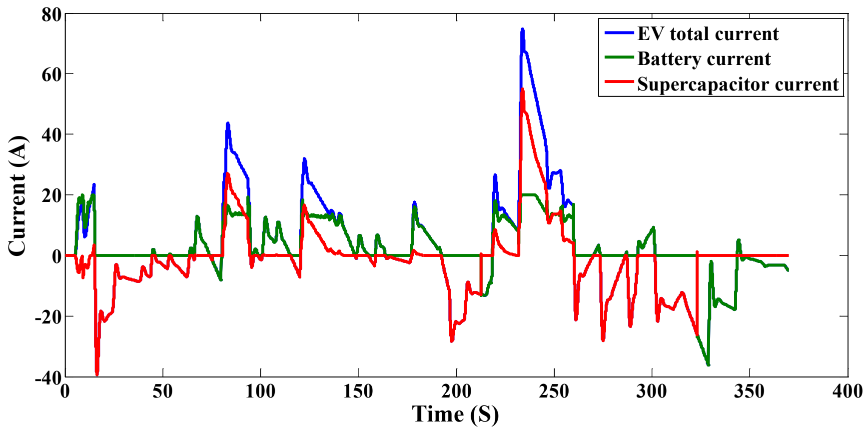

(a)

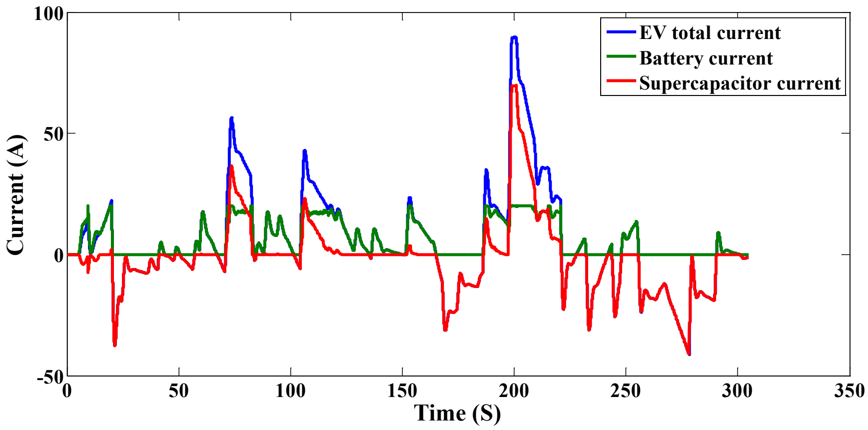

(b)

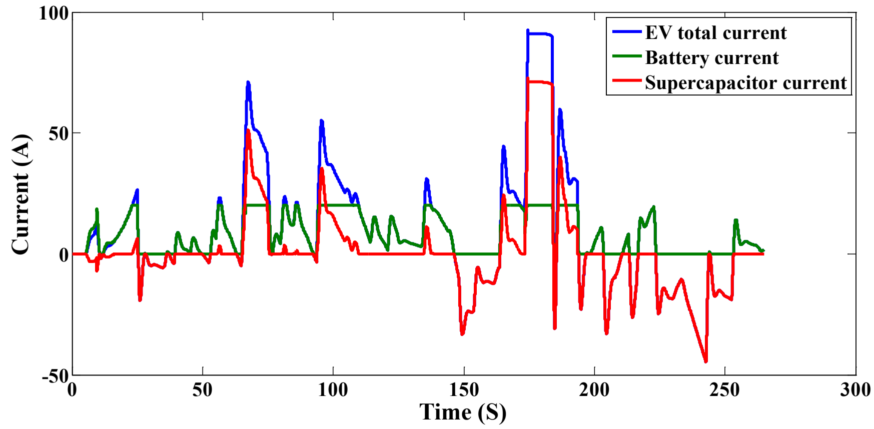

(c)

Figure 5.36 Total HESS currents based on a downhill drive cycle using the fuzzy adaptive rule-based controller (a) 50km/h, (b) 60km/h and (c) 70km/h

Figure 5.37 presents the changes of the battery states of charge during the downhill drive cycle with different speeds. The final values of the battery states of charge for the driving velocities (50, 60, and 70 Kilometres per hour) are 0.9471, 0.9448, and 0.9441. In the downhill drive cycle, the battery energy consumptions of the HESS with the fuzzy adaptive rule-based controller for the driving velocities (50, 60, and 70 Kilometres per hour) are 0.31%, 0.55% and 0.62% respectively. These results proved the battery energy consumption of the HESS using the fuzzy adaptive controller is bigger than the consumption of the HESS with the optimal adaptive controller on the downhill drive cycle.

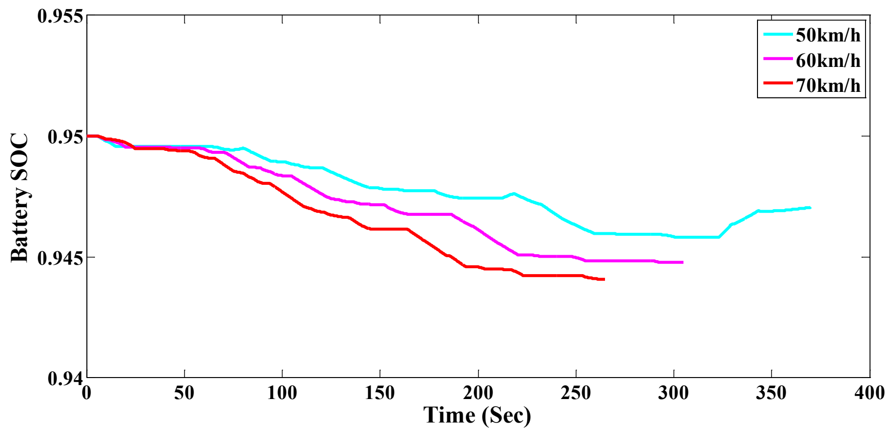

Figure 5.37 The battery states of charge in a downhill drive cycle using the fuzzy adaptive rule-based controller

Otherwise, Figure 5.38 illustrates the changes in the states of charge of the supercapacitor during the downhill drive cycle. The final value of the supercapacitor states of charge are 0.95, 0.9461, and 0.9030 for the driving velocities 50km/h, 60km/h, and 70km/h. These results prove the HESS earns more energy during the downhill drive cycle.

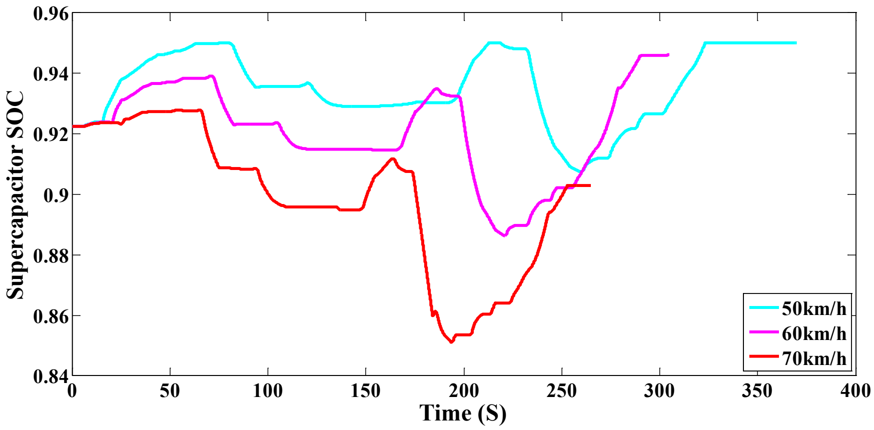

Figure 5.38 The supercapacitor states of charge in a downhill drive cycle using the fuzzy adaptive rule-based controller

Table 5.16 presents the total energy consumption of HESS with the fuzzy adaptive rule-based controller during the downhill drive cycles for the driving velocities (50, 60, and 70 Kilometres per hour). These results demonstrate that the fuzzy adaptive rule-based controller consumes less energy from the supercapacitor compared with the optimal adaptive rule-based controller for the downhill drive cycle. Furthermore, the number of possible downhill drive cycles for the HESS using the fuzzy adaptive rule-based controller are 242, 136, and 35 for the driving velocities (50, 60, and 70 Kilometres per hour) respectively. The total performance of the fuzzy adaptive controller is less than the optimal adaptive controller in terms of the number of the possible downhill drive cycles.

Table 5.16 The HESS details in downhill drive cycle using the fuzzy adaptive rule-based controller

	50km/h	*60km/h*	*70km/h*
$SOC_b(t)_{CPS}$	0.9471	0.9448	0.9441
$SOC_{sc}(t)_{CPS}$	0.95	0.9461	0.9030
Battery Consumption	0.31%	0.55%	0.62%
Supercapacitor Consumption	-3%	-2.57%	2.1%
Cycles No.	242	136	35

5.5.3 City-tour Drive Cycle

In the city-tour drive cycle, the HESS with fuzzy adaptive rule-based controller is supplied the load current by using the battery and the supercapacitor. The supercapacitor using to absorb the regenerated energy. Figure 5.39 shows the total load currents of the EV, the battery current, and the supercapacitor current based on the city-tour drive cycle in different driving velocities (50, 60, and 70 Kilometres per hour). The energy sharing percentage between the battery and the supercapacitor R is variable and calculated during the journey. The performance of the HESS elucidated the fuzzy adaptive rule-based controller is limiting the battery current to (I_{b_max}).

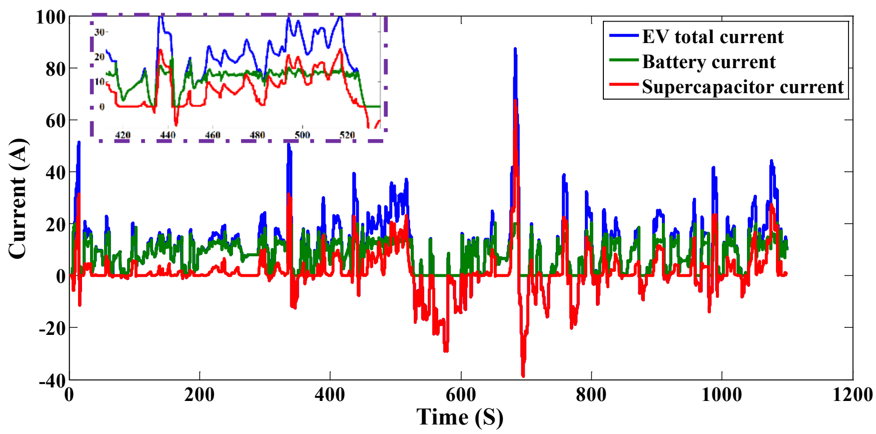

(a)

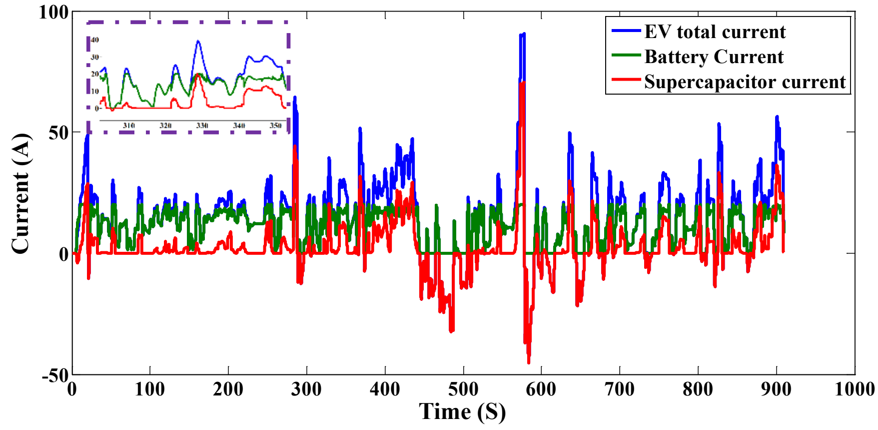

(b)

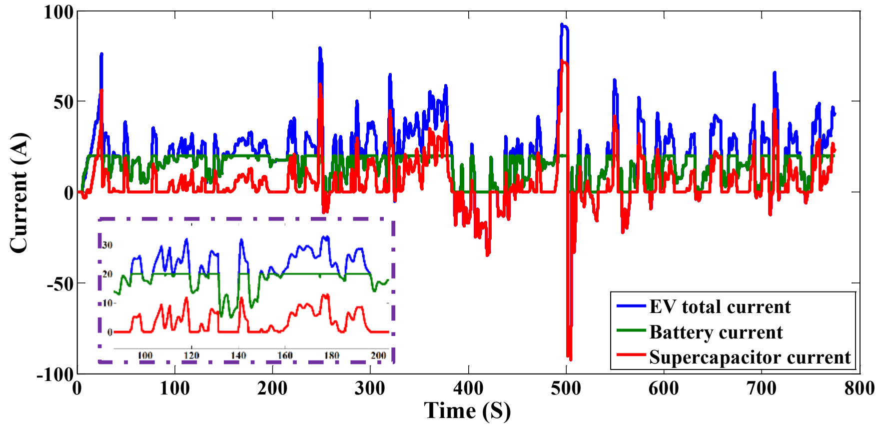

(c)

Figure 5.39 Total HESS currents based on city-tour drive cycle using the fuzzy adaptive rule-based controller (a) 50km/h, (b) 60km/h and (c) 70km/h

The battery states of charge during the city-tour drive cycle are illustrated in Figure 5.40. The final values of the battery states of charge for the driving velocities (50, 60, and 70 Kilometres per hour) are 0.9258, 0.9215, and 0.9193 respectively. Furthermore, the battery energy consumptions of the HESS with the fuzzy adaptive controller are less than the optimal adaptive controller in the city-tour drive cycles. In the driving speed 50km/h the battery energy consumption is 2.55% and the battery consumption is 3% for the driving speed 60km/h while the battery energy consumption for the driving velocities 70km/h is 3.23%.

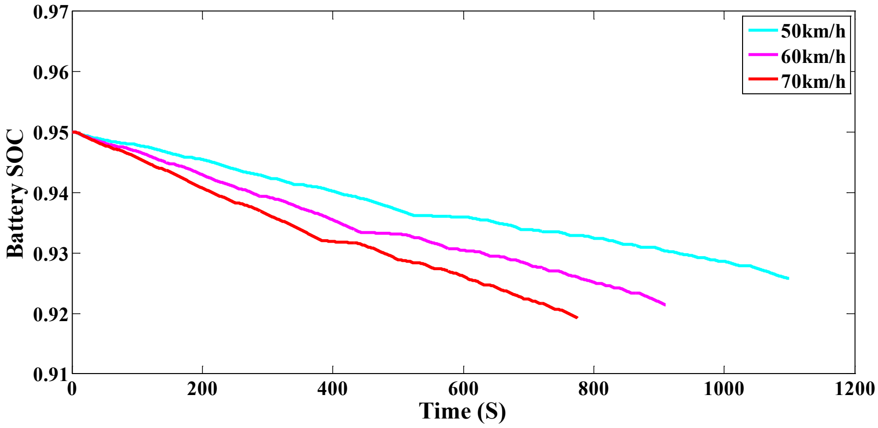

Figure 5.40 The battery states of charge in city-tour drive cycle using the fuzzy adaptive rule-based controller

On the other hand, Figure 5.29 presents the changes in the states of charge for the supercapacitor during the city-tour drive cycle. The final values of the supercapacitor states of charge for the driving velocities 50km/h, 60km/h, and 70km/h are 0.8220, 0.7650, and 0.6531. The results prove the supercapacitor energy consumption in the fuzzy adaptive controller increased proportionally with driving velocity.

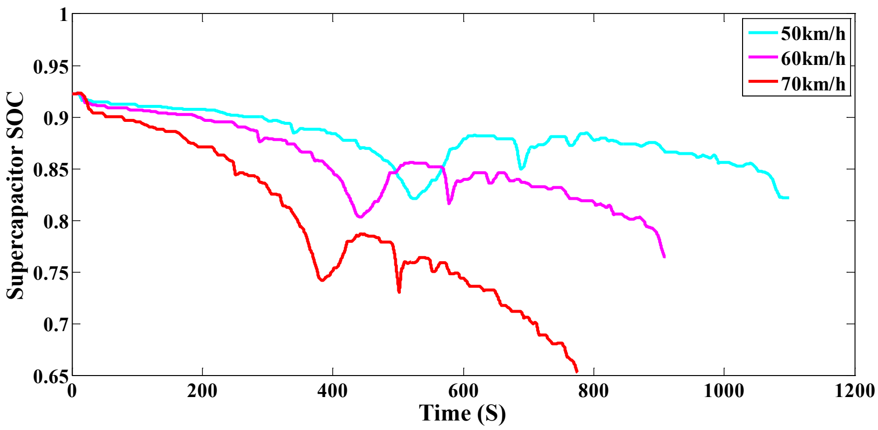

Figure 5.41 The supercapacitor states of charge in city-tour drive cycle using the fuzzy adaptive rule-based controller

Table 5.17 presents the total energy consumption for the battery and the supercapacitor during the city-tour drive cycles for the driving velocities (50, 60, and 70 Kilometres per hour) using the fuzzy adaptive rule-based controller. The total supercapacitor energy consumption is 10.89%, 17.06%, and 29.2% for the driving velocities (50, 60, and 70 Kilometres per hour). The number of the possible city-tour drive cycles in the fuzzy adaptive controller are 6.9, 4.4, and 2.6% for the driving velocities (50, 60, and 70 Kilometres per hour) respectively. The performance of the HESS with the optimal adaptive controller is better than the HESS with the fuzzy adaptive controller in terms of the number of the possible city-tour drive cycles.

Table 5.17 The HESS details in city-tour drive cycle using the fuzzy adaptive rule-based controller

	50km/h	***60km/h***	***70km/h***
$\mathrm{SOC_b(t)_{CPS}}$	0.9258	0.9215	0.9193
$\mathrm{SOC_{sc}(t)_{CPS}}$	0.8220	0.7650	0.6531
Battery Consumption	2.55%	3%	3.23%
Supercapacitor Consumption	10.89%	17.06%	29.2%
Cycles No.	6.9	4.4	2.6

5.5.4 Standard Drive Cycles

The responses of the HESS using the fuzzy adaptive rule-based controller based on three different standard drive cycles UDDS, NYCC, and Japan1015 drive cycle are analyzed in this section. The percentage of the energy sharing between the battery and the supercapacitor in the low load current is variable and it is estimated instantly during the drive cycle. The value of the energy sharing percentage between the battery and the supercapacitor depends on the vehicle speed. Figure 5.30 illustrates the total load currents of the EV, the battery current, and the supercapacitor current during the drive cycles (UDDS, NYCC, and Japan1015). The results of the HESS using the fuzzy adaptive rule-based controller for the EV demonstrate that the controller was succeed in reducing the battery stress compared to a single energy storage battery system and limited the battery current to (I_{b_max}) during the journey.

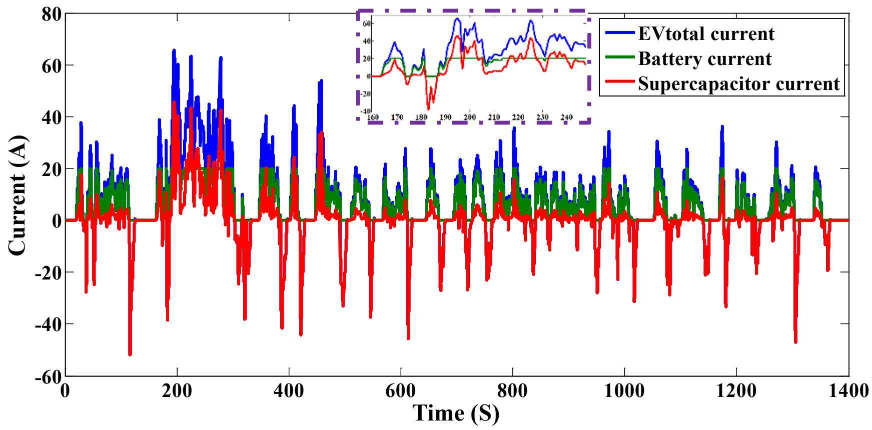

(a)

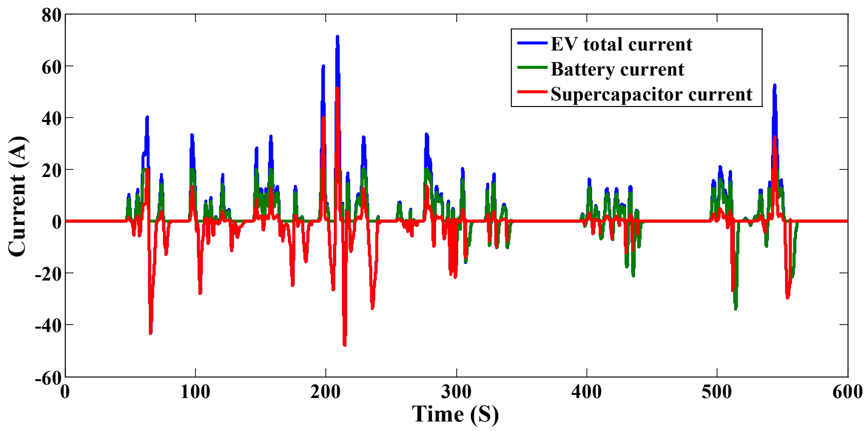

(b)

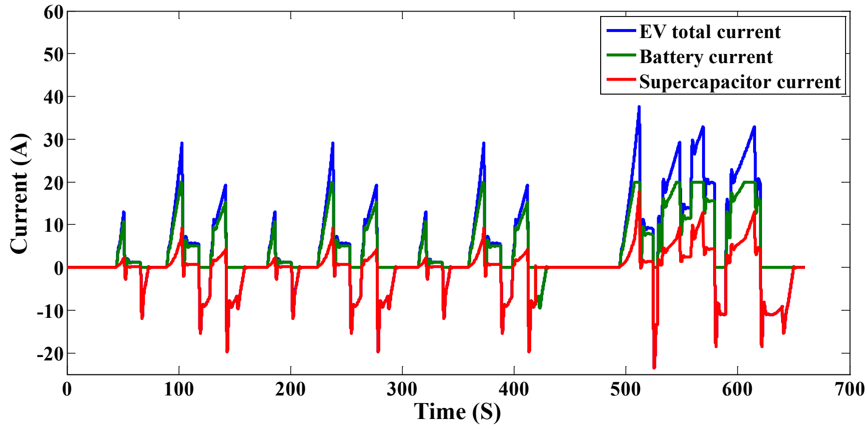

(c)

Figure 5.42 Total HESS currents based on standard drive cycle using the fuzzy adaptive rule-based controller (a) UDDS, (b) NYCC and (c) Japan1015

Figure 5.43 illustrated the changes of battery states of charge during (UDDS, NYCC, and Japan1015) drive cycles using the fuzzy adaptive controller. After a single drive cycle the final values of the battery states of charge are 0.9275, 0.9470, and 0.9425 for UDDS, NYCC, and Japan1015 drive cycles respectively. Furthermore, the battery energy consumption of the HESS using the fuzzy adaptive rule-based controller was increased comparing with the battery energy consumption of the HESS using the optimal adaptive controller. The battery energy consumption for UDDS, NYCC, and Japan1015 drive cycles is 2.37%, 0.32%, and 0.79%.

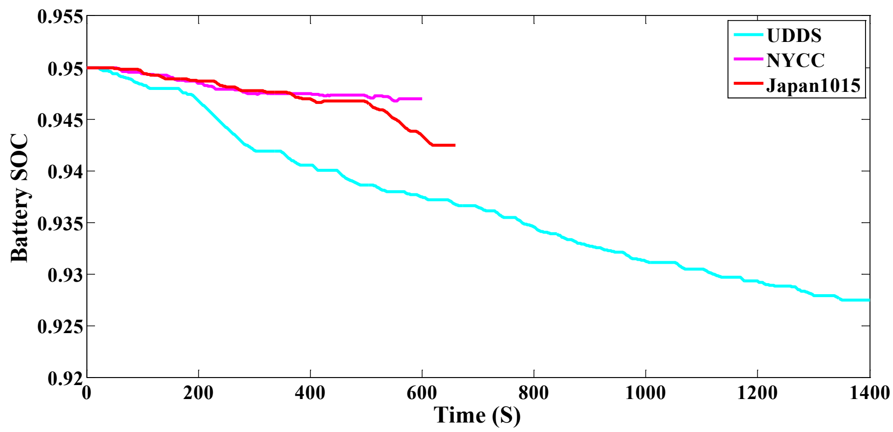

Figure 5.43 The battery states of charge in UDDS, NYCC, and Japan1015 drive cycles using the fuzzy adaptive rule-based controller

Otherwise, the final values of the supercapacitor states of charge for UDDS, NYCC, and Japan1015 drive cycles are 0.9291, 0.95, and 0.9453, respectively. These results elucidated the supercapacitor of the HESS using the fuzzy adaptive rule-based controller earns energy during all tested drive cycles. Figure 5.44 presents the changes in the states for supercapacitor during UDDS, NYCC, and Japan1015 drive cycle.

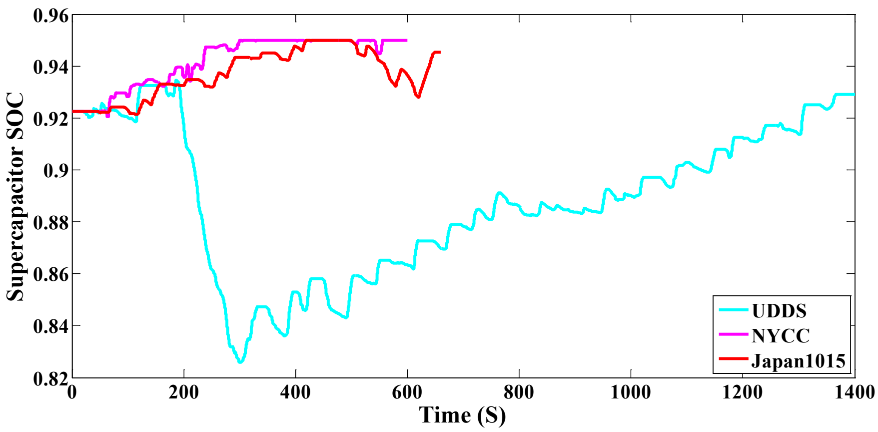

Figure 5.44 The supercapacitor states of charge in UDDS, NYCC, and Japan1015 drive cycles using the fuzzy adaptive rule-based controller

Table 5.18 summarizes the total energy consumption for the battery and the supercapacitor of HESS using the fuzzy adaptive rule-based controller during UDDS, NYCC, and Japan1015 drive cycles. The battery energy consumptions using the fuzzy adaptive controller for UDDS, NYCC, and Japan1015 drive cycles are increased compared with the battery energy consumptions using the optimal adaptive controller. Furthermore, in UDDS the number of drive cycles of the HESS was decreased using the fuzzy adaptive controller to 31.6 compared with 33 using the optimal adaptive controller. Likewise, in NYCC the number of drive cycles using the optimal adaptive rule-based controller decreased to 234 compared to 357 using the optimal adaptive controller. Besides, in Japan1015 drive cycle the number of drive cycles decreased by using the fuzzy adaptive controller to 95 compared with 102.7 in the optimal adaptive controller.

Table 5.18 The HESS details in UDDS, NYCC, and Japan1015drive cycles using the fuzzy adaptive rule-based controller

	UDDS	***NYCC***	***Japan1015***
$\mathrm{SOC_b(t)_{CPS}}$	0.9275	0.9470	0.9425
$\mathrm{SOC_{sc}(t)_{CPS}}$	0.9291	0.95	0.9453
Battery Consumption	2.37%	0.32%	0.79%
Supercapacitor Consumption	-0.73%	-3%	-2.5%
Cycles No.	31.6	234	95

Table 5.19 summarizes the comparison between the energy consumption on the single energy storage battery system ($\boldsymbol{EngCons_{BVE}}$) and the battery energy consumption on the HESS using the fuzzy adaptive rule-based controller($\boldsymbol{EngCons_{HESS}}$). The energy variance (*EngVar*) and the *Battery Energy Reduction Ratio* demonstrate the effectiveness of the HESS using the fuzzy adaptive rule-based controller in terms of decrease the battery stress and prolong the battery aging.

Table 5.19 The battery energy reduction ratio using the fuzzy adaptive rule-based controller

Drive cycle	***Speed***	$EngCons_{BVE}$	$EngCons_{HESS}$ *Fuzzy adaptive*	$EngVar$	***Battery Energy Reduction Ratio***
Uphill	50Km/h	2.04%	1.09%	0.95%	46.6%
	60Km/h	2.19%	1.16%	1.03%	47%
	70Km/h	2.42%	1.15%	1.27%	52.5%
Downhill	50Km/h	0.76%	0.31%	0.45%	59.2%
	60Km/h	0.86%	0.55%	0.31%	36%
	70Km/h	1.04%	0.62%	0.42%	40.4%
City tour	50Km/h	3.53%	2.55%	0.98%	27.8%
	60Km/h	4.15%	3%	1.15%	27.7%
	70Km/h	4.68%	3.23%	1.45%	31%
Standard drive cycles	UDDS	3.46%	2.37%	1.09%	31.5%
	NYCC	0.57%	0.32%	0.25%	44.9%
	Japan1015	1.07%	0.79%	0.28%	26.2%

5.6 Chapter Summary

This chapter presents the results of the proposed controller of HESS for EV. The results of the single energy storage system of the EV are presented for the selected real drive cycles and the standard drive cycles. Furthermore, the results of the proposed rule-based controller of HESS for the EV are presented and discussed in detail. In addition, the performance of the proposed optimal adaptive rule-based controller and the fuzzy adaptive rule-based controller are carried out and compared with the rule-based controller. The performances of the proposed controllers are validated using the three real drive cycles (uphill, downhill, and city-tour) at three different speeds (50,60, and 70) Km/h.

Moreover, three standard drive cycles (UDDS, NYCC, and Japan1015 drive cycle) are implemented to validate the performances of the proposed controllers. Table 5.19 presents the number of possible drive cycles using the rule-based controller, the optimal adaptive controller, and the fuzzy adaptive controller

Table 5.20 The number of the possible drive cycles using the proposed controllers

Drive cycle	***Speed***	***The Rule-Based***	***Optimal Adaptive Rule-Based***	***Fuzzy Adaptive Rule-Based***
Uphill	50Km/h	6.6	6.6	3.6
	60Km/h	3.6	3.6	3.1
	70Km/h	2.3	2.3	2.3
Downhill	50Km/h	242	250	242
	60Km/h	132	144	136
	70Km/h	35	35	35
City tour	50Km/h	23.7	24.8	6.9
	60Km/h	6.8	6.8	4.4
	70Km/h	2.6	2.6	2.6
Standard drive cycles	UDDS	29	33	31.6
	NYCC	227	357	234
	Japan1015	88	102.7	95

CHAPTER 6

CONCLUSION AND FUTURE WORK

6.1 Conclusion

The electric vehicle in the market uses batteries as the main energy source. The batteries in the EV have weaknesses in terms of the energy delivery and the life-cycle. Researchers tried to propose a hybrid energy storage system via the combination of two different types of energy storage devices (batteries and supercapacitor). Batteries are used as the main storage device due to their high energy density while the supercapacitor are used as an auxiliary storage device due to their high power density. There are many studies presented in the literature proposed several types of hybrid topologies of energy storage devices.

This thesis presents the proposed semi-active topology and the energy management system of the hybrid energy storage system for the electric vehicles. The proposed HESS is designed by connecting the battery directly to the DC bus while, the supercapacitor is connected to the DC bus via a bidirectional DC-DC converter. This topology aims to control the power flow of the supercapacitor by manipulating the duty cycle of the PWM of the bidirectional DC-DC converter.

In Hybrid energy storage applications, the rule-based strategy is commonly used as the energy management system to control the power flow to the DC-bus. The rule-based strategy lacks the ability to find the optimal solution compared with the optimization energy management strategy. The optimization methods are difficult to implement in a real-time control system due to the long computational time. Therefore, this research proposes an adaptive rule-based energy management strategy to control the power flow of the HESS for the electric vehicles. The road slope is involved in this work to estimate the energy consumption for the electric vehicle in a single drive cycle. The Contour Positioning System (CPS) is used to extract the road slope of the selected drive cycle along the journey. The characteristics of the road in the selected drive cycles are used to adapt the proposed energy management system of the HESS.

Three control layers are used in the proposed energy management strategy in this research. Three different types of rule-based controllers are proposed and investigated. The standard rule-based controller, the optimal adaptive rule-based controller, and the fuzzy adaptive rule-based controller are implemented to manage the energy flow of the HESS for the EV while the linear quadratic regulator is used to drive the DC-DC converter. The parameters of the standard rule-based controller are fixed and not related to the topographical conditions of the selected journey. The parameters of the optimal adaptive rule-based controller are modified after selecting the desired destination and before the movement of the electric vehicle. The parameters of the fuzzy adaptive rule-based controller are modified continuously along the journey.

The proposed control algorithms are tested in three real drive cycles (uphill, downhill, and city-tour) at three different speeds (50, 60, and 70 kilometres per hour) and in three different standard drive cycles (UDDS, NYCC, and Japan1015). The results demonstrate the variance of the energy consumption for the electric vehicle by considering and ignoring the topographical conditions. The results of the simulations prove that an uphill drive consumes more energy while the regenerative energy increases when going downhill. It is also found that the road slope has a limited effect for a city tour drive cycle. The state of charge and the energy consumption of the battery and supercapacitor are inspected for all drive cycles with the proposed controllers.

Furthermore, the results of the proposed HESS with the rule-based controller prove the controller success to reduce the current peak and the energy consumption of the battery compared with the single energy storage battery system. On the other hand, the proposed HESS with the fuzzy adaptive rule-based controller succeeds to reduce the battery current peak and the battery consumption while the number of possible drive cycles decreases compared with those of the rule-based controller and the optimal adaptive controller. Moreover, the proposed HESS with the optimal adaptive controller reduces the battery current peak and extends the number of possible drive cycles compared with those of the rule-based controller and the fuzzy adaptive controller. The proposed controllers extend the battery life-time by limiting the battery demand current.

6.2 Limitations and Future Work

The limitations of the proposed optimal adaptive controller are that it requires the driver to define the desired destination and the driving velocities before the vehicle starts moving. However, there is a difficulty in determining the appropriate vehicle speed for the selected journey by the driver. In addition, the road slope, the road situation, the weather conditions, and the traffic are the main factors to determine the vehicle speed during the journey. Furthermore, changing the destination path or the vehicle speed during the journey leads to a change in the total energy consumption of the drive cycle which requires a new calculation for the energy sharing percentage between the battery and the supercapacitor.

For future work, developing an algorithm to estimate the proper vehicle speed of the selected journey according to the topographical information, the weather conditions, and traffic conditions will improve the estimation of the energy consumption which in turn will lead to improve the accuracy of the energy sharing percentage between the battery and the supercapacitor to extend the number of the possible drive cycles. Moreover, in case of changing the destination, the road path, or the vehicle speed during the journey, the optimal adaptive algorithm should be improved to update the values of the controller parameters automatically. In addition, to validate whether the proposed HESS and the energy management system are suitable to perform practically, an experimental work for a down-scale prototype of HESS and the electric vehicle has to be carried out.

LIST OF REFERENCES

ABDULLAH, M., TAN, C. & YATIM, A. A simulation study of hybrid wind-ultracapacitor energy conversion system. 2014 IEEE Conference on Energy Conversion (CENCON), 2014 Johor Bahru, Malaysia. IEEE, 265-270.

ABDULLAH, M. A., TAN, C. W., YATIM, A. H., AL-MOTHAFAR, M. & RADAIDEH, S. M. 2012. Input current control of boost converters using current-mode controller integrated with linear quadratic regulator. *International Journal of Renewable Energy Research (IJRER),* 2**,** 262-268.

AHARON, I. & KUPERMAN, A. 2011. Topological overview of powertrains for battery-powered vehicles with range extenders. *IEEE Transactions on Power Electronics,* 26**,** 868-876.

AHMED, R., GAZZARRI, J., ONORI, S., HABIBI, S., JACKEY, R., RZEMIEN, K., TJONG, J. & LESAGE, J. 2015. Model-based parameter identification of healthy and aged li-ion batteries for electric vehicle applications. *SAE International Journal of Alternative Powertrains,* 4**,** 233-247.

AL SAKKA, M., GUALOUS, H., VAN MIERLO, J. & CULCU, H. 2009. Thermal modeling and heat management of supercapacitor modules for vehicle applications. *Journal of Power Sources,* 194**,** 581-587.

ALOBEIDLI, K. & KHADKIKAR, V. 2018. A New Ultracapacitor State of Charge Control Concept to Enhance Battery Lifespan of Dual Storage Electric Vehicles. *IEEE Transactions on Vehicular Technology,* 67**,** 10470-10481.

ARMENTA, J., NúñEZ, C., VISAIRO, N. & LáZARO, I. 2015. An advanced energy management system for controlling the ultracapacitor discharge and improving the electric vehicle range. *Journal of Power Sources,* 284**,** 452-458.

BALOG, R. S. & DAVOUDI, A. 2013. Batteries, Battery battery Management Battery Management, and Battery battery Charging Technology battery charging techniques. *Transportation Technologies for Sustainability.* Springer.

BAMPOULAS, A., GIANNAKIS, A., TSAKLIDOU, S. & KARLIS, A. Modeling, simulation and performance evaluation of a low-speed battery electric vehicle. 2016 Eleventh International Conference on Ecological Vehicles and Renewable Energies (EVER), 2016. IEEE, 1-8.

BARSALI, S. & CERAOLO, M. 2002. Dynamical models of lead-acid batteries: implementation issues. *IEEE Transactions on energy conversion,* 17**,** 16-23.

BECKER, H. I. 1957. Low voltage electrolytic capacitor. Google Patents.

BERTRAND, N., SABATIER, J., BRIAT, O. & VINASSA, J.-M. 2010. Embedded fractional nonlinear supercapacitor model and its parametric estimation method. *IEEE Transactions on industrial electronics,* 57**,** 3991-4000.

BHARATH, K. V. S. & PANDEY, K. Fuzzy-Based Multi-Objective Optimization for Subjection and Diagnosis of Hybrid Energy Storage System of an Electric Vehicle. Proceeding of International Conference on Intelligent Communication, Control and Devices, 2017. Springer, 299-307.

BORIBOONSOMSIN, K. & BARTH, M. 2009. Impacts of road grade on fuel consumption and carbon dioxide emissions evidenced by use of advanced navigation systems. *Transportation Research Record,* 2139**,** 21-30.

BURKE, A. 2000. Ultracapacitors: why, how, and where is the technology. *Journal of power sources,* 91**,** 37-50.

CAO, J. & EMADI, A. 2012. A new battery/ultracapacitor hybrid energy storage system for electric, hybrid, and plug-in hybrid electric vehicles. *IEEE Transactions on Power Electronics,* 27**,** 122-132.

CAPASSO, C., LAURIA, D. & VENERI, O. 2018. Experimental evaluation of model-based control strategies of sodium-nickel chloride battery plus supercapacitor hybrid storage systems for urban electric vehicles. *Applied energy,* 228**,** 2478-2489.

CERAOLO, M. 2000. New dynamical models of lead-acid batteries. *IEEE transactions on Power Systems,* 15**,** 1184-1190.

CHEN, B.-C., WU, Y.-Y. & TSAI, H.-C. 2014. Design and analysis of power management strategy for range extended electric vehicle using dynamic programming. *Applied Energy,* 113**,** 1764-1774.

CHEN, M. & RINCON-MORA, G. A. 2006. Accurate electrical battery model capable of predicting runtime and IV performance. *IEEE transactions on energy conversion,* 21**,** 504-511.

CHENG, A., XIONG, Q., WANG, L. & ZHANG, Y. Design of drive control strategy for mini pure electric vehicles on the condition of slope climbing. 2019 Chinese Control And Decision Conference (CCDC), 2019. IEEE, 4828-4832.

CHEW, K. W., LEONG, C. & GOI, B. M. Contour data acquisition system for electric vehicle distance estimation method. Applied Mechanics and Materials, 2014. Trans Tech Publ, 503-507.

COELINGH, E. & SOLYOM, S. 2012. All aboard the robotic road train. *Ieee Spectrum,* 49**,** 34-39.

CONWAY, B. E. 2013. *Electrochemical supercapacitors: scientific fundamentals and technological applications*, Springer Science & Business Media.

DEVILLERS, N., JEMEI, S., PERA, M.-C., BIENAIME, D. & GUSTIN, F. 2014. Review of characterization methods for supercapacitor modelling. *Journal of Power Sources,* 246**,** 596-608.

DIXON, J. Energy storage for electric vehicles. 2010 IEEE International Conference on Industrial Technology, 2010. IEEE, 20-26.

DOUGLAS, H. & PILLAY, P. Sizing ultracapacitors for hybrid electric vehicles. 31st Annual Conference of IEEE Industrial Electronics Society, 2005. IECON 2005., 2005. IEEE, 6 pp.

ECKERT, J. J., DE ALKMIN SILVA, L. C., DEDINI, F. G. & CORREA, F. C. 2020. Electric vehicle powertrain and fuzzy control multi-objective optimization, considering dual hybrid energy storage systems. *IEEE Transactions on Vehicular Technology,* 69**,** 3773-3782.

EHSANI, M., GAO, Y. & EMADI, A. 2009. *Modern electric, hybrid electric, and fuel cell vehicles: fundamentals, theory, and design*, CRC press.

EHSANI, M., GAO, Y. & EMADI, A. 2010. *Modern electric, hybrid electric, and fuel cell vehicles: fundamentals, theory, and design,* Boca Raton, CRC press.

ERICSSON, E. 2000. Variability in urban driving patterns. *Transportation Research Part D: Transport and Environment,* 5**,** 337-354.

FARAH, N., TALIB, M. H. N., SHAH, N. S. M., ABDULLAH, Q., IBRAHIM, Z., LAZI, J. B. M. & JIDIN, A. 2019. A novel self-tuning fuzzy logic controller based induction motor drive system: An experimental approach. *IEEE Access,* 7**,** 68172-68184.

FARANDA, R., GALLINA, M. & SON, D. A new simplified model of double-layer capacitors. 2007 International Conference on Clean Electrical Power, 2007 Capri, Itlay. IEEE, 706-710.

FATHABADI, H. 2018. Novel fuel cell/battery/supercapacitor hybrid power source for fuel cell hybrid electric vehicles. *Energy,* 143**,** 467-477.

FOTOUHI, A., AUGER, D. J., PROPP, K., LONGO, S. & WILD, M. 2016. A review on electric vehicle battery modelling: From Lithium-ion toward Lithium–Sulphur. *Renewable and Sustainable Energy Reviews,* 56**,** 1008-1021.

FOTOUHI, A., PROPP, K. & AUGER, D. J. Electric vehicle battery model identification and state of charge estimation in real world driving cycles. 7th Computer Science and Electronic Engineering Conference (CEEC), 2015 Colchester, UK. IEEE, 243-248.

GOLCHOUBIAN, P. & AZAD, N. L. 2017. Real-time nonlinear model predictive control of a battery–supercapacitor hybrid energy storage system in electric vehicles. *IEEE Transactions on Vehicular Technology,* 66**,** 9678-9688.

GOMOZOV, O., TROVãO, J. P. F., KESTELYN, X. & DUBOIS, M. R. 2016. Adaptive energy management system based on a real-time model predictive control with nonuniform sampling time for multiple energy storage electric vehicle. *IEEE Transactions on Vehicular Technology,* 66**,** 5520-5530.

GONSRANG, S. & KASPER, R. 2018. Optimisation-Based Power Management System for an Electric Vehicle with a Hybrid Energy Storage System. *International Journal of Automotive and Mechanical Engineering,* 15**,** 5729-5747.

GONZLEZ, B. I. M. A. F. 2009. *Multiple Input-Converter for a Battery-Ultracapacitor Hybrid Electric Vehicle.*

HALEY, P. 2012. *Effect of Electrical Vehicles on Residential Distribution Systems.* Faculty of the Louisiana State University and Agricultural and Mechanical College in partial fulfillment of the requirements for the degree of Masters of Science in Electrical Engineering In The Department of Electrical and Computer Engineering By Paul Haley BS, Louisiana State University.

HAN, W., LI, Y. & CHEN, L. High-precision DEM production in complex urban area using LiDAR data. 2012 20th International Conference on Geoinformatics, 2012. IEEE, 1-5.

HU, J., LIU, D., DU, C., YAN, F. & LV, C. 2020. Intelligent energy management strategy of hybrid energy storage system for electric vehicle based on driving pattern recognition. *Energy***,** 117298.

HURIA, T., CERAOLO, M., GAZZARRI, J. & JACKEY, R. High fidelity electrical model with thermal dependence for characterization and simulation of high power lithium battery cells. IEEE International Electric Vehicle Conference (IEVC), 2012 Greenville, USA. IEEE, 1-8.

IANNUZZI, D. & TRICOLI, P. 2012. Speed-based state-of-charge tracking control for metro trains with onboard supercapacitors. *IEEE Transactions on power electronics,* 27**,** 2129-2140.

JACKEY, R., SAGINAW, M., SANGHVI, P., GAZZARRI, J., HURIA, T. & CERAOLO, M. 2013. Battery Model Parameter Estimation Using a Layered Technique: An Example Using a Lithium Iron Phosphate Cell. SAE Technical Paper.

JAVORSKI ECKERT, J., CORREA DE ALKMIN E SILVA, L., MAZZARIOL SANTICIOLLI, F., DOS SANTOS COSTA, E., CORREA, F. C. & GIUSEPPE DEDINI, F. 2018. Energy storage and control optimization for an electric vehicle. *International Journal of Energy Research,* 42**,** 3506-3523.

JOHANSSON, P. & ANDERSSON, B. 2008. Comparison of simulation programs for supercapacitor modelling. *Master of Science Thesis. Chalmers University of Technology, Sweden*.

JORDáN, J., PALANCA, J., DEL VAL, E., JULIAN, V. & BOTTI, V. 2018. A multi-agent system for the dynamic emplacement of electric vehicle charging stations. *Applied Sciences,* 8**,** 313.

JU, F., ZHANG, Q., DENG, W. & LI, J. Review of structures and control of battery-supercapacitor hybrid energy storage system for electric vehicles. IEEE International Conference on Automation Science and Engineering (CASE), 2014 Taipei, Taiwan. IEEE, 143-148.

KALOKO, B. S., SOEBAGIO, M. H. P. & PURNOMO, M. H. 2011. Design and Development of Small Electric Vehicle using MATLAB/Simulink. *International Journal of Computer Applications,* 24**,** 19-23.

KATSHIKO, O. 2010. *Modern Control Engineering,* USA, New Jersey: prentice Hall.

KEDJAR, B. & AL-HADDAD, K. 2009. DSP-based implementation of an LQR with integral action for a three-phase three-wire shunt active power filter. *IEEE transactions on industrial electronics,* 56**,** 2821-2828.

KĘDRA, B. & MALKOWSKI, R. Comparison of Supercapacitor and Flywheel Energy Storage Devices Based on Power Converters and Simulink Real-Time. 2018 IEEE International Conference on Environment and Electrical

Engineering and 2018 IEEE Industrial and Commercial Power Systems Europe (EEEIC/I&CPS Europe), 2018. IEEE, 1-5.
KHALIGH, A. & LI, Z. 2010. Battery, ultracapacitor, fuel cell, and hybrid energy storage systems for electric, hybrid electric, fuel cell, and plug-in hybrid electric vehicles: State of the art. *IEEE transactions on Vehicular Technology,* 59**,** 2806-2814.
KUPERMAN, A. & AHARON, I. 2011. Battery–ultracapacitor hybrids for pulsed current loads: A review. *Renewable and Sustainable Energy Reviews,* 15**,** 981-992.
LALDIN, O., MOSHIRVAZIRI, M. & TRESCASES, O. 2013. Predictive algorithm for optimizing power flow in hybrid ultracapacitor/battery storage systems for light electric vehicles. *IEEE Transactions on Power Electronics,* 28**,** 3882-3895.
LARMINIE, J. & LOWRY, J. 2003. Electric vehicle technology explained, 2003. *John Wiley&Sons, Ltd.*
LI, G., YANG, Z., LI, B. & BI, H. 2019a. Power allocation smoothing strategy for hybrid energy storage system based on Markov decision process. *Applied energy,* 241**,** 152-163.
LI, Y., HUANG, X., LIU, D., WANG, M. & XU, J. 2019b. Hybrid energy storage system and energy distribution strategy for four-wheel independent-drive electric vehicles. *Journal of Cleaner Production,* 220**,** 756-770.
LIU, S., XIE, X. & YANG, L. 2020. Analysis, Modeling and Implementation of a Switching Bi-Directional Buck-Boost Converter Based on Electric Vehicle Hybrid Energy Storage for V2G System. *IEEE Access,* 8**,** 65868-65879.
LU, X., CHEN, Y., FU, M. & WANG, H. 2019. Multi-Objective Optimization-Based Real-Time Control Strategy for Battery/Ultracapacitor Hybrid Energy Management Systems. *IEEE Access,* 7**,** 11640-11650.
MACHADO, F., TROVãO, J. P. F. & ANTUNES, C. H. 2015. Effectiveness of supercapacitors in pure electric vehicles using a hybrid metaheuristic approach. *IEEE Transactions on Vehicular Technology,* 65**,** 29-36.
MAHMUD, K. & TOWN, G. E. 2016. A review of computer tools for modeling electric vehicle energy requirements and their impact on power distribution networks. *Applied Energy,* 172**,** 337-359.
MARIE-FRANCOISE, J.-N., GUALOUS, H. & BERTHON, A. 2006. Supercapacitor thermal-and electrical-behaviour

modelling using ANN. *IEE Proceedings-Electric Power Applications,* 153**,** 255-262.

MELLOR, P., SCHOFIELD, N. & HOWE, D. Flywheel and supercapacitor peak power buffer technologies. Electric, Hybrid and Fuel Cell Vehicles (Ref. No. 2000/050), IEE Seminar, 2000. IET, 8/1-8/5.

MESBAHI, T., RIZOUG, N., BARTHOLOMEUS, P., SADOUN, R., KHENFRI, F. & LE MOIGNE, P. 2017. Optimal energy management for a li-ion battery/supercapacitor hybrid energy storage system based on a particle swarm optimization incorporating Nelder–Mead simplex approach. *IEEE Transactions on Intelligent Vehicles,* 2**,** 99-110.

MOHAN, N. & UNDELAND, T. M. 2007. *Power electronics: converters, applications, and design,* USA, John Wiley & Sons.

NEAIMEH, M., HIGGINS, C., HILL, G., HUBNER, Y. & BLYTHE, P. 2012. Investigating the effects of topography and traffic conditions on the driving efficiency of electric vehicles to better inform smart navigation.

NEUBAUER, J., PESARAN, A., BAE, C., ELDER, R. & CUNNINGHAM, B. 2014. Updating United States Advanced Battery Consortium and Department of Energy battery technology targets for battery electric vehicles. *Journal of Power Sources,* 271**,** 614-621.

OSTADI, A., KAZERANI, M. & CHEN, S.-K. Hybrid Energy Storage System (HESS) in vehicular applications: A review on interfacing battery and ultra-capacitor units. Transportation Electrification Conference and Expo (ITEC), 2013 IEEE, 2013. IEEE, 1-7.

PALADINI, V., DONATEO, T., DE RISI, A. & LAFORGIA, D. 2007. Super-capacitors fuel-cell hybrid electric vehicle optimization and control strategy development. *Energy Conversion and Management,* 48**,** 3001-3008.

PAN, C., LIANG, Y., CHEN, L. & CHEN, L. 2019. Optimal Control for Hybrid Energy Storage Electric Vehicle to Achieve Energy Saving Using Dynamic Programming Approach. *Energies,* 12**,** 588.

PEARRE, N. S., KEMPTON, W., GUENSLER, R. L. & ELANGO, V. V. 2011. Electric vehicles: How much range is required for a day's driving? *Transportation Research Part C: Emerging Technologies,* 19**,** 1171-1184.

PERGER, T. & AUER, H. 2020. Energy efficient route planning for electric vehicles with special consideration of the topography and battery lifetime. *Energy Efficiency,* 13**,** 1705-1726.

QU, L., ZHUANG, W. & CHEN, N. Instantaneous Velocity Optimization Strategy of Electric Vehicle Considering Varying Road Slopes. 2019 Chinese Control And Decision Conference (CCDC), 2019. IEEE, 5483-5488.

RAFIK, F., GUALOUS, H., GALLAY, R., CRAUSAZ, A. & BERTHON, A. 2007. Frequency, thermal and voltage supercapacitor characterization and modeling. *Journal of power sources,* 165**,** 928-934.

REDDY, T. 2002. *Handbook of batteries*, McGraw-Hill Pub.

REKIOUA, D. 2014. Wind Power Electric Systems. *Green Energy and Technology, London Springer*.

REN, G., SHAN, S., MA, G., SHANG, X., ZHU, S., ZHANG, Q. & YANG, T. 2019. Review of Energy Storage Technologies for Extended Range Electric Vehicle. *Journal of Applied Science and Engineering,* 22**,** 69г82.

RICHARDSON, D. B. 2013. Electric vehicles and the electric grid: A review of modeling approaches, Impacts, and renewable energy integration. *Renewable and Sustainable Energy Reviews,* 19**,** 247-254.

ROY, B. U. & RENGARAJAN, N. 2015. Application of Supercapacitors for Short term Energy Storage Requirements. *Sciences,* 8**,** 158-164.

SADEQ, T. & WAI, C. K. Model the DC-DC Converter with Supercapacitor Module based on System Identification. 2019 IEEE International Conference on Automatic Control and Intelligent Systems (I2CACIS), 2019. IEEE, 185-188.

SADEQ, T. & WAI, C. K. Linear Quadratic Regulator Control Scheme on Hybrid Energy Storage System. 2020 IEEE International Conference on Automatic Control and Intelligent Systems (I2CACIS), 2020. IEEE, 219-223.

SADEQ, T., WAI, C. K., MORRIS, E., TARBOSH, Q. A. & AYDOĞDU, Ö. 2020. Optimal Control Strategy to Maximize the Performance of Hybrid Energy Storage System for Electric Vehicle Considering Topography Information. *IEEE Access*.

SADOUN, R., RIZOUG, N., BARTHOLOMEUS, P., BARBEDETTE, B. & LE MOIGNE, P. Optimal sizing of hybrid supply for electric vehicle using Li-ion battery and supercapacitor. 2011 IEEE Vehicle Power and Propulsion Conference, 2011. IEEE, 1-8.

SCHALTZ, E. 2011. *Electrical vehicle design and modeling*, INTECH Open Access Publisher.

SELLALI, M., ABDEDDAIM, S., BETKA, A., DJERDIR, A., DRID, S. & TIAR, M. 2019. Fuzzy-Super twisting control implementation of battery/super capacitor for electric vehicles. *ISA transactions*.

SHAFIEI, A., MOMENI, A. & WILLIAMSON, S. S. Battery modeling approaches and management techniques for plug-in hybrid electric vehicles. 2011 IEEE Vehicle Power and Propulsion Conference, 2011. IEEE, 1-5.

SHAH, V. A., KUNDU, P. & MAHESHWARI, R. 2012. Improved method for characterization of ultracapacitor by constant current charging. *International Journal of modeling and optimization,* 2**,** 290.

SHARMA, P. & BHATTI, T. 2010. A review on electrochemical double-layer capacitors. *Energy Conversion and Management,* 51**,** 2901-2912.

SHEN, D., KARBOWSKI, D. & ROUSSEAU, A. 2020. A minimum principle-based algorithm for energy-efficient eco-driving of electric vehicles in various traffic and road conditions. *IEEE Transactions on Intelligent Vehicles,* 5**,** 725-737.

SHEN, J. & KHALIGH, A. 2016a. Design and real-time controller implementation for a battery-ultracapacitor hybrid energy storage system. *IEEE Transactions on Industrial Informatics,* 12**,** 1910-1918.

SHEN, J. & KHALIGH, A. Predictive control of a battery/ultracapacitor hybrid energy storage system in electric vehicles. 2016 IEEE Transportation Electrification Conference and Expo (ITEC), 2016b. IEEE, 1-6.

SHIM, J. W., CHO, Y., KIM, S.-J., MIN, S. W. & HUR, K. 2013. Synergistic control of SMES and battery energy storage for enabling dispatchability of renewable energy sources. *IEEE Transactions on Applied Superconductivity,* 23**,** 5701205-5701205.

SUN, L., FENG, K., CHAPMAN, C. & ZHANG, N. 2017. An adaptive power-split strategy for battery–supercapacitor powertrain—design, simulation, and experiment. *IEEE Transactions on Power Electronics,* 32**,** 9364-9375.

TARBOSH, Q. A., AYDOĞDU, Ö., FARAH, N., TALIB, M. H. N., SALH, A., ÇANKAYA, N., OMAR, F. A. & DURDU, A. 2020. Review and investigation of simplified rules fuzzy logic speed controller of high performance induction motor drives. *IEEE Access,* 8, 49377-49394.

THOMAS, C. 2009. Fuel cell and battery electric vehicles compared. *international journal of hydrogen energy,* 34, 6005-6020.

TIE, S. F. & TAN, C. W. 2013. A review of energy sources and energy management system in electric vehicles. *Renewable and Sustainable Energy Reviews,* 20, 82-102.

UDHAYA SANKAR, G., GANESA MOORTHY, C. & RAJKUMAR, G. 2019. Smart storage systems for electric vehicles–a review. *Smart Science,* 7, 1-15.

VENERI, O., CAPASSO, C. & PATALANO, S. 2018. Experimental investigation into the effectiveness of a super-capacitor based hybrid energy storage system for urban commercial vehicles. *Applied Energy,* 227, 312-323.

WAI, C. K., RONG, Y. Y. & MORRIS, S. 2015. Simulation of a distance estimator for battery electric vehicle. *Alexandria Engineering Journal,* 54, 359-371.

WANG, J., BESSELINK, I. & NIJMEIJER, H. 2015. Electric vehicle energy consumption modelling and prediction based on road information. *World Electric Vehicle Journal,* 7, 447-458.

WANG, J., BESSELINK, I. & NIJMEIJER, H. 2018a. Battery electric vehicle energy consumption prediction for a trip based on route information. *Proceedings of the Institution of Mechanical Engineers, Part D: Journal of Automobile Engineering,* 232, 1528-1542.

WANG, X., TAO, J. & ZHANG, R. Fuzzy energy management control for battery/ultra-capacitor hybrid electric vehicles. Control and Decision Conference (CCDC), 2016 Chinese. IEEE, 6207-6211.

WANG, Y., YANG, Z. & LI, F. 2018b. Optimization of energy management strategy and sizing in hybrid storage system for tram. *Energies,* 11, 752.

WANGSUPPHAPHOL, A., IDRIS, N., JUSOH, A. & MUHAMAD, N. 2013. Power converter design for electric vehicle applications. *J. Teknologi,* 67, 25-31.

WIPKE, K., CUDDY, M., BHARATHAN, D., BURCH, S., JOHNSON, V., MARKEL, A. & SPRIK, S. 1999. ADVISOR 2.0: A second-generation advanced vehicle simulator for systems analysis. *NAEVI,* 98, 3-4.

XIANG, C., WANG, Y., HU, S. & WANG, W. 2014. A new topology and control strategy for a hybrid Battery-

Ultracapacitor energy storage system. *Energies,* 7**,** 2874-2896.
YANG, S. & KNICKLE, H. 2002. Design and analysis of aluminum/air battery system for electric vehicles. *Journal of Power Sources,* 112**,** 162-173.
ZHANG, J., ZHANG, L., SUN, F. & WANG, Z. 2018. An overview on thermal safety issues of lithium-ion batteries for electric vehicle application. *IEEE Access,* 6**,** 23848-23863.
ZHANG, L., WANG, Z., HU, X., SUN, F. & DORRELL, D. G. 2015. A comparative study of equivalent circuit models of ultracapacitors for electric vehicles. *Journal of Power Sources,* 274**,** 899-906.
ZHANG, L., YE, X., XIA, X. & BARZEGAR, F. 2020. A real-time energy management and speed controller for an electric vehicle powered by a hybrid energy storage system. *IEEE Transactions on Industrial Informatics*.
ZHANG, Q. & DENG, W. 2016. An adaptive energy management system for electric vehicles based on driving cycle identification and wavelet transform. *Energies,* 9**,** 341.
ZHANG, Y., JIANG, Z. & YU, X. Control strategies for battery/supercapacitor hybrid energy storage systems. Energy 2030 Conference, 2008. ENERGY 2008. IEEE, 2008. IEEE, 1-6.
ZHAO, B., LV, C. & HOFMAN, T. 2019. Driving-cycle-aware energy management of hybrid electric vehicles using a three-dimensional Markov chain model. *Automotive Innovation,* 2**,** 146-156.
ZHENG, C., LI, W. & LIANG, Q. 2018. An energy management strategy of hybrid energy storage systems for electric vehicle applications. *IEEE Transactions on Sustainable Energy,* 9**,** 1880-1888.
ZUBIETA, L. & BONERT, R. 2000. Characterization of double-layer capacitors for power electronics applications. *IEEE Transactions on industry applications,* 36**,** 199-205.